PhD Dissertation

Auditory nerve function in mouse models of *ATP11A* and *CABP1-CABP2* related hearing loss

for the award of the degree

"Doctor of Philosophy"

Division of Mathematics and Natural Sciences of the

Georg-August-Universität Göttingen

within the doctoral program

"Sensory and Motor Neuroscience"

of the Georg-August University School of Science (GAUSS)

submitted by

Shashank Sharad Chepurwar

born in Gadchiroli, India

Göttingen, 2024

Thesis Committee

Prof. Dr. Nicola Strenzke

Institute for Auditory Neuroscience, University Medical Center, Göttingen

Prof. Dr. Martin Göpfert

Department of Cellular Neurobiology, University of Göttingen

Dr. Andreas Neef

Göttingen Campus Institute for Dynamics of Biological Networks, Göttingen

Members of the Examination Board Reviewer

Reviewer: **Prof. Dr. Nicola Strenzke**

Institute for Auditory Neuroscience, University Medical Center, Göttingen

Second Reviewer: **Prof. Dr. Martin Göpfert**

Department of Cellular Neurobiology, University of Göttingen

Additional Reviewer: **Dr. Andreas Neef**

Göttingen Campus Institute for Dynamics of Biological Networks, Göttingen

Further members of the Examination Board:

Prof. Dr. Michael Sereda

Max Planck Institute for Multidisciplinary Sciences, Göttingen

Dr. Brett Carter

European Neuroscience Institute, Göttingen

Dr. Thomas Frank

European Neuroscience Institute, Göttingen

Date of oral examination: 2nd of October 2024

Abstract

Hearing loss can be caused by varied factors affecting diverse structures of the auditory system such as the middle ear, the stria vascularis, the outer hair cells (OHC), inner hair cells (IHC), the spiral ganglion neurons (SGN), and the central auditory system. Auditory synaptopathy/neuropathy is a hearing disorder caused by deficits of the IHC ribbon synapses or the SGNs. Clinically, it is characterized by absent or severely abnormal auditory brainstem responses (ABRs) and conserved function of the OHCs determined by preserved Distortion Product Otoacoustic Emissions (DPOAEs). Here, I use genetically modified mouse models to study the mechanisms of two independent genetic causes of auditory neuropathy, autosomal dominant auditory neuropathy type II (AUNA2) caused by mutations in *ATP11A* and autosomal recessive auditory synaptopathy DFNB93 caused by mutations in *CABP2*.

Like AUNA2 patients, conditional *Atp11a* knockout mice showed an age-dependent reduction in ABR amplitudes. However, the single unit responses of their SGNs were quite normal. Interestingly, we observed a reduction in peak firing rates which together with a reduction in the number of IHC-SGN synapses may explain the ABR phenotype. In contrast, the very strong ABR amplitude reduction in *Cabp1-Cabp2* double knockout mice was found to correlate with a drastic reduction of SGN action potential firing. Enhanced synaptic $Ca_V1.3$ Ca^{2+} channel inactivation in the IHCs led to enhanced SGN firing rate adaptation. By increasing the duration of the silent interstimulus interval, I observed that the sound onset spike rates of mutants improved with an increased jitter and latency of the first-spike. These observations suggest the synergistic action of *Cabp1-Cabp2* is crucial for maintaining the calcium channels in a non-inactivated state and for sustained synaptic transmission at IHC ribbon synapses.

The comparison between the two mutants underlines that very diverse processes can cause auditory neuropathy and suggest that the clinical interventions to restore hearing need to thus focus on specific functional units of the auditory system. This study implicates the electrophysiological investigations in the auditory nerve as a crucial and essential experiment to confirm and assess the severity of an auditory deficit, to functionally characterize the phenotype of auditory neurotransmission and effectively elucidate the disease mechanism of etiologically diverse hearing disorders.

Acknowledgement

Scientific endeavour, just like life, becomes a worthy journey when one has the right companions. I am fortunate enough to always meet people of high calibre and favourable nature in my scientific career. A doctoral work is not only to push boundaries through carefully planned original investigation but also to live an experience of unadulterated inquiry into a phenomenon. Dedicating this long continuous time for making inroads into an unsolved problem filled me with a sense of confidence and awe towards the scientific discipline.

I would like to thank Prof. Dr. Nicola Strenzke for suggesting me a difficult scientific problem and simultaneously ensuring top-notch support that is ideal for a doctoral student. Ensuring that I received ample supervision while encouraging me to think critically made my doctoral experience joyful and complete. I am thankful to Prof. Dr. Tobias Moser for insightful discussions and his exceptional approachability. It was a rewarding experience to collaborate with Prof. Dr. Tina Pangršič Vilfan, discussions with whom always provided me with a fresh and nuanced perspective for which I am thankful. I would also like to thank Dr. Barbara Vona and Dr. Marcus Jeschke for helpful and cordial discussions. I would want to express my gratitude towards Prof. Dr. Martin Göpfert and Dr. Andreas Neef, members of my thesis committee who along with a critical evaluation of my progress, always encouraged me to improve. I would like to thank the further members of thesis examination board Prof. Dr. Michael Sereda, Dr. Brett Carter and Dr. Thomas Frank for investing their valuable time in evaluating my work. I would like to thank Dr. Antoine Huet for his practical and insightful suggestions regarding experiments. I would like to extend my gratitude towards Dr. Lina Maria Jaime Tobón, Christoph Kampshoff, Dr. Daniel Keppeler, Dr. Thomas Mager, Dr. Jakob Neef, Dr. Kathrin Kusch, Dr. Fritz Kobe and Dr. Lukasz Jablonski for being helpful and greatly resourceful.

I would like to thank Dr. Anna Vavakou for her collaboration and data contribution in the single-unit experiments. I would want to thank Iman Bahader for help with initial experiments, Stefan Thom for helping with Systems Physiology experiments and David Oestreicher for the fantastic collaboration on studying Cabp proteins. I would like to thank Dr. Bettina Wolf whose practical suggestions were immensely helpful to me during experimentation. I would like to specially thank Dr. Anupriya Thirumalai, Dr. Alfonso Malpede, Mehar Monga, Dr. Mohona Mukhopadhyay, Dr. Aida Garrido, Lennart Roos, Lakshay Khurana, Dr. Rohan Kapoor, Dr. Han Chen, Fadhel El May, Roos Voorn, Theocharis Alvanos, Sabina Nowakowska, Jonathan Götz, Jana Henseler, Elisabeth Koert, Artur Mittring and Tilman Horn for being exceptional labmates and all other members of the Institute for Auditory Neuroscience whose names I might have inadvertently missed.

I thank Daniela Gerke for help with the cryosections and Sina Langer, Christiane Senger-Freitag, Sandra Gerke and members of the ZTE for their help that ensured all my experiments ran smoothly. I am thankful to Ludwig Ehrenreich and Gerhard Hoch for quality technical support and also to Klara Dinter and Patricia Räke-Kügler who made all the office-work seem easy.

I thank Dominik Reimenschneider for the great office-sharing time and unplanned tea-breaks. I thank Dominik Sobczak for his very sincere effort under my guidance and lastly, I would like to thank Albert Justin Franke for being the best rotation student.

I feel elated and fortunate to have been in the company of such exceptional scientists during the course of my work. It encourages me to improve and contribute my Highest Endeavor.

Declaration

Hereby I declare that this thesis has been written independently and with no other sources and aids than quoted.

Shashank Sharad Chepurwar

Göttingen, 3 January 2024

Table of Contents

Table of Contents ..... **I**
Index of figures ..... **II**
Index of tables ..... **III**
Abbreviations ..... **IV**
1 Introduction **1**
1.1 Introduction to the auditory system 1
1.1.1 Anatomy of the cochlea and the traveling wave 1
1.1.2 Hair cell mechanotransduction and the receptor potential 2
1.1.3 Inner hair cell ribbon synapses 3
1.1.4 Sound encoding by SGNs 5
1.2 Hearing loss 5
1.2.1 Auditory synaptopathy and neuropathy 6
1.2.2 AUNA2 8
1.2.3 Calcium Binding Proteins 13
1.2.4 The *Otof* TDA mutant 17
1.3 Objective measures of auditory function 18
1.3.1 Auditory Brainstem Response 18
1.3.2 Distortion Product Otoacoustic Emissions (DPOAE) 20
2 Methods **22**
2.1 Mouse line generation 22
2.2 Immunohistochemistry 22
2.3 ABR and DPOAE 22
2.4 Single-Unit Electrophysiology 23
2.5 Analysis of neuronal activity data 26
2.6 Plotting and statistical tests 27
3 Results **28**
3.1 Calcium binding proteins 1 and 2 28
3.2 ATP11A 36
3.3 OTOF TDA 45
3.4 Current and future work 47
4 Discussion **49**
4.1 Cabp1 and Cabp2 49
4.2 Atp11a 51
4.3 Perspective 52
5 References **55**

Index of figures

Figure 1: Schematic depicting the human auditory system highlighting the components of outer, middle and the inner ear. 2
Figure 2: Schematic of a general mammalian Organ of Corti 2
Figure 3: Schematic depicting the ten transmembrane spanning domains of the alpha subunit of P4 ATPase along with the supporting CDC50 beta subunit. 9
Figure 4: Phylogenetic tree of the 14 human P4-ATPases with their class depicted. 12
Figure 5: Schematic of the function of a flippase 13
Figure 6: Inner hair cell ribbon synapse number and calcium currents in Cabp1/2 DKO mice. 14
Figure 7: Ca^{2+} currents in IHCs of *Cabp1/2* DKO mice 15
Figure 8: Recovery of Ca^{2+} currents in *Cabp1/2*-DKO IHCs 16
Figure 9: recovery of Ca^{2+}-currents in *Cabp1/2*-DKO IHCs 16
Figure 10: Voltage- and Ca^{2+} -dependent inactivation are enhanced after deletion of Cabp1 and Cabp2. 17
Figure 11: Impaired auditory brainstem responses in *Cabp1/2* DKO mice 28
Figure 12: DPOAE thresholds measurements for *Cabp1/2*-DKO mice. 29
Figure 13: : DPOAE intensities in *Cabp1/2* DKO mice 30
Figure 14: SGN responses in *CaBP1/2* DKO mice 31
Figure 15: Adapted spike rates for different interstimulus rates 31
Figure 16: Strength of adaptation in DKO. 32
Figure 17: Spike rates in *Cabp1/2*- DKO SGNs 33
Figure 18: Functional properties of DKO 34
Figure 19: SGN response properties in *Cabp1/2* DKO mice 35
Figure 20: Atp11a expression in the organ of Corti 36
Figure 21: ABR recordings at age 23 weeks 37
Figure 22: ABR data at lower ages 37
Figure 23: ABR thresholds at advanced ages 38
Figure 24: ABR in Atp11a cKO mice 38
Figure 25: ABR latencies in *Atp11a* cKO mice 39
Figure 26: Normal DPOAE in *Atp11a* cKO mice 40
Figure 27: Spontaneous Rate in *Atp11a* cKO 41
Figure 28: *Atp11a* cKO Post-stimulus time histogram 41
Figure 29: Functional properties of SGNs in *Atp11a* cKO mice 42
Figure 30: Properties of SGNs to complex stimuli 42
Figure 31: Correlations of functional properties 43
Figure 32: Images of *Atp11a* cKO inner hair cell synapses 44
Figure 33: Reduction in synapse numbers in ATP11a cKO 44
Figure 34: ABR and DPOAE in OtofTDA 45
Figure 35: Image Segmentation in SGNs 47

Index of tables

Table 1: Implications of P4 ATPases in disease conditions (Folmer et al. 2009).....9
Table 2 Biological functions of P-type ATPases (Andersen et al. 2016) 11
Table 3: Generator cells of specific ABR peaks..... 19

Abbreviations

ABR	Auditory Brainstem Response
AEP	Auditory Evoked Potential
AIC	Akaike's Information Criterion
AIFM1	Apoptosis-Inducing Factor Mitochondria-associated-1
AMPA	α-amino-3-hydroxy-5-methyl-4-isoxazolepropionic acid
AN	auditory nerve
ANOVA	Analysis of Variance
ARHL	Age-related hearing loss
Atp11a	Phospholipid-transporting ATPase 11A
AUNA	Auditory Neuropathy
AVCN	Anteroventral Cochlear Nucleus
BK	Big Potassium (Kalium)
Cabp1	Calcium Binding Protein 1
Cabp2	Calcium Binding Protein 2
CACNA1D	The gene encoding for Calcium Voltage-gated Channel subunit alpha1 D
CaM	Calmodulin
CAP	Compound Action Potential
CAPOS syndrome	Cerebellar ataxia, Areflexia, pes cavus, Optic atrophy and SNHL
Cas9	CRISPR-associated protein 9
CDC50	aminophospholipid translocase regulatory protein
CDI	Ca^{2+}-dependent inactivation
CF	Characteristic Frequency
cKO	Conditional Knockout
CMT	Charcot–Marie–Tooth disease
CN	cochlear nucleus
CRISPR	Clustered Regularly Interspaced Short Palindromic Repeats
CtBP2	C-terminal-binding protein 2
dB	Decibels
DDON	Deafness–Dystonia–Optic Neuropathy
DDP1	Deafness–Dystonia Peptide-1
DFNA	Autosomal dominant non-syndromic sensorineural deafness

DFNB	recessive non syndromic hearing loss gene
DFNM	modifier non syndromic hearing loss gene
DFNX	x-linked non syndromic hearing loss gene
DFNY	y-linked non syndromic hearing loss gene
Diaph	Diaphanous-3
DOA	Dominant Optic Atrophy
DPOAE	Distortion Product Otoacoustic Emission
EAAT	Excitatory Amino Acid Transporter
ECochG	Electrocochleogram
EM	Expectation-Maximization
ESC	Embryonic Stem Cell
FRT	Flippase Recombination Target
GLAST	GLutamate-ASpartate Transporter
GUI	Graphical User Interface
IC	inferior colliculus
IHC	Inner Hair Cell
KO	Knockout
KOMP	Knockout Mouse Project
LEM3	Ligand Effect Modulator 3
LL	lateral lemniscus
MET	Mechano-Electrical Transducer
MPZ	Myelin Protein Zero
MRTNR, MTTS	mitochondrial hearing loss gene
NARS2	Asparaginyl-tRNA Synthetase 2
NF-*κ*B	Nuclear factor kappa-light-chain-enhancer of activated B cells
NSHL	Nonsyndromic hearing loss
OAE	Otoacoustic Emission
OC	Organ of Corti
OHC	Outer Hair Cell
OPA1	Optic Atrophy 1
OTOF	Otoferlin gene
OTSC	Otosclerosis
PBS	Phosphate-Buffered Saline
PC	Phosphatidylcholine
PE	Phosphatidylethanolamine
PI	Phosphatidylinositol
PJVK	Pejvakin gene
PMP22	Peripheral Myelin Protein 22
Po	open probability
PS, PtSer	Phosphatidylserine
PSD	Post-Synaptic Density
PSTH	Post-Stimulus Time Histogram
PV	Parvalbumin

RM	Reissner's Membrane
ROR1	Receptor Tyrosine Kinase Like Orphan Receptor 1
RRP	Readily Releasable Pool
SANDD	Sinoatrial node Dysfunction and Deafness
SHL	Syndromic hearing loss
SI	Synchronization Index
SLa	Spiral Lamina
SLi	Spiral Limbus
SOAE	Spontaneous Otoacoustic Emission
SOC	superior olivary complex
SP	Summating Potential
SPL	Sound Pressure Level
SQL	Structured Query Language
TEOAE	Transient Evoked Otoacoustic Emission
TIMM8A	Translocase of Mitochondrial inner Membrane 8A
tm1a	Targeted mutation 1 a
tRNA	transfer Ribonucleic Acid
VDI	voltage-dependent inactivation
VGCC	Voltage Gated Calcium Channels
Vglut	Vesicular Glutamate Transporter
WHO	World Health Organization
WT	Wildtype

1 Introduction

The ability to hear is crucial for survival of animals in the wild. In humans, the sense of hearing is indispensable for day-to-day interactions which maintains healthy social life. Moreover, intact hearing is required for appreciation of music. Impairment of hearing can be a socially-isolating experience resulting from limited contact with others. An estimated 466 million people around the world have a disabling form of deafness (WHO). Deafness can be congenital or acquired later in life. Syndromic forms of hearing loss include syndromes such as Usher, Alport, Treacher Collins, etc. Infections such as those caused by Toxoplasma gondii, Rubella virus, Cytomegalovirus, etc can cause acquired congenital hearing loss (Korver et al. 2017). Early intervention in cases of hearing loss in newborns is crucial to obtain a better outcome of treatment (Finitzo et al. 1998).

1.1 Introduction to the auditory system

1.1.1 Anatomy of the cochlea and the traveling wave

The human auditory system is divided into the outer ear, middle ear and the inner ear (Fig. 1). The auricle or the ear pinna which is the externally visible part of the ear and the ear canal that leads to ear drum or tympanic membrane form the outer ear. Sound enters through the ear canal and vibrates the tympanic membrane. The tympanic membrane is connected to malleus bone which further joins incus and stapes. These ossicles constitute the middle ear. The vibrations of the tympanic membrane are conducted through the coordinated movement of the ossicles to the inner ear. The inner ear is composed of cochlea, which is the hearing organ and the semicircular canals of the vestibular system which regulate the balance of the body. The cochlea is a snail shaped structure consisting of two and half coiled turns of tubular chambers. The chambers are filled with fluid housed in three compartments, the scala vestibuli, scala tympani and scala media. The cochlea has two openings called the round and oval windows. The middle ear ossicle stapes contacts the oval window via the stapedial footplate and transmits the generated motion to the cochlear fluid.

The motion of cochlear fluids sets up a travelling wave along the basilar membrane, a structure that separates the scala media from the scala tympani and houses the organ of Corti (Fig. 2). The organ of Corti contains the inner and outer hair cells. Hair cells sense the motion of the surrounding fluids through hair-like structures called the stereocilia. The stereociliar bundle is deflected by the surrounding forces of the fluids which leads to opening of mechanically gated K^+ channels (Sukharev & Corey, 2004). Outer hair cells are electromotile and respond to the incoming vibrations thus amplifying the travelling wave (Oghalai et al. 2004). Inner hair cells transduce the sound signal into SGN nerve impulses at specialized synapses. SGNs form the eighth cranial nerve in the modiolus, the centre of the cochlea.

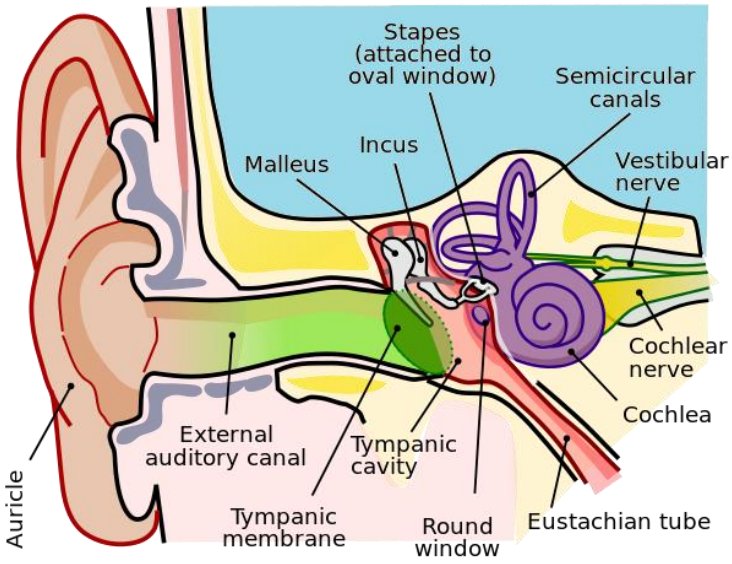

Figure 1: Schematic depicting the human auditory system highlighting the components of outer, middle and the inner ear.

(adapted from Wikimedia under Creative Commons Attribution licence)

1.1.2 Hair cell mechanotransduction and the receptor potential

On the apical surface of hair cells, an array of projections anchored to an actin network called the cuticular plate forms the stereociliar bundle. The bundle is arranged in a staircase pattern consisting of 50 to 100 actin-rich stereocilia and a single kinocilium which is microtubule-based (Siemens et al. 2004). The stereocilia are connected to each other through tip, lateral and ankle links while kinocilium connects through kinocilia links. The filamentous tip link connecting a stereocilium to its neighbour is formed by cadherin 23 on the top part connected to protocadherin 15 on the lower part (Bartsch & Hudspeth 2018).

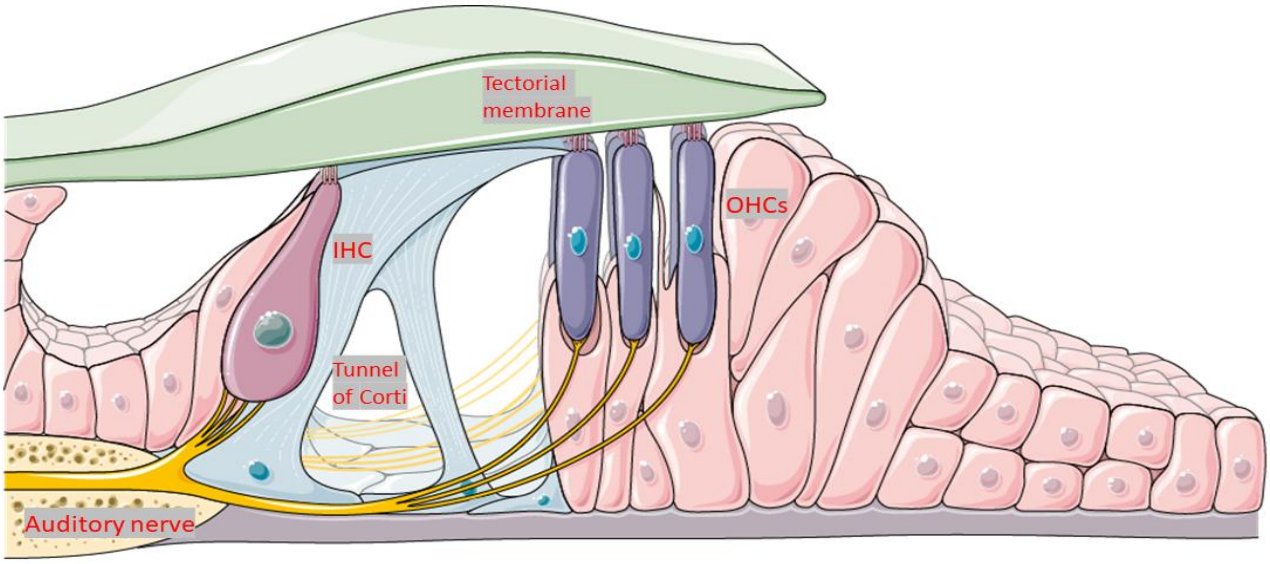

Figure 2: Schematic of a general mammalian Organ of Corti

(adapted from Wikimedia under Creative Commons Attribution licence)

The lower end of the tip link is coupled with mechanically gated ion channels. Sounds as low as a whisper and as high as a jet engine are capable of deflecting the stereocilia on a range of picometers to nanometers. Deflections towards the taller edge of the bundle causes tension in the tip link to increase leading to opening of the Mechano-Electrical Transducer (MET) channels. This opening causes an influx of cations which constitutes the MET current. The negative deflections however, close the channels. The MET current is carried predominantly by K^+ while the contribution from Ca^{2+} ions is minor. The ions enter through the hair bundle membrane at the apex of the hair cells. It exits through the basolateral membrane of the hair cell down a concentration gradient with K^+ ions leaving into the low K^+ perilymph (Fettiplace et al. 2019). Hair cells do not generate action potentials but a receptor potential. Their resting potential is shaped by various K^+ channels located on the basolateral membrane (Kros et al. 2007). The depolarization activates L-type Voltage Gated Calcium Channels (VGCCs) which in turn open the voltage-gated potassium channels such as the calcium sensitive BK type potassium channels (Fuchs et al. 2003). The contact of inner hair cells with its target, the afferent auditory neurons which is one of the main focus of this thesis is organized into specialized zones characterized by thickening of plasma membrane called the active zones (AZ).

1.1.3 Inner hair cell ribbon synapses

A striking feature of inner hair cells, unobserved in most other synapses is the presence of the ribbon nano-structure at their active zones. The ribbon is an ovoid vesicle docking structure with a diameter of about 400 nm attached to a monolayer of about 100 vesicles via 20nm filaments (Fuchs et al. 2003, Lenzi et. al 1999). Additional vesicles reside in the cytoplasmic proximity of ribbon by an as yet unknown mechanism. A ribbon is tethered to the active zone with a small number (<5%) of ribbons classified as 'floating' ribbons, probably reflecting the ribbon turnover (Zenisek et al. 2004, Khimich et al. 2005). In an event of sustained activation of the hair cell, the vesicles on the plasma membrane of the active zone are rapidly depleted while those at the opposite end of the ribbon are less affected (Lenzi et al. 2002). The inner hair cell uses graded potentials that can transmit information at higher rates than that achieved through spiking. This needs the synapse to sustain periods of high exocytosis. Vesicles tethered to the ribbon provide a pool for sustained release that is about five folds larger than the membrane tethered fast release pool (Sterling et al. 2005).

Each ribbon synapse is associated with one afferent nerve fibre thus a single active zone acts as an input to one spiral ganglion neuron. Although this holds true for mammals, multiple ribbon synapses associate with a single afferent in nonmammalian systems such as turtle and frog (Keen et al. 2006, Schnee et al. 2005). Ribbons are formed mainly by ribeye/CtBP2 protein (Schmitz et al. 2000) while bassoon and piccolo act as scaffolding proteins (Dick et al. 2001). Bassoon anchors the ribbons to the active zone and is implicated in fast exocytosis at the synapse (Khimich et al. 2005). Another difference between IHC ribbon synapse and canonical synapses is the absence of molecular players such as the SNARE (Soluble NSF Attachment protein) complex that mediates vesicle fusion, priming factors of the Munc family (Vogl et al. 2015) and the Ca^{2+} sensor synaptotagmin. The SNARE complex is replaced by as yet unknown proteins and synaptotagmin is replaced by C2 domain protein otoferlin

(Roux et al. 2006, Safieddine et al. 2012). In *Otof* knockout mice, the exocytosis at IHC ribbon synapses is almost completely abolished, despite preserved ribbons and Ca^{2+} currents (Roux et al. 2006). These mice are profoundly deaf and hence serve as a model for DFNB9 nonsyndromic human deafness caused by mutations in the gene *OTOF* (Yasunaga et al. 1999). To encode prolonged sound stimuli such as the continuous background noise, the inner hair cell synapse must maintain sustained neurotransmitter release. This needs extensive vesicle endocytosis and exocytosis and the presence of ribbon along with its vesicles. Otoferlin may underlie rapid replenishment and fusion of vesicles as evidenced by reduced synaptic exocytosis and slowed priming of vesicles into Readily Releasable Pool (RRP) in the C2F domain otoferlin mutant pachanga (Pangršič et al. Vogl et al. 2015). Nonsyndromic human deafness DFNA25 as well as deafness in mice is caused by mutation in *VGLUT3* gene SLC17A8 (Ruel et al. 2008, Seal et al. 2008). Vesicular Glutamate Transporter (Vglut3) is required for glutamate loading of synaptic vesicles, crucial for synaptic transmission and hearing function.

The calcium entry at the IHC synapse occurs through $Ca_V1.3$ L-type voltage gated Ca^{2+} channels. These channels are clustered on the plasma membrane beneath the ribbon and are opposed to the post-synaptic density. It is thought that Ca^{2+} channels form a cloud of cytoplasmic Ca^{2+} in the vicinity of docked vesicles of the RRP, when opened by depolarization. About 95% of type I auditory afferent neurons synapse on IHCs while the remaining 5% are Type II afferent neurons synapsing onto the OHCs. Type I neurons are myelinated while type II are thin and unmyelinated. Deflections of the hair bundles in IHC results in modulations of membrane potential from rest resulting in the sound-evoked receptor potentials. In mouse neonates, Ca^{2+} dependent action potentials are observed in the IHC, driving spontaneous firing of the auditory neurons. However, in the adults, action potentials are replaced by graded receptor potentials (Marcotti et al. 2003). At low sound frequencies the discharge of the auditory nerve is phase-locked with the receptor potential matching the sound stimulus. At sound frequencies above ~2 kHz a sustained increase in firing is observed instead (Kiang 1984, Rose et al. 1967).

In response to depolarization, glutamate filled vesicles are released into the synaptic cleft where they activate AMPA receptors (Matsubara et al. 1996). These glutamate receptors line the border of the postsynaptic density (PSD). Excess glutamate is taken up by glutamate transporters (EAAT) (Furness and Lehre 1997, Furness and Lawton 2003, Rebillard et al. 2003). Another instance of heterogeneity across the synapses is observed in the distribution of glutamate-aspartate transporters (GLAST) which are present in higher abundance on the pillar side of IHC with its high spontaneous rate fibres as compared to the modiolar side populated by low spontaneous rate fibres (Liberman 1982, Furness and Lawton 2003).

The release of neurotransmitter is accompanied by changes in membrane surface area of the hair cell mediated by vesicle exocytosis and endocytosis. These events can be studied by measuring the membrane capacitance (Cm) which increases with an increase in membrane surface in an event of fusion of synaptic vesicle with plasma membrane. The membrane capacitance measurements segregate into two kinetic components. The fast kinetic component mediates exocytosis at very high rates but saturates within a few milliseconds suggesting it represents exocytosis of a finite and relatively small pool of vesicles. It is thought that this component is mediated by the RRP of vesicles docked on the plasma membrane in the active zone (Moser & Beutner, 2000; Khimich et al. 2005; Schnee et al. 2005; Rutherford & Roberts, 2006) and possibly the release of ribbon-associated vesicles (Edmonds et al. 2004; Spassova et al. 2004). The subsequent slower kinetic component of exocytosis represents the process of resupply of vesicles to the active zone as well as extrasynaptic turnover of synaptic vesicles.

1.1.4 Sound encoding by SGNs

Each IHC is contacted by 8 to 20 SGN nerve terminals with heterogeneous response patterns which transmit sound information from cochlear inner hair cells (IHCs) to the brainstem. Spontaneous firing rate exhibits variability among fibres ranging from few spikes to 100 spikes/s. Fibres with low spontaneous rate have high thresholds (low sensitivity) while high spontaneous rate fibres have low thresholds (high sensitivity) (Liberman 1978, Ohlemiller et al. 1991, Winter et al. 1990). Although being functionally diverse, SGNs show comparable frequency tuning, suggesting that they contact neighbouring or even the same IHC at a given tonotopic position (Liberman 1978, Liberman 1982, Merchan-Perez & Liberman 1996). Low spontaneous fibres are thin and tend to be placed towards the modiolar side while the high spontaneous and high sensitivity fibres which are large in diameter with a higher number of mitochondria synapse on the pillar side of the IHC (Liberman 1980). Ribbons on the modiolar side are larger and more elongated. There also is systematic presynaptic heterogeneity in the $Ca_V1.3$ channels: those on the pillar side show high Ca^{2+}sensitivity by allowing entry at weaker depolarizations, thus getting activated at more hyperpolarized potentials than those at the modiolar side (Ohn et al. 2016).

Lately, single-cell RNA sequencing experiments have revealed that in addition to presynaptic heterogeneity there are also three molecularly defined type I SGN subtypes which likely contributes to heterogeneity of SGN coding properties (Shrestha et al. 2018).

1.2 Hearing loss

Hearing loss originates from both environmental and genetic factors. Exposure to high intensity noise can cause temporary/permanent shift in hearing thresholds. Environmental factors such as viral infections, neonatal anoxia and hyperbilirubinemia as well as use of ototoxic drugs such as aminoglycoside and gentamicin antibiotics are responsible for causing hearing defects (Yorgason et al. 2006). Unlike the genetic factors, environmental factors are avoidable through awareness and preventive measures. The clinical diagnosis of hearing loss is heterogeneous depending on multiple factors such as onset, severity and co-occurrence of other malformations. Hearing loss occurring prior to acquisition of speech is termed as prelingual deafness which can be congenital or appearing after birth. Prelingual deafness and deafness appearing in early childhood have major consequences on language acquisition. Age-related hearing loss (ARHL) occurs with a prevalence of about 60% of the population aged above 65. Hearing loss is described with terms such as severe, mild and moderate in descending order of severity. Nonsyndromic hearing loss (NSHL) is used to refer to cases where hearing loss is the only abnormality while in Syndromic hearing loss (SHL) other malformations occur along with hearing loss. Genetic factors are however responsible for hearing loss in 50-60% of all children born with hearing loss (Morton & Nance, 2006).

Genes responsible for hearing loss can be classified according to the varied molecular pathways and auditory function they can impair such as gene regulation, fluid homeostasis of the inner ear, mechanotransduction, junctional complex and tight junctions, synaptic transmission and the auditory pathway. To date, more than 50 genes and an additional set of 80 loci have been linked to hearing loss of varying order (Dror & Avraham, 2010). The nonsyndromic genes or loci are classified according to their inheritance mode into DFNA (dominant), DFNB (recessive), DFNX (x-linked), DFNY (y-linked), and DFNM (modifier). Other forms of hearing loss include

otosclerosis (OTSC), auditory neuropathy (AUNA), and mitochondrial (MRTNR, MTTS) genes. The number next to the name of the locus denotes the chronological order of its discovery, as listed on the Hereditary Hearing Loss Homepage (http:// hereditaryhearingloss.org/).

1.2.1 Auditory synaptopathy and neuropathy

The majority of the forms of hearing loss affect the normal functioning of sensory hair cells thus impairing the transduction of sound stimulus. This can include morphological defects in the structure of hair cell stereocilia, the cell itself or the IHC-SGN synapse. However, without apparent disruption of hair cell activity, the transmission of the auditory signal from the cochlea to the brain along the auditory nerve can be affected. Such a scenario is clinically classified as auditory neuropathy marked by improper function of auditory nerve while the cochlear sensory machinery is functional (Starr et al. 1996). Patients with auditory neuropathy score higher in speech disability as compared to patients with sensorineural hearing loss with similar hearing thresholds (Starr et al. 2000). The clinical diagnostic criteria for auditory neuropathy is absent or abnormal auditory brainstem response (ABR) with a preserved otoacoustic emission (OAE) thus pointing towards impairment of auditory nerve alongside functional OHCs. Thus, ABR responses directly point at the synchronic activity of the auditory nerve. It is constituted by 5 consecutive waves corresponding to continuous destinations in the auditory cascade. Several genes have been associated with auditory neuropathy phenotype, including vesicular glutamate transporter-3 (*VGLUT3*), otoferlin (*OTOF*), pejvakin (*PJVK*) and diaphanous-3 (*DIAPH3*). Of note, some of these genes are involved in inner hair cell function and synaptic transmission. Hence, the term "neuropathy" is actually not very precise.

VGLUT3 is one of the three subtypes of vesicular glutamate transporters involved in the accumulation of glutamate in the synaptic vesicles at the afferent synapse of cochlear inner hair cells. Vglut3 null mice show no response to sound stimulus as measured by auditory brainstem response but preserved OAE indicating normal OHC function (Seal et al. 2008). Further, mutations in the SLC17A8 gene, which encodes *VGLUT3,* underlies a NSHL termed DFNA25 in humans (Ruel et al. 2008). The synaptic vesicles of IHC are loaded with glutamate by the Vglut3 transporter. These vesicles then fuse with the plasma membrane releasing their contents onto the receptors of auditory nerve terminals. Absence of Vglut3 leads to severe synaptic deficiency caused by the loss of glutamate release.

Another protein implicated in the functioning of the IHC is otoferlin encoded by *OTOF* gene which is linked with auditory neuropathy (DFNB9) (Chaïb et al. 1996; Yasunaga et al. 1999). Otoferlin is a calcium sensor for neurotransmitter release at the IHC-SGN synapse (Roux et al. 2006). The membrane-anchored cytosolic protein, otoferlin is present in long and short isoforms, with the long isoform being affected in all DFNB9 mutations (Yasunaga et al. 2000). Otof knockout mice show no visible ABR with normal OAE recordings, satisfying the criterion of auditory neuropathy. However, ABR could be elicited by direct electrical stimulation, indicating that auditory neurons are not the target of otoferlin dysfunction. Recent studies have established otoferlin to be involved in calcium-dependent exocytosis and vesicle fusion at auditory hair cells synapses (Beurg et al. 2008; Dulon et al. 2009).

Pejvakin encoded by gene *PJVK* is implicated in nonsyndromic auditory neuropathy DFNB59 (Delmaghani et al. 2006). Pejvakin is expressed in hair cells and spiral ganglion neurons acting as a sensor to activate autophagy mechanism to degrade peroxisomes in oxidative stress events such as noise-induced damage (Defourny et al. 2019, Delmaghani et al. 2006, Schwander et al. 2007). The *CACNA1D* gene codes for a subunit of $Ca_V1.3$, a Ca^{2+} channel in IHCs that triggers the glutamate release at the synaptic site (Brandt et al. 2003). Since these channels are distributed across different sites such as in OHCs, IHCs, cardiomyocytes, neuroendocrine cells and neurons, this mutation may lead to a syndrome called "sinoatrial node dysfunction and deafness" (SANDD syndrome) in mice as well as in humans (Baig et al. 2011, Platzer et al. 2000). Cabp2 (Calcium binding protein 2) is a protein that interacts with voltage-gated Ca_V channels in regulating Ca^{2+} influx at the IHC presynaptic site (Haeseleer et al. 2002, Christel et al. 2012), leading to the vesicular release of synaptic glutamate. Mutations in *CABP2* gene causes the autosomal-recessive nonsyndromic deafness DFNB93 (Schrauwen et al. 2012).

A variety of factors disrupt the functioning of auditory signal cascade downstream of IHC synapse and are a cause of postsynaptic neuropathies. Mutations in the *OPA1* gene coding for a mitochondrial protein result in the syndromic dominant optic atrophy (DOA+) which is associated with hearing impairment (Alexander et al. 2000, Delettre et al. 2000). DOA+ results in visual impairment due to optic atrophy and hearing impairment due to degeneration of terminal axons of SGNs. ROR1 gene encodes for receptor tyrosine kinase-like orphan receptor 1 protein involved in NF-ϰB pathway for neural outgrowth. Mutation in this gene results in lack of innervation of sensory hair cell synapses and a deficiency of SGN axons. Presence of profound SNHL with preserved OAEs suggests an auditory postsynaptic synaptopathy (Diaz-Horta et al. 2016). Mutations in *ATP1A3* gene result in a syndromic phenotype characterized by cerebellar ataxia, areflexia, pes Cavus, optic atrophy and SNHL denoted by acronym CAPOS syndrome (Nicolaides et al. 1996). Clinical audiological measurements in CAPOS reveal preserved OAEs and absent or abnormal ABRs.

DIAPH3 gene encoding the protein Diaphanous homolog 3 mapped to the AUNA1 (auditory neuropathy, dominant, 1) locus in an American family (Kim et al. 2004) exhibits an auditory neuropathy phenotype. It was found that Diap3 overexpression causes progressive hearing loss and inner hair cell defects in a mouse model of AUNA1 (Schoen et al. 2013). Apart from these genes, certain other forms of deafness involving a lesion of peripheral neurons are also classified as auditory neuropathies. Charcot–Marie–Tooth disease (CMT) is a progressive motor and sensory neuropathy which involves a disproportionately poor speech perception as compared to the loss expected solely from cochlear impairment (Goswamy et al. 2012). Mutations in the MPZ gene and the *PMP22* gene are associated with the auditory neuropathy phenotype of CMT. Histological analysis reveals a normal hair cell morphology with considerable SGN fibre demyelination (Verhagen et al. 2005, Varga et al. 2003, Kabzinska et al. 2007). Friedreich ataxia is another sensorimotor neuropathy involving similar damage to SGNs resulting in auditory neuropathy phenotype (Rance et al. 2008). The deafness–dystonia peptide-1/translocase of mitochondrial inner membrane 8A (*DDP1/TIMM8A*) protein is involved in the transfer of metabolites into the mitochondrial inner membrane from the cytoplasm. An X-linked recessive progressive neurodegenerative syndrome results from mutation in the gene *TIMM8A* known as deafness–dystonia–optic neuropathy (DDON or Mohr–Tranebjærg syndrome) (Tranebjærg et al. 2003). Affected individuals present auditory neuropathy characterized by progressive degeneration of neurons (Bahmad et al. 2007, Brookes et al. 2008). *AIFM1*, the apoptosis-inducing factor mitochondria-associated-1 protein codes for a flavin adenine of the

mitochondrial intermembrane space and is expressed in inner and outer hair cells along with SGNs. Mutations of the *AIFM1* gene are responsible for an X-linked auditory neuropathy associated with a progressive neuromuscular degeneration known as Cowchock syndrome. Another early-onset progressive neurodegenerative disorder known as Leigh syndrome is caused by a mutation in the mitochondrial asparaginyl-tRNA synthetase (NARS2). NARS2 mutation leads to mitochondrial respiratory chain deficiency causing damage to SGNs as seen in DFNB94 (Simon et al. 2015).

The generation of a mouse model propels the field of discovery of any hearing mutation. Many of the hearing diseases along with syndromic hearing loss disorders do not have a mouse model available for conducting research on hearing loss. This handicaps the efforts to investigate the disease processes. In this thesis we have used two mouse lines the *Cabp1-Cabp2* and *Atp11a*, thus generating data that is translatable and adds to the already available rich dataset of mouse studies for hearing loss.

1.2.2 AUNA2

Another type of autosomal dominant auditory neuropathy is the AUNA2 auditory neuropathy described in a large German family. AUNA2 is exhibited as a non-syndromic slowly progressive post lingual hearing loss. Moreover, AUNA2 in humans has an age of onset in the second decade and progression to severe hearing loss by the fifth decade. The gene linkage is to chromosome 12q24 or 13q34.(Lang-Roth et. al 2017). Out collaborator Alexander Volk now found a heterozygous 5500 bp deletion in ATP11A on chromosome 13q34, segregating with the phenotype in this family. Atpa11a is a phospholipid flippase, crucial for maintaining lipid asymmetry. He showed that the mutated protein has reduced flippase activity for phosphatidylserine.

1.2.2.1 What is membrane lipid asymmetry?

In a healthy asymmetric membrane, Phosphatidylcholine (PC), sphingomyelin and glycolipids are enriched on exoplasmic leaflet, and phosphatidylserine (PS), phosphatidylethanolamine (PE), and phosphatidylinositol (PI) are confined to the cytoplasmic leaflet. (Zachowski 1993; Lenoir et al. 2007). Membrane lipid asymmetry is essential for a wide variety of cellular processes such as cell signalling, apoptosis, fertilization, vesicle budding and trafficking, membrane stability and permeability and membrane protein regulation. Additionally, it is important for blood coagulation, bile and cholesterol homeostasis. Lipid asymmetry also affects cell and organellar shaping and dynamics. In case of neurons, neurite extension and neuronal cell survival falls under the effects of membrane asymmetry perturbation (Andersen et al. 2016). Asymmetric lipid distribution may induce membrane curvature. The latter is a prerequisite for vesicle formation. Hence, cells that maintain high flow of exocytosis of vesicles may have impaired function via the secretory pathway. Disruption of lipid symmetry in a controlled manner is crucial for cell fusion, cytokinesis and host-virus interactions (Lopez-Marques 2014). Differential distribution of lipids across the bilayer is a characteristic eukaryotic cell membrane feature.. Asymmetric distribution of specific lipids is critical in physiological processes such as blood coagulation,, cell fusion, and host–virus interactions.

1.2.2.2 P4 ATPases and their functions

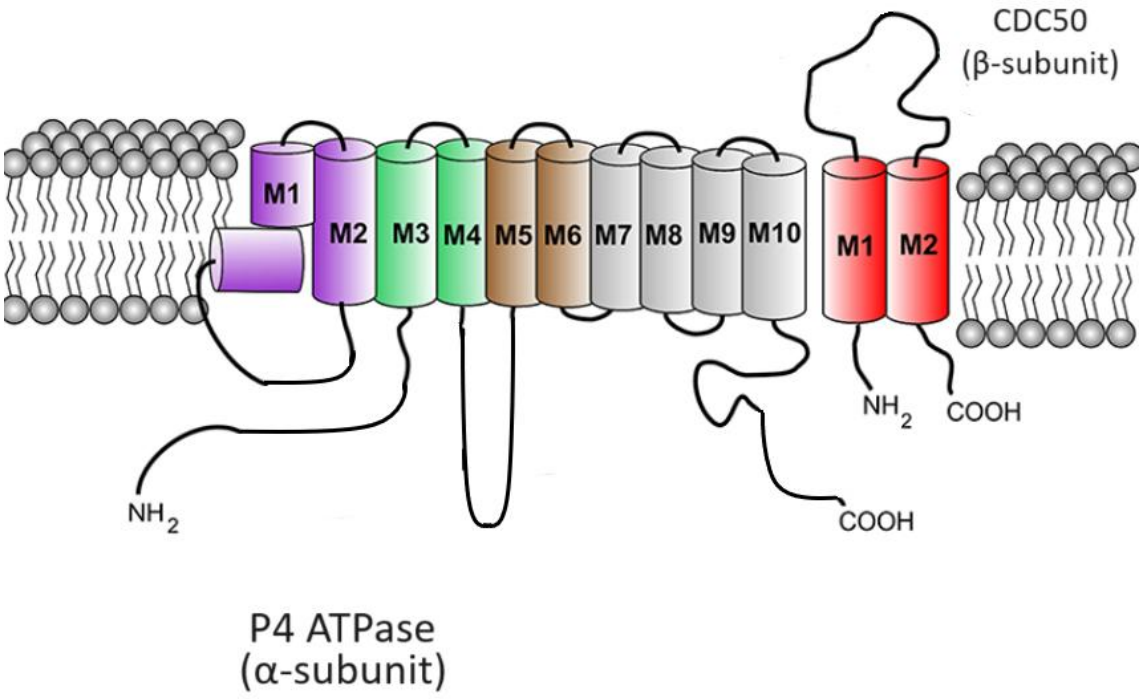

Figure 3: Schematic depicting the ten transmembrane spanning domains of the alpha subunit of P4 ATPase along with the supporting CDC50 beta subunit.

(Adapted from Andersen et al. 2016)

P4-ATPases are a subfamily of P-type ATPase consisting of members that are multispan transmembrane proteins involved in the translocation of phospholipids from the exoplasmic side to the cytoplasmic side (Fig. 3). In the mammals, there are fourteen members) (fifteen in mouse) divided into five classes (Class 1a, 1b, 2, 5 and 6) (Fig. 4). P4-ATPases excluding ATP9A and ATP9B form a heteromeric complex (likely heterodimer) by assembling with an accessory b(beta)-subunit from the CDC50/LEM3 family ubiquitously present in all eukaryotes (Katoh and Katoh, 2004; Saito et al. 2004). In humans, three CDC50 proteins are found: CDC50A (also named TMEM30A), CDC50B (TMEM30B) and CDC50C (TMEM30C).

Many of the P4 ATPases are implicated in severe human disorders on account of genetic aberrations in them. (Andersen 2016, Folmer at al. 2016, Liou et al. 2019) (

Table 1) Although the data is scarce, new studies focusing on P4 ATPases in disease conditions are increasingly available suggesting renewed interest in scientific community.

Table 1: Implications of P4 ATPases in disease conditions (Folmer et al. 2009)

Class	P4 ATPase	Pathophysiology
1 a	ATP8A1	
	ATP8A2	Tumorigenicity (unclear)

1 b	ATP8B1	Intrahepatic cholestasis
	ATP8B2	
	ATP8B3	Sperm capacitation abnormalities
	ATP8B4	Alzheimer's disease (unclear)
2	ATP9A	
	ATP9B	
5	ATP10A	Insulin resistance, Obesity
	ATP10B	
	ATP10D	Obesity
6	ATP11A	Hearing loss
	ATP11B	
	ATP11C	Blood and liver disorders

1.2.2.3 Flippases in the plasma membrane

In healthy cells, phospholipids are maintained asymmetrically in the plasma membrane with a differential composition among the two leaflets (Balasubramanian & Shroit, 2003). The amine-containing lipids, PtdSer and phosphatidylethanolamine (PtdEtn), are localized to the inner cytoplasmic leaflet of the plasma membrane, while on the other hand phosphatidylcholine (PtdCho) and sphingomyelin are concentrated in the outer exoplasmic leaflet. Aminophospholipid translocase(s) or flippase(s) are proposed to establish this asymmetrical phospholipid distribution by transporting PtdSer and PtdEtn from the outer to the inner leaflet of the lipid bilayer by employing ATP-dependent processes. Type IV P-type ATPases (P4-ATPases) are candidate flippases that include the large family with 14 human and 15 murine members of ten transmembrane segment membrane proteins. CDC50 protein functions as a chaperone for the correct subcellular localization of P4-ATPases, and is indispensable for their lipid transport activity (Nagata et al. 2016). Biological functions of P4-ATPases are outline in Table 2.

1.2.2.4 Flippase and scramblase regulation in apoptosis

It has been known that apoptotic PtdSer externalization is caspase-dependent (Martin et al. 1996) and accompanied by both scramblase activation and flippase inactivation at the plasma membrane (Verhoven et al. 1995, Bratton et al. 1997). Caspase cleavage at specific cleavage sites apparently inactivates flippase activity of P4 ATPase for example, ATP11C. It was observed that cells expressing caspase-resistant ATP11C could not expose PtdSer during apoptosis (Segawa et al. 2014), thus the flippase must be inactivated for apoptotic PtdSer exposure. Further studies also established that caspase cleavage activates the scramblase activity thus pointing at a concerted activity of multiple pathways. These findings together reveal how PtdSer is kept at the inner leaflet of the plasma

membrane in living cells, and how during apoptosis this asymmetrical distribution undergoes disruption to expose PtdSer. In healthy cells, a flippase actively or ATP dependently translocates PtdSer and PtdEtn from the outer to the inner leaflet of the plasma membrane, while scramblase such as Xkr8 remains inactive, thus PtdSer is confined to the inner leaflet. During apoptosis, caspases simultaneously inactivate flippase and activate scramblase, enabling rapid PtdSer exposure on the cell surface. This model is verified in several human and mouse cell lines studied (Segawa et al. 2015, Suzuki et al. 2013). When cells lose flippases, for example, by the lack of CDC50A (cell division cycle protein 50A), the asymmetrical distribution of phospholipids in the cells can no longer be maintained, thus exposing PtdSer to the cell surface of living cells but with no involvement of scramblases. The PtdSer thus exposed does not flip-flop at the plasma membrane, and undergoes efficient recognition by PtdSer receptor or PtdSer-binding proteins. Thus, macrophages engulf living, PtdSer-exposing cells lacking flippase in a PtdSer-dependent manner, pointing at the sufficient and necessary role of PtdSer for cells to be removed.

Table 2 Biological functions of P-type ATPases (Andersen et al. 2016)

P1A-ATPases	found in some bacteria and transport K^+
P1B-ATPases	transport heavy metal ions such as Ag^+, Zn^{2+}, Cd^{2+}, and Cu^{2+}
P2A-ATPases	sarco(endo)plasmic reticulum Ca^{2+}ATPase (SERCA) and secretory pathway Ca^{2+}-ATPase (SPCA)
P2B-ATPases	plasma membrane Ca^{2+}-ATPase (PMCA) transport $Ca^{2+}$and Mn^{2+}
P2C-ATPases	transport monovalent ions and include Na^+/K^+-ATPases and H^+/K^+-ATPases
P2D-ATPases	found in fungi and transport Na^+
P3A-ATPases	transport H^+
P3B-ATPases	transport Mg^{2+}
P4-ATPases	transport or flip phospholipids across membranes
P5-ATPases	substrate yet to be determined

1.2.2.5 Engulfment of Apoptotic Cells

Apoptotic cells are engulfed by multiple cell types namely macrophages and immature dendritic cells as well as epithelial and mesenchymal cells in a process known as phagocytosis (as well as via the complement-mediated phagocytosis called as efferocytosis) (deCathelineau & Henson, 2003). Macrophages are ubiquitously active throughout animal tissues with their parallel cellular machinery in the liver and brains called Kupffer cells and microglia, respectively. These cells engulf apoptotic cells efficiently. However, macrophages in varying tissues are heterogeneous (Gordon et al. 2014). Depending on the tissue context, macrophages seem to use a different and diverse set of molecules to engulf apoptotic cells. In normal resting cells, a flippase such as ATP11C translocates PtdSer and phosphatidylethanolamine (PtdEtn) from outer to inner leaflets, while Ca^{2+} or caspase-dependent scramblases are inactive. This keeps PtdSer, the 'eat me' signal hidden by localizing it in the inner leaflet of the plasma membrane, and macrophages cannot engulf them.

Thus, a collaboration between apoptotic cells and phagocytes is required for the evolutionarily conserved apoptotic cell clearance process to work. Although how PtdSer is externalized to the cell surface and is recognized by phagocytes had long been a mystery (Bevers and Williamson, 2010, Sahu et al. 2007, Wolf et al. 2007), the molecular identity of flippase was brought to light recently with identification of the molecules that support the scrambling and flipping of phospholipids at the plasma membrane.

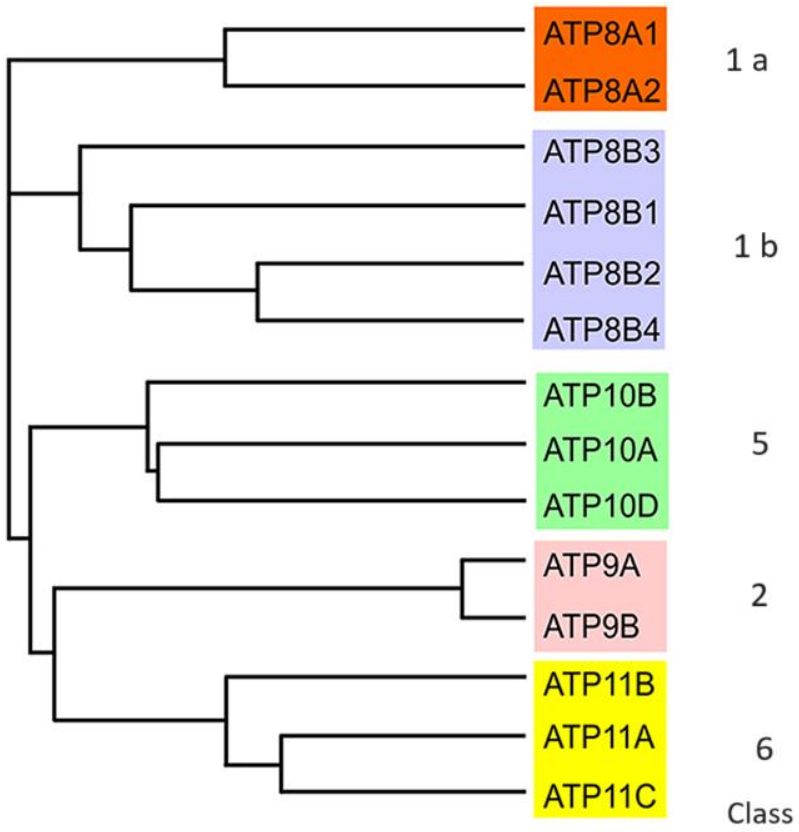

Figure 4: Phylogenetic tree of the 14 human P4-ATPases with their class depicted.

(Adapted from Andersen et al. 2016).

1.2.2.6 Phosphatidylserine Exposure during Apoptosis

Macrophages clear almost a billion senescent or damaged cells in the body every day which undergo apoptosis. Macrophages exclusively engulf apoptotic cells without damaging the healthy cells (Fadok et al. 1992), suggesting that apoptotic cells expose a specific 'Eat me' signal to phagocytes for efficient marking. Of the many 'Eat me' signals proposed, including phosphatidylserine (PtdSer), carbohydrates (amino sugars or mannose), intercellular adhesion molecule-3 (ICAM3), and calreticulin (Gardai et al. 2006), PtdSer is the most studied and also the most likely 'eat me' signal candidate.

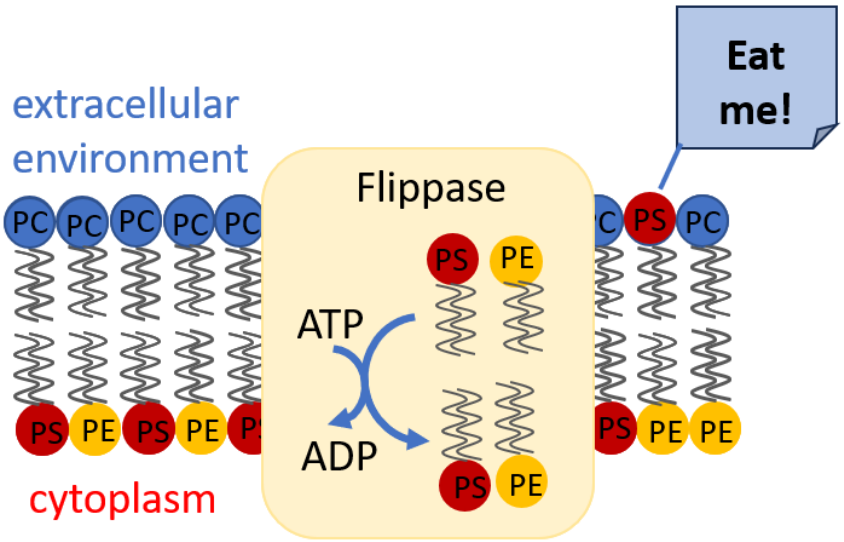

Figure 5: Schematic of the function of a flippase

PtdSer is exposed to the outer leaflet, thus acting as an 'Eat me' signal

The normal localization of PtdSer is to the inner leaflet of the plasma membrane, but during apoptosis it is exposed to the cell surface, becoming visible to the cell death machinery of the body (Leventis & Grinstein, 2010). For example, red blood cells that heavily display PtdSer are recognized and engulfed by macrophages (Tanaka and Shroit, 1983). Even though PtdSer exposure and PtdSer-dependent apoptotic cell engulfment have high evolutionarily conservation from lower organisms (Caenorhabditis elegans and Drosophila) to mammals (van den Eijnde et al. 1998, Venegas & Zhou, 2007), only recently the molecular mechanism that externalizes PtdSer to the plasma membrane during apoptosis has been identified (Segawa and Nagata, 2015).

1.2.3 Calcium Binding Proteins

Ca^{2+}-binding proteins (Cabps) are involved in regulation of numerous voltage-gated and ligand-gated ion channels. Ca^{2+}-binding proteins perform the functions of regulation of inactivation, activation, open probability (Po) and Ca^{2+}-dependent facilitation of the voltage-dependent Ca^{2+} (Cav) channels. Inactivation acts as a preventive mechanism against excessive Ca^{2+} entry via Cav channels. The two routes by which Ca_V1 and Ca_V2 channels undergo inactivation are: voltage-dependent inactivation (VDI) and Ca^{2+}-dependent inactivation (CDI). Cabps are expressed in the retina and the cochlea. Cabp1/caldendrin is also expressed in other neuronal tissues, including the brain (Seidenbecher et al. 1998; Menger et al. 1999; Haeseleer et al. 2000, 2004; Yang et al. 2006; Cui et al. 2007; Kim et al. 2014). The expression of Cabp1 is high in the brain and retina. Multiple Cabps are expressed in the cochlea (Cui et al. 2007; Yang et al. 2006) among which Cabp1 and Cabp2 are the most abundantly expressed (Yang et al. 2016; Yang 2018). Playing an opposing role to that of Ca^{2+}/CaM, which stabilize the inactivated state of $CaV_{1.2}$ channels, Cabp1 eliminates CDI completely by prolonging channel opening (Zhou et al. 2004; Cui et al. 2007) while supporting Ca^{2+}-dependent facilitation. In addition to regulating CDI, Cabp1 also regulates activation gating and VDI of Ca^{2+} (Ca_V) channels. Ca^{2+} binding proteins (Cabps) also suppress CDI in

heterologous expression systems (Hardie and Lee, 2016). The mechanism of suppression of CDI by Cabps is thought to occur by competitive displacement of CaM from the channel complex (Findeisen et al. 2013; Zhou et al. 2004) and by modulation allosterically (Oz et al. 2013; Yang et al. 2014).

In the visual system, light responses of retinal ganglion cells of mice deficient in Cabp1 and Cabp2 show abnormal amplitude and kinetics from those of wild-type mice. Cabp1/caldendrin and Cabp2 are not essential for normal gross retinal and synapse morphology but are required for the proper transmission of retinal light responses. Within the cochlea, Cabp1 and Cabp2 have distinct expression with Cabp1 being most highly expressed in spiral ganglion neurons (SGNs) and possibly in satellite glial cells, which have no Cabp2 expression (Yang et al. 2016). It is known that the gene encoding *CABP2* causes autosomal recessive hearing loss DFNB93 in humans (Picher et al. 2017; Schrauwen et al. 2012). Cabp1 and Cabp2 were implicated in the function of peripheral auditory system. In *Cabp1* Knockout (KO) mice, ABR wave I was larger in amplitude, and with shorter latency, hinting at enhanced synchrony of auditory nerve fibres. In whole-cell patch clamp recordings of spiral ganglion neurons in culture Cabp1 KO neurons showed greater excitability along with normal presynaptic function of IHCs supporting the enhanced synchrony interpretation. For Cabp1 KO mice, DPOAEs and ABR thresholds were normal in 4-week old, but elevated at 32 kHz in 9 weeks old mice, and also at 8 and 16 kHz by age of 6 months. In Cabp2 KO mice, significant ABR threshold elevations were visible at 4 weeks of age and increased in severity at mid-frequency range by age 9 weeks. DPOAEs in Cabp2 KO mice were normal at 4 weeks, but by 9 weeks of age they were significantly reduced in the mid-frequency range. (Yang et al. 2018).

CaBP1 and CaBP2 proteins have been studied individually in previous studies (Picher et al. 2017, Yang et al. 2018) but the combined effect of these proteins have not yet been studied. Having taken into consideration the varied phenotypes exhibited by Cabp1 and Cabp2 single knockouts we hypothesized that Cabp1 compensates for some of the functions of Cabp2. Thus, to bring out the effect of total loss of CaBP1-CaBP2 without any overlapping compensation I designed the following study. I investigated the effect of combined removal of Cabp1 and Cabp2 genes by studying the Cabp1-Cabp2 double knockout mice here. Using ex-vivo patch clamp recordings from mouse inner hair cells David Oestreicher and Tina Pangršič investigated their calcium current properties.

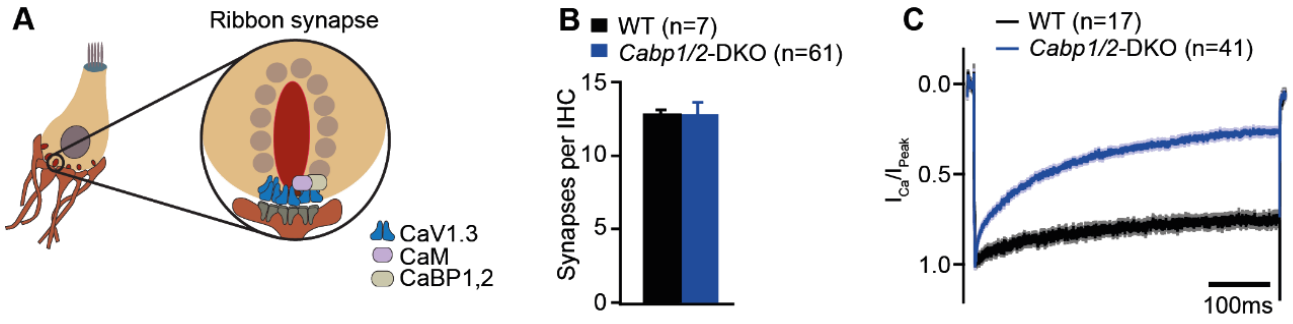

Figure 6: Inner hair cell ribbon synapse number and calcium currents in Cabp1/2 DKO mice.

(A) Schematic of the IHC and one of its many ribbon synapses. Cabps and CaM modulate voltage-gated calcium channels at the IHC ribbon synapses thus shaping the presynaptic Ca^{2+} signal. (B) Synapse density in apical IHCs was normal at 3-4 weeks of age for the Cabp1/2-DKO animals. (C) Peak normalized Ca^{2+}-currents after a 500-

ms depolarization step to the maximum current potential in apical IHCs of WT and Cabp1/2-DKO animals. A pronounced inactivation of the Ca^{2+} current in the absence of Cabp1 and 2 is evident. [Data acquired by David Oestreicher]

In an attempt to investigate possible synergistic functions of the two major IHC Cabps, they first measured Ca^{2+} currents in the IHCs of *Cabp1/2*-DKO mice and WT animals aged 3-4-weeks in the presence of 1.3 mM extracellular Ca^{2+} using perforated patch-clamp method. They observed that employing 500 ms-long depolarization steps to maximal Ca^{2+}-current potential at (-25 to -15 mV) leads to pronounced inactivation of $Ca_V1.3$ channels in the DKO IHCs (Fig. 6 C). As compared to the inactivation observed in the IHCs of Cabp1 or Cabp2 single KOs, this was significantly stronger under similar conditions (Yang et al. 2018, Picher et al. 2017, Oestreicher et al. 2021), and even when comparing to data from 5-week-old Cabp2 KO mice acquired at physiological temperature. This further substantiates the evidence of severity as well as early onset of the observed DKO phenotype.

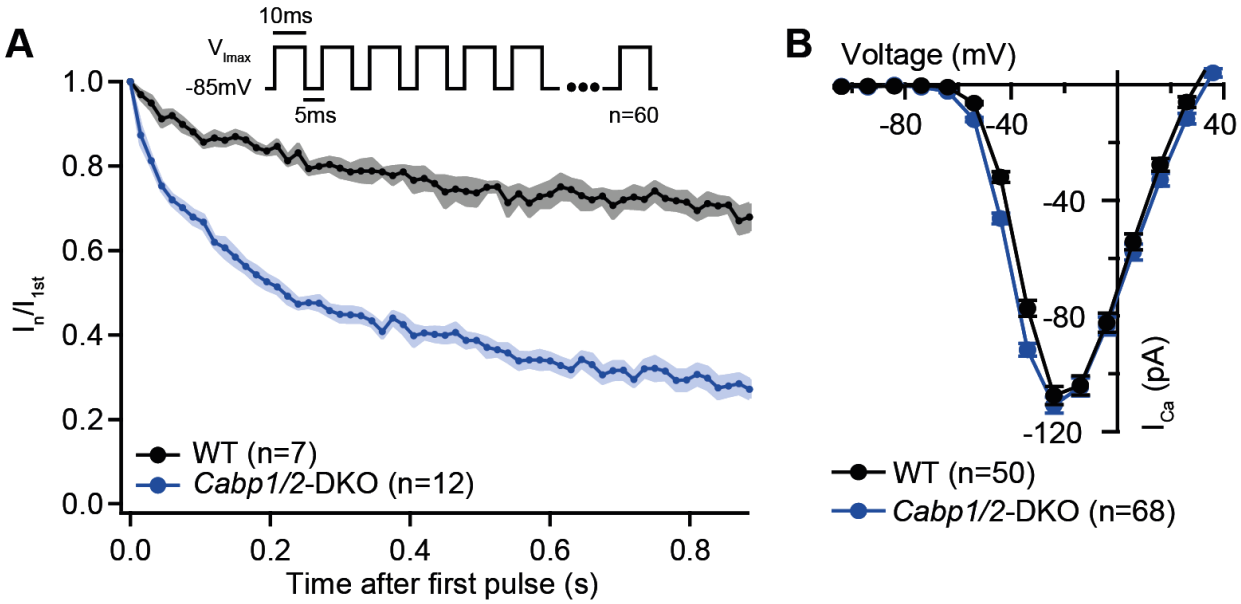

Figure 7: Ca^{2+} currents in IHCs of *Cabp1/2* DKO mice

(A) Ca^{2+}-currents upon a train of 10-ms long depolarization steps, normalized to the amplitude of the first pulse. (B) Ca^{2+}-current-voltage relationships show slightly reduced amplitudes in the IHCs of the *Cabp1/2*-DKO animals and WT. [Data acquired by David Oestreicher]

Ca^{2+} currents were greatly reduced upon application of short train stimuli (Fig. 7 A). Short stimuli at different potentials revealed maximal Ca^{2+}-current amplitudes in the IHCs of DKO mice to be comparable to controls (Fig. 7 B). Immunolabeling of the organs of Corti indicated normal presynaptic $Ca_V1.3$ clustering with no apparent change in size or shape of the clusters (Fig. 6 B), and comparable abundance of ribbon synapses in the apical IHCs of WT and DKO animals (12.9 ± 0.2 vs 12.8 ± 0.8; respectively) at 3 weeks of age. Using transgenic expression of WT Cabp2, they could partially restore the "non-inactivating" nature of the IHC $Ca_V1.3$ channels in the

Cabp1/2- DKOs ($p < 0.0001$, Student's t-test). The speed of recovery from $Ca_V1.3$ inactivation was probed using an initial 5-ms long pulse followed by a conditioning stimulus and a series of 5-ms long pulses to test the kinetics of recovery of the Ca^{2+}-current amplitude (Fig. 8).

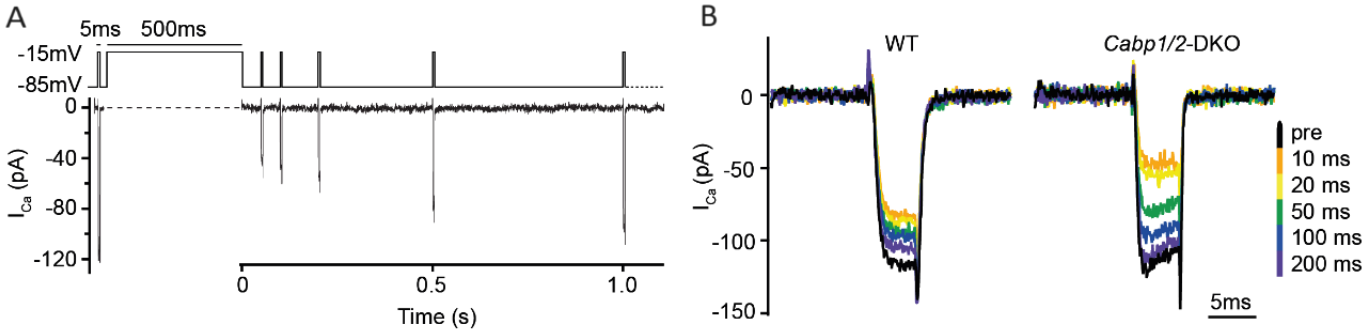

Figure 8: Recovery of Ca^{2+} currents in *Cabp1/2*-DKO IHCs

Ca^{2+} currents measurements by 5-ms long depolarization steps to the maximum current potential, followed by a 500-ms depolarization step or a 120-s long sine wave conditioning stimulus. Ca^{2+} currents were then tested at various time points to assess the recovery of Ca^{2+}-current amplitudes. (A) Example Ca^{2+}-current recording using a 500-ms long depolarization step as a conditioning stimulus. (B) Example Ca^{2+}-current traces in WT and *Cabp1/2*-deficient IHCs after a 500-ms long conditioning stimulus measured at different time points. [Data acquired by David Oestreicher]

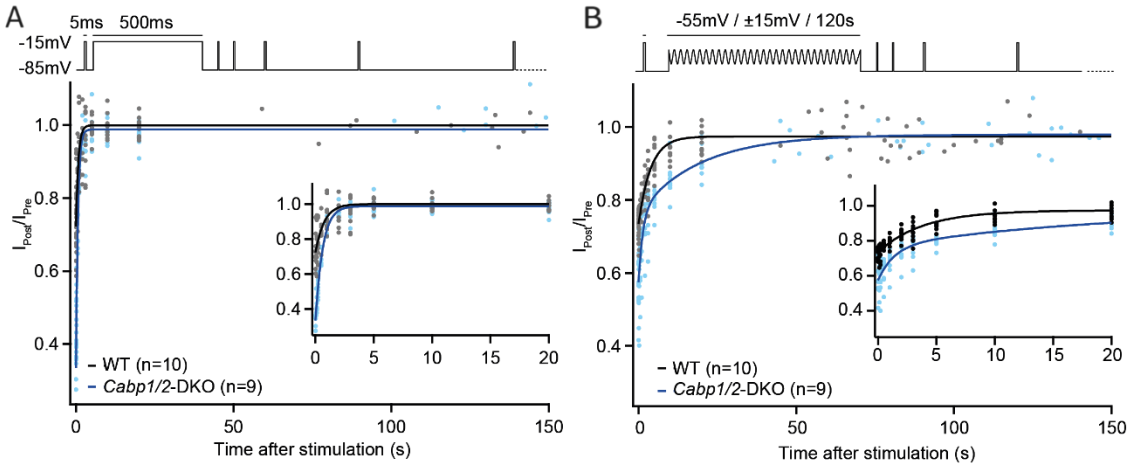

Figure 9: recovery of Ca^{2+}-currents in *Cabp1/2*-DKO IHCs

Ca^{2+}-current amplitudes normalized to the amplitude of the pre-conditioning test pulse up to 150 sec after either a 500-ms depolarization step (A) or a 2-min long sine wave stimulus (B). The initial 20 s after the conditioning stimulus are shown in the insert plots. The data were fitted by a single or double exponential function. [Data acquired by David Oestreicher]

In response to a 500-ms depolarization step (Fig. 9 A), the speed of recovery from inactivation was fast both in DKO as well as WT IHCs where a much smaller fraction of channels underwent inactivation (time constants of 0.62 and 0.75 second in DKO and WT IHCs, respectively). A 2-min long sine wave (± 15 mV) from -55 mV to mimic a milder but prolonged hair cell stimulation (Fig. 9 B) elicited smaller inactivation of $Ca_V1.3$ channels as compared to a 500-ms depolarization step. For this sine stimulation, the recovery from inactivation was slowest in the DKO IHCs (time constants of 1.36 and 3.83 s in DKO and WT IHCs, respectively). This suggests the tendency of significant fraction of $Ca_V1.3$ channels to go into "deep-state" of inactivation with very slow recovery in the absence of Cabp 1 and 2 in response to a mild but prolonged stimulation of IHCs, as was described for Na_V, K_V and Ca_V channels (Bezanilla et al. 1982, Payandeh et al. 2012, Olcese at al. 1997, Ferreira et al. 2003), thus limiting efficient sound encoding.

To further probe the nature of the enhanced $Ca_V1.3$ inactivation, David Oestreicher also recorded $Ca_V1.3$ currents in the presence of extracellular concentration of 2 mM Ca^{2+} or Ba^{2+} (Fig. 10 A), and analyzed the two types of inactivation as previously described in Tadross et al. 2010. The lack of Cabp1 and 2 significantly enhanced both, VDI and CDI of IHC $Ca_V1.3$ channels, those being approx. two- and six-times larger than those in WT IHCs (Fig. 10 B; VDI: 0.30 ± 0.02 vs 0.13 ± 0.02 and CDI: 0.65 ± 0.01 vs 0.11 ± 0.02 in *Cabp1/2* DKO and WT IHCs, respectively; $p < 0.0001$, Student's t-test).

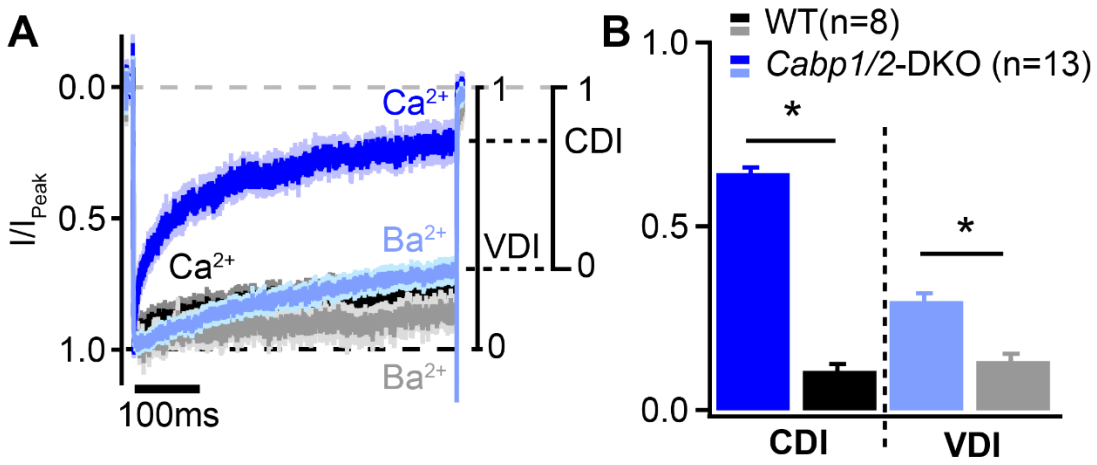

Figure 10: Voltage- and Ca^{2+} -dependent inactivation are enhanced after deletion of Cabp1 and Cabp2.

Peak normalized Ca^{2+}- and Ba^{2+} currents in WT and *Cabp1/2*-deficient IHCs recorded in the extracellular solution containing 2 mM of the respective divalent cation. (B) VDI and CDI were both significantly enhanced in the IHCs of *Cabp1/2*-DKO animals (asterisks; Student's t-test, $p < 0.0001$).

1.2.4 The *Otof* TDA mutant

One important example of genetic auditory synaptopathies (review in Moser et al. 2006; Santarelli et al. 2015; Moser & Starr, 2016), is DFNB9, caused by mutations in the *OTOF* gene. It encodes otoferlin, a hair cell-specific tail-anchored (Vogl et al. 2016) multi-domain protein (Roux et al. 2006), which belongs to the ferlin protein family

mainly involved in membrane trafficking and repair (review in Lek et al. 2012; McNeil & Kirchhausen, 2005; Pangršič et al. 2012). Otoferlin has broad distribution within IHCs (Roux et al. 2006; Pangršič et al. 2010; Revelo et al. 2014; Strenzke et al. 2016), supporting its presynaptic function in the basolateral IHC pole region and its role in constitutive, non-synaptic membrane trafficking (Revelo et al. 2014). Close to 90 pathogenic mutations of OTOF have been reported till date; the majority of these mutations result in DFNB9- type hearing impairment by causing inactivation of otoferlin (Santarelli et al. 2015). Ca^{2+}-triggered exocytosis is nearly abolished in IHCs of Otoferlin knock-out mice (Pangršič et al. 2010, Roux et al. 2006) while synaptic vesicles were found close to the active zone membrane, suggesting that a late step of exocytosis was disrupted without an absence of vesicles limiting signal transduction (Roux et al. 2006). Along with roles in Ca^{2+} and phospholipid binding it is hypothesized that otoferlin serves as a Ca^{2+} sensor in hair cell exocytosis, similar to synaptotagmins 1 and 2 in conventional synapses.

More roles for otoferlin have been suggested in Ca^{2+} dependent vesicle replenishment (Pangršič et al. 2010; Strenzke et al. 2016; Vogl et al. 2016; Tertrais et al. 2019; Michalski et al. 2017) and acting as a Ca^{2+} sensor of SV fusion (Roux et al. 2006; Johnson & Chapman, 2010; Michalski et al. 2017). Synaptic vesicles could also be primed for fusion by otoferlin, potentially via promoting short tether formation between synaptic vesicles and the AZ membrane (Vogl et al. 2015). Another functional implication is in mediating exocytosis-endocytosis coupling (Jung et al. 2015; Kroll et al. 2019, 2020; Tertrais et al. 2019). To dissect the function of otoferlin we focused on the potential Ca^{2+} binding region of the C2E domain of the protein. It likely involves the highly conserved aspartates D1508, D1514, D1563, D1565, and D1570/D1571 out of which 3 were targeted for alanine substitution by CRISPR/Cas9 genome-editing thus generating homozygous OtofD1563/1565/1570A mice abbreviated as OtofTDA/TDA, for "triple D (aspartate) to A (alanine)".

1.3 Objective measures of auditory function

To assess the function of the auditory system different techniques are used of which Auditory Brainstem Response (ABR) and DPOAE (Distortion Product Otoacoustic Emission) are tools of choice. These techniques are noninvasive and can be performed in a time-intensive way without extensive preparation for the procedure. Both techniques are standard measures in the clinical setting and thus allow for a direct comparison between human patients and mouse models. In contrast, the single unit recordings used in this project are a highly invasive procedure and cannot be obtained from patients. They can be instrumental for the interpretation of abnormal ABRs, as they allow to differentiate between reductions in spike rate and impairments of temporal precision.

1.3.1 Auditory Brainstem Response

ABR is a type of Auditory Evoked Potential (AEP) that captures the electrical potentials occurring at various levels of the auditory system. AEPs can be classified according to the latency into short, middle or long latency-type recorded at about <10, 10 to 50 and >50ms respectively. The latency corresponds to a level of auditory system and the group of neurons responsible for the particular response. AEPs can also be classified on the basis of distance of the point of recording from the origin of the activity into near-field and far-field potentials. Near-

field potentials are recorded directly from a nerve or nucleus while far-field potentials such as the potentials in ABR are recorded at a distance from the active neural structures. Near-field potentials are large in amplitude being limited to capturing the activity of only one structure while low amplitude far-field potentials measure the contributions from many neural structures and even muscles. Examples of near-field potentials include those encountered in recordings from the auditory nerve and the cochlear nucleus.

Strong far-field potentials can be obtained from a nucleus whose dendrites are organized uniformly and are known to have open field potentials. Nuclei with dendrites organized randomly in all directions generate weak far-field potential known as closed field (Lorente de No, 1947). Short latency responses constitute electrocochleogram (ECochG) and ABR while the sources of long latency responses are Cortical regions. ABR is visualized as a group of five waves (peaks I to V) seen as alternating potentials in positive and negative directions. ABR activity originates from the brainstem as well as peripheral locations. A peripherally evoked potential such as ECochG is composed of Summating Potential (SP) which originates from cochlear hair cells, and Compound Action Potential (CAP) originating from the auditory nerve. These peripherally evoked potentials form the early component of the ABR. The neuronal generators of different ABR peaks are listed below (Melcher et al. 1996). Wave I is generated solely by the auditory nerve (AN), whereas waves II–V have contributions from multiple anatomical structures. Wave II is mainly generated by the cochlear nucleus (CN), wave III by the superior olivary complex (SOC), wave IV by the lateral lemniscus (LL), and wave V by the inferior colliculus (IC) (Ruttiger et al. 2017)(Table 3).

Table 3: Generator cells of specific ABR peaks

Peak	Generator
I	Spiral Ganglion cells
II	Globular bushy cells of posterior Anteroventral Cochlear Nucleus (AVCN)
III	Spherical bushy cells of anterior AVCN, cells of the contralateral medial nucleus of the trapezoid body
IV	principal cells of the ipsilateral and contralateral medial superior olivary nuclei
V	nuclei of the lateral lemniscus and inferior colliculus

The ABR setup is designed to extract evoked activity from the background of spontaneous activity. Amplitudes of ABR are typically less than 0.5 μV, much smaller than the ongoing spontaneous activity of the brain. The instrumentation is simple and consists of stainless-steel needle electrodes placed at the vertex of the mouse and the mastoid, plus a common a ground electrode placed on the back of the mouse. The difference potential between the vertex and the mastoid is amplified and bandpass-filtered. Acoustic stimuli such as

broadband clicks or tone bursts are used. An averaged waveform is obtained by acquiring responses from repeated stimuli. Measures such as threshold, morphology of the waveform, peak amplitude, latency, inter-peak latency are used in the analysis. Studies use ABR to probe the mouse auditory system by characterizing strains, mutants and hearing loss caused by various factors such as aging, noise-induced hearing loss and ototoxicity.

The amplitude of ABR decreases with decreasing stimulus intensity, while the peak latencies increase. With decreasing stimulus intensity, the amplitude of early peaks (I, II, III) decreases more than peak V, rendering only peak V discernible at low intensities. The amplitude of sharp peaks in far-field potentials depends on the degree of synchronicity of the neural activity of the generator (nerve, fiber tracts, nuclei). ABR is widely used to study the effect of insult or injury to the auditory nerve. Lesions in the auditory nerve are a common cause of auditory nerve disorders. A high degree of temporal coherence is maintained in the nerve fibres reaching the cochlear nucleus by restricting the variability of conduction velocity of the fibres. Temporal coherence may be important for normal speech discrimination and the reduced speech discrimination typical to injuries of the auditory nerve can be attributed to impaired temporal coherence. Injuries cause a reduction in conduction velocity of nerve fibres leading to impaired temporal coherence. An injury of the intracranial portion of the auditory nerve leads to increase in latency of all peaks except peak I, which is generated by the most peripheral portion of the auditory nerve. In individuals whose auditory nerve is injured, peaks II and III of the ABR are missing while only peak I and V are discernible.

Features of ABRs are widely used to infer the functional status of auditory system. ABR wave I to IV were found to have increased latency in mutant mice lacking βIVΣ1 spectrin which could be a result of delay in generation of action potentials by spiral ganglion neurons and/or impaired conduction along the auditory pathway (Lacas-Gervais et al. 2004). In mutant mice lacking myelin components proteolipid protein (PLP) and glycoprotein M6B, ABR waves II to V were significantly delayed as a result of hypomyelination (Werner 2013). ABR wave I to V interval may be used for monitoring disease progression in paediatric Charcot Marie Tooth disease (Giuliani et al. 2019). ABR wave amplitudes also show differences as seen in the myelin deficient shiverer mutant mice with decreased wave II and III amplitudes with an increased amplitude of waves IV and V (Moore et al. 2019). A flat ABR wave as seen in patients with Friedreich's ataxia signals an absence of neural synchrony in the auditory pathway (Giraudet et al. 2018).

1.3.2 Distortion Product Otoacoustic Emissions (DPOAE)

OHCs are electromotile active elements of the cochlea that act as 'motors' reducing the dampening of basilar membrane motion. This increases the vibration amplitude of the basilar membrane for low sound intensities by approximately 50dB and enhances its frequency selectivity. The cochlea generates low-intensity sounds that are conducted backwards through the ossicular apparatus to the tympanic membrane setting it in motion. These sounds can be picked up by a sensitive microphone placed in the auditory canal. This is known as Otoacoustic Emission (OAE). There are several kinds of OAEs- a) TEOAE (Transient Evoked Otoacoustic Emission) elicited by a transient sound and generated as a result of reflection of traveling wave on basilar membrane. b) SOAE (Spontaneous Otoacoustic Emission) is a sustained sound generated spontaneously without applying any sound to the ear. c) DPOAE (Distortion Product Otoacoustic Emission) is a measure of non-linear distortion in the

cochlea obtained by applying two tones to the ear and measuring the amplitude of a difference tone generated as a result.

When two pure tones (primaries) of slightly different frequencies f1 and f2 (f2/f1=1.2) are applied to the ear, new frequency components not present in the input can be recorded in the ear canal with its largest component occurring at frequency 2f1-f2. The primaries non linearly interact within the cochlea giving rise to the DPOAE. There are two sources of DPOAE, the primary frequency place (nonlinear distortion emission) and other at the distortion frequency plane (reflection emission) (Kim et al. 1980). The relative contribution of these two components varies depending upon the stimulus conditions (Shera & Guinan, 1999, Knight & Kemp, 2000). DPOAE amplitude is influenced by the primary tone level separation, which is kept about 10 to 15 dB (L1 > L2) for the largest amplitude in adult humans (Abdala 1996).

2 Methods

2.1 Mouse line generation

The *Atp11A-PvCre* mouse line was derived from conditional ready knockout reporter strain *Atp11A*$^{tm1a(KOMP)Wtsi}$ (ATPase, class VI, type 11A; targeted mutation 1a) from the Wellcome Trust Sanger Institute (ESC clone ID EPD0111_4_B04). More information about the strain is available here: https://www.informatics.jax.org/allele/MGI:4363953. This genetic construct initially leads to any of the wildtype, heterozygous or knockout mice with the heterozygous and KO expressing the LACZ reporter. We and others observed that knockout mice were never born which is explained probably due to placental insufficiency (Ochiai et al. 2022). We chose the heterozygous mice to initially test for hearing phenotype, because the patients with the *ATP11A* mutations have an autosomal dominant inheritance pattern. We found that haploinsufficiency would induce the ABR phenotype, but it did not. We cross-bred the heterozygous line with ROSA-FLIP mice leading to removal of DNA fragment between the FRT sites followed by further breeding with the Parvalbumin-Cre-mice thus using the two flox sites to create a conditional KO mouse line lacking Atp11a in Parvalbumin-expressing cells (*Atp11a*$^{fl/fl}$ Cre+, abbreviated as cKO mice in this study). *Atp11a fl/fl* Cre- littermates were used as controls.

2.2 Immunohistochemistry

Apical turns of organs of Corti from C57Bl/6 mice at 24 weeks were locally fixed in 4% formaldehyde in PBS (for 15 minutes). After incubation in 1× goat serum dilution buffer for 1 h at 4◦C, samples were incubated with primary antibodies with mouse polyclonal CtBP2 (1:50 dilution, Catalog No. 612044, BD Bioscience), chicken Homer1 (1:50 dilution, Synaptic Systems #160006), rabbit ATP11A (1:50 dilution, Biomol (US Biological) # 146698) overnight at 4◦C. Samples were then washed 3× and were incubated with appropriate secondary antibodies (goat anti-chicken 488 and goat anti-mouse 568, 1:200 dilution, Invitrogen) for 1 h at room temperature and were washed 4×, mounted and imaged using a SP5 confocal microscope (Leica, Germany) with a 63× objective.

Co-localization of ribbon and post-synapse puncta marked by CtBP2 and Homer respectively were manually ascertained by presence of closely spaced individually marked ribbon and post-synapse spots using ImageJ and Imaris software.

2.3 ABR and DPOAE

Animals were anesthetized intraperitoneally with a combination of ketamine (125 mg/kg) and xylazine (2.5 mg/kg) while the heart rate was constantly monitored to control the depth of anaesthesia by administering additional doses as needed. The core body temperature was maintained constant at 37°C using a rectal temperature-controlled heating blanket (Hugo Sachs Elektronik; Harvard Apparatus). For the purpose of stimulus

generation, presentation, and data acquisition the TDT System II (Tucker-Davis Technologies) run by BioSig32 software (TDT) was used. Sound pressure levels are provided in two ways: in dB SPL RMS for tonal stimuli and dB SPL peak equivalent (PE) for clicks and the sound calibration was done using a 1⁄4 "microphone (D 4039, Brüel & Kjær GmbH). Tone bursts (12 kHz, 10 ms plateau, 1 ms cos 2 rise/fall) or clicks of 0.03 ms duration were presented at 20 Hz or 100 Hz in a sound-proof free field setup ipsilaterally using a JBL 2402 speaker (JBL GmbH & Co.) for sound input. Subdermal needles were placed on the vertex and mastoid and the difference potential between them was amplified (50,000-fold), filtered (low pass: 4 kHz, high pass: 400 Hz) and sampled at a rate of 50 kHz for 20 ms, 2 X 2000 times to obtain two mean auditory brainstem responses (ABRs) per sound intensity. Hearing threshold was determined using visual inspection as the lowest stimulus intensity that evoked a reproducible response waveform in both recorded traces with 10 dB precision. For distortion product otoacoustic emissions, we used an ED1/EC1 speaker system (Tucker-Davis) to generate the two primary tones (frequency ratio f2/f1: 1.2, intensity f2 = intensity f1 + 10 dB). For the coupling of primary tones into the ear canal, a custom-made probe containing an MKE-2 microphone (Sennheiser) was used and adjusted to the desired sound intensities at the position of the eardrum. The microphone signal was amplified and digitized (DMX 6 Fire; Terratec) and then analysed by fast Fourier transformation (MATLAB, MathWorks).

2.4 Single-Unit Electrophysiology

The mouse lines *Atp11a-Pv-Cre* (AUNA2 auditory neuropathy), *Cabp1-Cabp2* (Calcium Binding protein) double knock-out and *Otof*$^{TDA/TDA}$ (Otoferlin point mutant) are used for single-unit electrophysiology experiments. In these experiments, the cochlear portion of the VIII cranial nerve is accessed through the use of sharp pipette electrodes. The glass pipettes are pulled using an electrode puller machine (Sutter Instruments) resulting in sharp pipettes with a clearly formed tip. For the recording, a silver chloride coated silver electrode is inserted in the formed glass pipette filled with a solution of saline and the dye Methylene blue. In preparation for the experiment, it is ensured that the mouse has not undergone any other invasive experiment in the past week for suitability in the experiment. After a few minutes of habituation in the experimental room, the mouse is injected with a mixture of Urethane 1.32g/kg and Xylazine 5mg/kg (mixed together in single dose) and Buprenorphine 0.1mg/kg (every 4 hours) intraperitoneally adjusted according to its weight supplemented by 0.25 ml Sterofundin G5 solution (containing glucose) subcutaneously every hour. The onset of anaesthesia is confirmed by the observation of mouse stopping to move and when the toe-pinch reflex is absent. The mouse is then shifted for surgical procedure and next experiments to the sound-proof room designed to prevent outside sound from entering. The mouse is oriented on its dorsal surface flat on the ground and an incision is made at the throat to perform tracheostomy. Using a fine forceps the trachea is held and the surrounding tissue is teased away while making it prominent by slight elevation using a bent forceps directed below the trachea. While applying mild pressure from below the trachea, a fine incision is made on the ventral side of the trachea immediately posterior to the cricoid cartilage creating an opening. Fine paper tips are used to clean the trachea towards the posterior direction a few times to remove excess fluid while making sure not to venture deep towards the lungs. A hollow plastic tube with a 'V'-shaped cut is carefully inserted into the posterior trachea such that it fits tightly in the tracheal space. Once the

tube is in place, a fine cotton thread is tied around the trachea-tube region to secure the tube in place. The mouse now has a clear breathing way making the mouth and nose region accessible.

After the tracheostomy, the mouse is carefully inverted with its ventral side facing down. Using sharp scissors, the ear pinnae of both the ears are carefully clipped such that the skin of the ear canal attached to the head is retained as a marker for position of ear canal. A head holder that fits on to the snout is placed by directing the tongue out and putting the holder into the mouth. The holder fits onto the experimental platform such that the shoulders of the mouse are held raised and the posterior part is resting on the floor. This position ensures that the ear is accessible for projection of sound onto it. Two metal bars originating from top of raised bars placed equally away from each ear are used to accurately position the head in lateral directions by using the visible ear canals to orient. Once the mouse is held in place as explained, a hole is made into the cranium to make way for the recording electrode under the view of a stereo microscope. After removing the skin over the cranium, the posterior musculature connecting to the upper neck is carefully removed. Using a sharp rongeur chip away the cranial bone on the ipsilateral side of sound incidence directly above the ear canal to maintain proximity with the auditory nerve. After exposing about a quarter of ipsilateral half of the cranium, the visible portion of the brain comprising the cerebellum is pneumatically removed using a pump till the point the bony ridge is visible which corresponds to a position conducive to accessing the VIII cranial nerve. At this point, the glass electrode is positioned and the tip of the electrode is used to direct the electrode to the suitable recording position. Here, presence of Methylene blue in the saline solution used for filling glass pipettes leads to better visibility of the electrode tip.

The tip of the electrode is placed next to the dark spot, a region of dark pigmentation on the posterior half of the bony ridge which is useful for orientation. After placing the electrode at its starting point, it is then stereotactically oriented to a goldilocks zone ideal for intercepting the auditory nerve determined from many similar experiments which is 30 μm lateral and 30 μm posterior to the starting point. After each attempt of advancing the electrode through into the brain towards the auditory nerve is completed during recordings, the electrode is retracted and a novel position is sought. Generally, a position within the radius of 15-20 μm is chosen and the electrode is used again while maintaining the electrode impedance of approximately 30 MΩ. If the tip of the electrode breaks as signalled by very low impedance a new recording position is again sought by using the dark spot as a reference being careful of not entering the previously explored area. The reference electrode is placed in a pocket of skin flaps near the neck on the contralateral side of sound incidence. The pocket is irrigated with Saline and regularly checked for intactness. To balance for the blood-loss during surgery, Sterofundin solution is administered in the aforementioned dosage throughout the experiment.

To record from the auditory nerve, the electrode tip is manoeuvred proximal to the active neurons to obtain juxtacellular signals while the ear is receiving sound stimulus from a speaker. A custom-written MATLAB code is used to visualise the electric potentials as read through the electrode. The speaker is placed 30 cm away from the ear so as to align the centre of speaker with that of the ear canal. Using the speaker, a high intensity sound stimulus in the range of 70-80 dB is incident upon the ear so as to activate the majority of SGNs thus making it statistically favourable to encounter them while the electrode is traversing the bulk of the nerve. Using the manipulator, the electrode is advanced rapidly for approximately 1000μm after which a step size of 3-5 μm is used to slowly advance the electrode while simultaneously visualising the potential of the electrode. The signal from the electrode is also

converted into sound output via an output speaker to amplify the activity encountered at the electrode and conspicuously knowing the presence of spiking activity which are heard as sharp sounds.

A standard stimulus of 5 Hz inter-stimulus frequency and 50 ms stimulus duration is used with either noise bursts consisting of a spread of frequencies ideal for activating neurons across the frequency-range or a tone burst sound stimulus consisting of a single frequency to activate a small subset of neurons. For locating the sound-responsive neurons and finding the primary auditory neurons, a standard noise burst stimulus is used. If a neuron with auditory activity corresponding to sound-following response of spikes is encountered, its spontaneous activity is recorded by recording the neuronal output during a silent period. Following which a tuning curve is obtained composed of the response of the neuronal unit to an array of frequency-intensity combinations resulting in a stereotypic pattern with a prominent minima corresponding to a frequency with the lowest threshold of activity known as the Characteristic Frequency (CF). Once the CF is determined a Post-Stimulus Time Histogram (PSTH) is generated at sound stimulus set to intensity 30dB above the threshold at CF by recording the spiking activity following the sound stimulus repeatedly for 50-100 times and superimposing this activity from multiple trials. The shape of the PST is stereotypic with a high onset rate followed by lowering of the rate over time saturating to a lower adapted rate characteristic of primary auditory neurons. Other neuron types encountered apart from primary neurons consist of Primary-like with Notch, Chopper and Onset populating the Antero-Ventral Cochlear Nucleus (AVCN). The primary-like with notch neurons can be identified with a short negatively pointing notch after the peak onset while the chopper neurons which have a highly regular response pattern as visible in the PSTH with spike Covariance below 0.4 for this type. The chopper neurons are also highly synchronised with sound onset making them possible to distinguish from the primary neurons by hearing their characteristic sound through the output speaker. The onset neurons consist of a PSTH with a single onset peak activity and no following activity.

Once the unit is identified through the PSTH the neuron can be tested for custom paradigms such as forward masking, rate level sweep or a PSTH for a custom sound stimulus with a different stimulus frequency and length. For the forward masking the activity of the neuron is recorded for the signal sound in presence of a preceding 'masker' sound and the extent of masking or suppression in activity owing to the masker is assessed. For the rate level sweep the response of the unit for increasing stimulus intensities at CF is measured. The response to a custom stimulus with a defined interstimulus frequency and duration can be used to test the neuron for its response to stimulus with a non-standard inter stimulus interval between the sounds and a higher/lower duration of the stimulus. A higher duration is ideal to visualise the response to continuous sound stimulus while a stimulus with varying inter-stimulus interval is suitable for experiments focusing on questions of ability of the neurons to faithfully follow continuous bursts of discrete sound pulses.

To assess recovery from adaptation, we used a forward masking paradigm (Harris & Dallos, 1979; Spassova et al. 2004) in which a 100 ms masking stimulus was separated from a 15 ms probe stimulus by a variable silent interval of 4, 16, 64 and 256 ms (Frank et al. 2010).

Neural synchrony was assessed using transposed tones (Bernstein & Trahiotis, 2002), consisting of a carrier tone at the fibre's CF that was amplitude modulated by a half-wave-rectified sinusoid of 0.5 kHz. The level of this modulated tone was varied in 5 dB steps, from 30 below threshold to 50 dB SPL above threshold. The synchronization index (SI) for spike times at each modulation frequency and level was defined as the average of a

vector sum, where t_i is the time of the i^{th} spike in a train of n spikes, and ω is the angular frequency of the modulator (Buran et al. 2010):

$$SI = \frac{\left\| \sum_{i=1}^{n} e^{-j\omega t} \right\|}{n}$$

2.5 Analysis of neuronal activity data

Custom-written MATLAB codes are used for processing the data starting from filtering of spikes to analysing the trends of the data. To filter the spikes from noise, a GUI based program is used consisting of a dual filter level that filters-in spikes that are have higher amplitude than a manually set threshold level and simultaneously filters-out spikes that are close to the noise level. Among the spikes considered high and conspicuous enough it is checked that the spikes form a group distinct from the filtered out low amplitude spike group. If both the groups are overlapping then the filtering is assumed to have been unsuccessful in separating the spikes into two groups- the spike and non-spike groups. The process of filtering is iteratively repeated by choosing another suitable filtering level that distributes the spikes into distinct 'in' and 'out' groups. The performance of the filtering program is manually rated for each recording and only the highly rated runs are used for analysis. In addition to filtering real spikes from noise, the raw data is filtered for any interfering artefacts such as those from other electronic devices nearby. The identity of each of the neuronal units is assigned by considering the PSTH, tuning curves and other associated data. The identification is performed by two independent experimenters to reduce experimenter bias.

Quantifications from the filtered recording data are stored in a Microsoft Access database and SQL-based commands are used to interface with the database. A useful analysis to assess the coding ability of the neurons is the jitter of the first spike as a readout of the ability of the neuron to fire at similar intervals after the onset of sound. The first-spike latency is calculated as the delay in appearance of the first spike in the neuron after the onset of sound. The variance of first-spike latency is then considered as the jitter of neuronal spiking response. For the units undergoing adaptation, the kinetics of the adaptation are quantified by fitting a single exponential to the PSTH response to the 50 ms tone burst presented at 5 Hz and the time constant of adaptation (τ) is determined.

A transient artificial signal composed of closely spaced positive and negative potentials that are close in appearance to the real action potentials was observed in about 10% of the single-unit recordings due to interference from the electronic setup. A standalone MATLAB routine was used to mark these transient disturbances by making use of the peculiarities of transient signal as seen in a fixed distance in time between the positive and negative potentials and the difference in waveforms between transient waveform and the waveforms exhibited by action potentials. After removal of transients, the empty time space generated was replaced by the native noise floor to keep the signal properties constant.

2.6 Plotting and statistical tests

The box plots were generated by MATLAB. The central mark on each box indicates the median, and the top and bottom edges of the box indicate the 75th and 25th percentiles, respectively. The whiskers extend to the most extreme data points that are not considered outliers, and the outliers are plotted individually using the '+' marker symbol. For the statistical testing to compare means of two vectors, Jarque Bera test was used to determine whether each of the vectors has a normal distribution. If the test rejects the null hypothesis within the p value less than 0.05, the vector is determined to have non-normal distribution. Then a non-parametric test such as Mann-Whitney U test is used. However, if both of the vectors are normally distributed, Student's t test is used for determining the statistical significance of the mean comparison of the two vectors. A p-value below 0.05 was considered significant.

3 Results

3.1 Calcium binding proteins 1 and 2

An initial assessment of hearing function was performed using non-invasive ABR and DPOAE recordings , (Fig. 11 A, B, Fig. 12 A, B). David Oestreicher performed these recordings in young mice aged 3-4 weeks, I performed them in young adult mice. *Cabp1/2*-DKO animals showed ABR thresholds that were highly elevated. Tone bursts stimulus up to a maximum intensity of 90 dB barely elicited any ABR response. Click responses were better preserved but greatly reduced in amplitude. ABR wave I, reflecting synchronous spiking of SGNs, was greatly reduced in size in the younger mice and not measurable in the older mice (Fig. 11 B). Later ABR peaks were better preserved as observed in other mouse mutants with defects in the IHC synapse (Khimich et al. 2005, Strenzke et al. 2016), indicating a partial preservation of neuronal activation of the auditory brainstem.

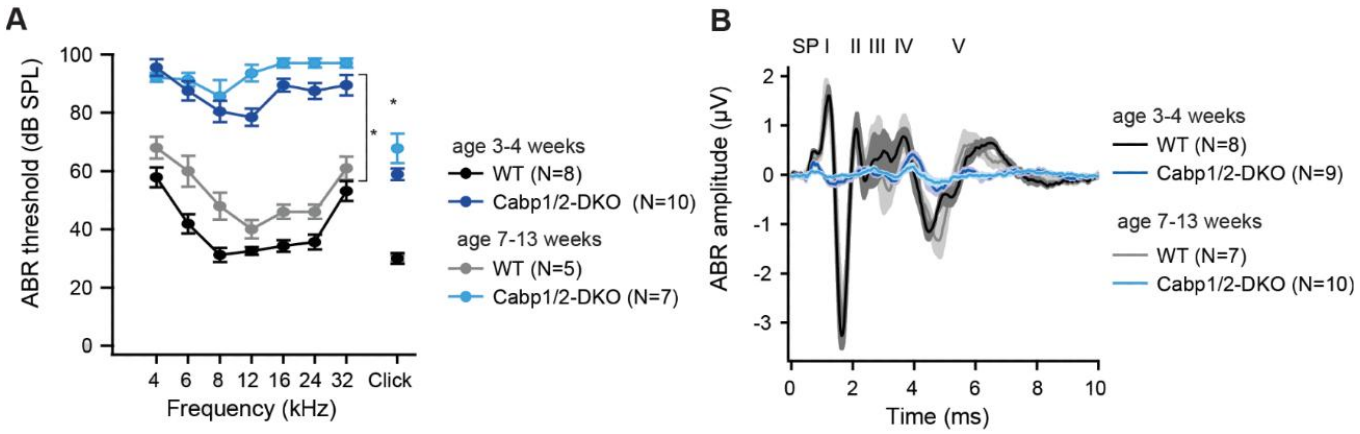

Figure 11: Impaired auditory brainstem responses in *Cabp1/2* DKO mice

(A) ABR thresholds to tone burst and click stimulation show an age-progressive pantonal severe hearing impairment in *Cabp1/2*-DKO mice (asterisks: 2 way ANOVA for tone burst, Student's t-tests for click thresholds; $p \leq 0.0001$). When thresholds exceeded 90 dB for the tone burst stimulation, they were assigned a value of 100 dB for calculation of the mean and SEM. (B) Grand averages of ABR waveforms to 80-dB click stimuli presented at a rate of 20 Hz show a strong decrease in ABR amplitudes in *Cabp1/2*- DKO mice at 3-4 weeks of age. At age 7- 13 weeks there are only minimal responses remaining, which are dominated by a delayed wave IV. The ABR wave peaks are labeled by roman numbers. Wave I is preceded by the summating potential (SP) [co-performed along with David Oestreicher].

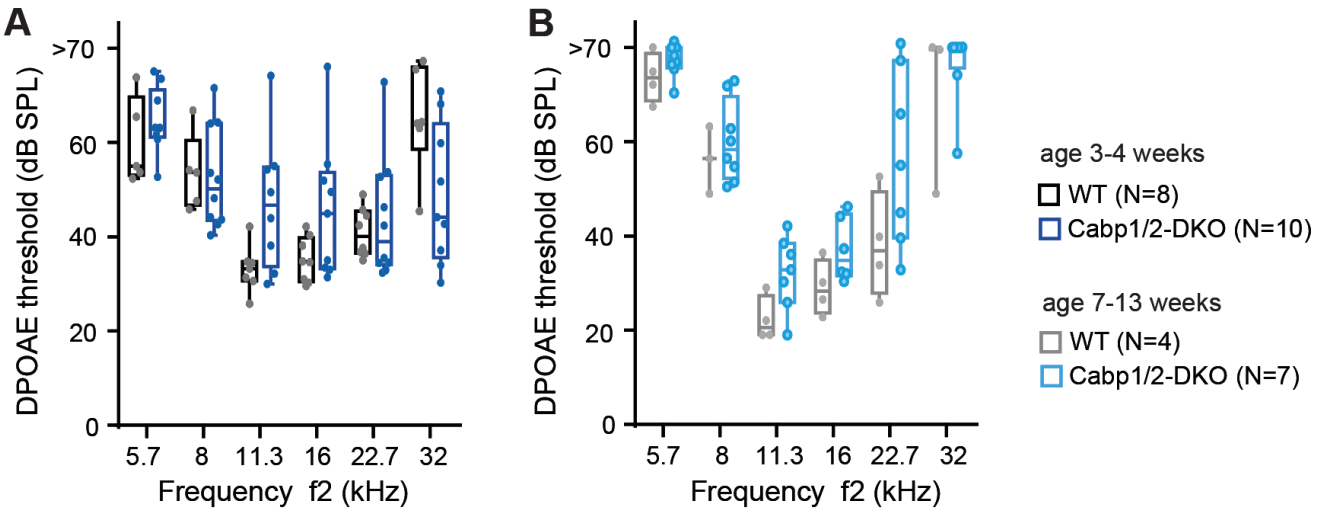

Figure 12: DPOAE thresholds measurements for *Cabp1/2*-DKO mice.

An increase in DPOAE thresholds was observed in some *Cabp1/2*-DKO mice, and was significant at the age of 7-13 weeks ($p < 0.002$, 2-way ANOVA). However, note that even at 7-13 weeks of age some *Cabp1/2*-DKO mutants retained normal DPOAE thresholds.[co-performed along with David Oestreicher]

To assess active cochlear amplification efficacy by the outer hair cells (OHCs), we recorded distortion product otoacoustic emissions (DPOAEs). In human DFNB93 patients, OAEs were only detectable in some of the younger patients (Picher et al. 2017, Bharadwaj et al. 2014). Mouse work in Cabp2 knockout mutants corroborates this notion of at least initially intact cochlear amplification (Yang et al. 2018, Picher et al. 2017, Oestreicher et al. 2021). Our results suggest that cochlear amplification is largely preserved in DKO animals as well (Fig. 12 A, B). The DPOAEs thresholds and amplitudes were found to be normal in about half of the DKO animals in both age groups. In the other half, they were reduced in amplitude and had higher thresholds, but they were still detectable (Fig. 13 A, B). Overall, our data suggests that loss of Cabp1 and Cabp2 does not per se compromise cochlear amplification. However, there may be (likely secondary) degeneration of outer hair cells) in some mutant animals. On the basis of previous ex-vivo studies and my studies on DPOAE and ABR, it was found that DPOE was near normal and ABR was severely impaired and calcium dependent inactivation was enhanced. The ABR phenotype was a bit surprising because exocytosis was not so bad and synapse numbers were also normal, hence I chose to conduct single-unit electrophysiology recordings in the Spiral Ganglion neurons.

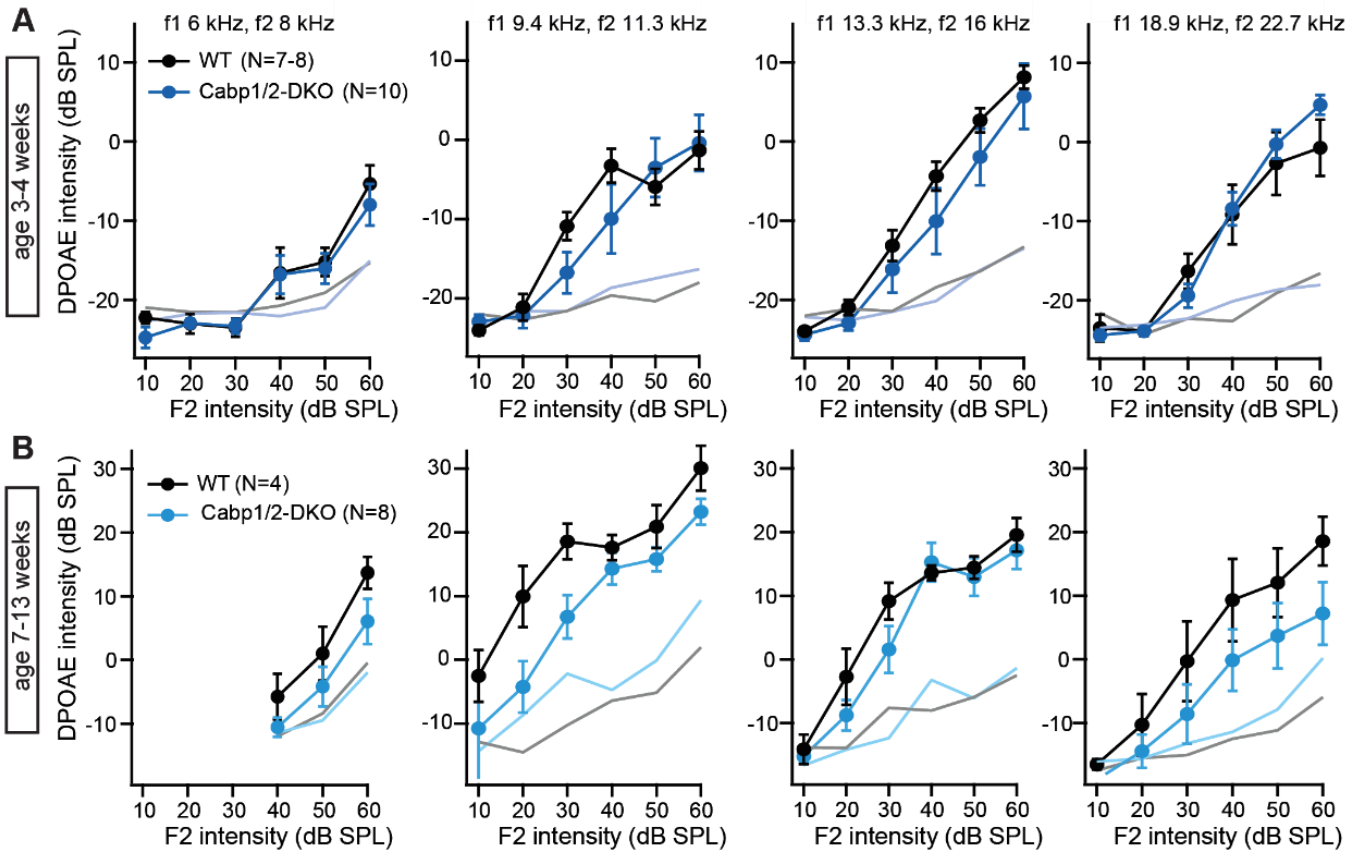

Figure 13: : DPOAE intensities in *Cabp1/2* DKO mice

DPOAE amplitude growth functions for different primary tone frequency combinations at the age of 3-4 weeks (A) and 7-13 weeks (B). The two datasets (A and B) were acquired at different experimental setups calibrated with different artificial mouse ear couplers, resulting in different absolute amplitudes. Light colored lines depict average noise floor level.

Next, I studied the properties of sound encoding by measuring sound-induced spiking responses of SGNs. A total of 39 neurons were recorded from WT mice, which were classified as SGNs based on parameters such as their location, response patterns, spike waveforms and recording stability. Their responses were well comparable to typical WT SGN data (Picher et al. 2017, Jean et al. 2018, Jing et al. 2013, Taberner et al. 2005, Vogl et al. 2017). After characterizing their spontaneous rate and frequency tuning, we tested sound-responsive neuron by assessing its response to 50 or 500 ms tone bursts at the characteristic frequency 30 dB above threshold (i.e. where the sigmoidal rate-intensity functions have saturated spike rates) using 5 Hz stimulus repetition rate. Neurons classified as SGNs exhibited a typical response pattern with a high onset firing rates and gradual adaptation to steady-state rates between100 and 400 Hz(Fig. 14 A, Fig. 16). We also observed that in the single unit recordings, the changes in onset rates and adapted rates is both significant with a drop in rates seed in mutants [Fig. 14 A]

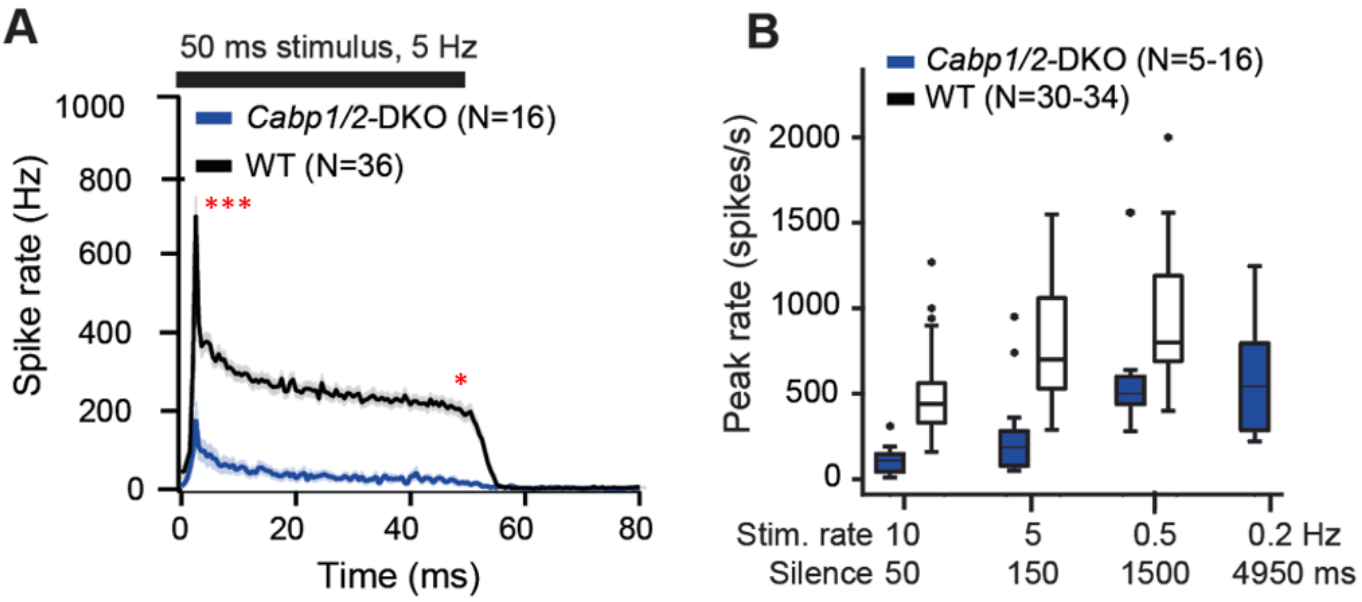

Figure 14: SGN responses in *CaBP1/2* DKO mice

WT post stimulus time histograms of SGNs to 50-ms suprathreshold tone or noise burst stimuli presented at a rate of 5 Hz showed a very high sound onset rate gradually adapting to a sustained rate persisting throughout the stimulus duration. Spike rates were much lower in the mutants. The peak rate ($p < 0.001$) and adapted rate ($p < 0.05$) are significantly lower for mutants (*, Wilcoxon rank sum test) (B) Peak rates for different stimulus rates/interstimulus intervals in WT SGNs strongly increase between 10 and 5 Hz, while in DKOs the strongest increase in peak rate is between 150 and 1500 ms of silence.

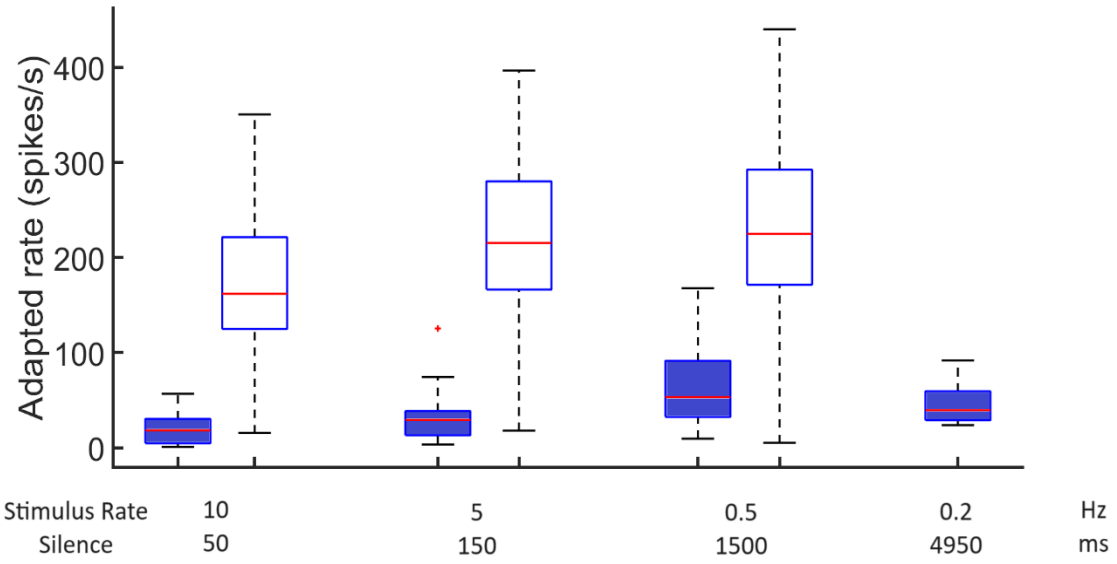

Figure 15: Adapted spike rates for different interstimulus rates

Adapted rates for different stimulus rates / interstimulus intervals follows a trend similar to that observed for peak rates with an incremental trend up to 0.5 Hz followed by a lowering in rate at 0.2 Hz for DKOs as compared to a steady increase with lowering of frequency in WT [Fig. 15].

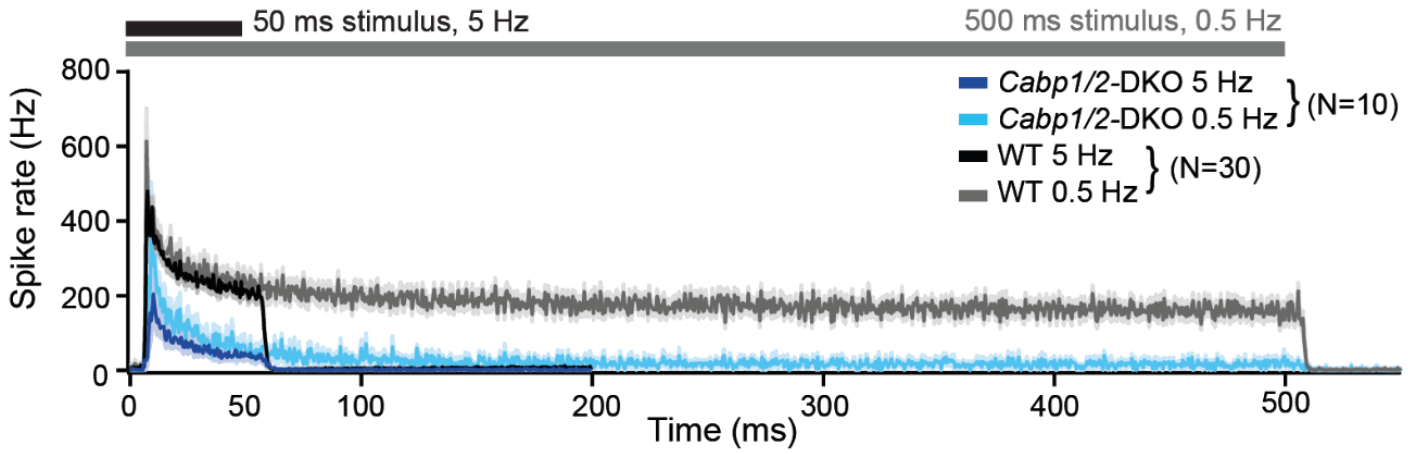

Figure 16: Strength of adaptation in DKO.

Applying a lower stimulus rate of 0.5 Hz partially restored sound onset responses in *Cabp1/2*-DKOs, highlighting the enhanced strength of adaptation. WT and mutant neurons sustained their adapted spiking response throughout the longer 500 ms stimulus used in these recordings. For direct comparison, the average 5-Hz post stimulus time histograms from the same neurons are shown.

Using the same approach in *Cabp1/2* DKO mice aged 8-14 weeks, sound-responsive neurons were extremely scarce and were only found in 4 out of 10 tested mutant animals (compared to 11 out of 12 WT animals). We assume that the sound thresholds of the primary and secondary neurons of the auditory pathway were too high for our 80-90 dB noise burst search stimulus to elicit spiking. Only one out of the 20 sound-responsive neurons we recorded and analyzed from DKO animals showed a normal response in our automated tuning curve algorithm with a 35 dB threshold at 7.8 kHz, while all others displayed thresholds above 80 dB and exhibited extremely low spike rates.

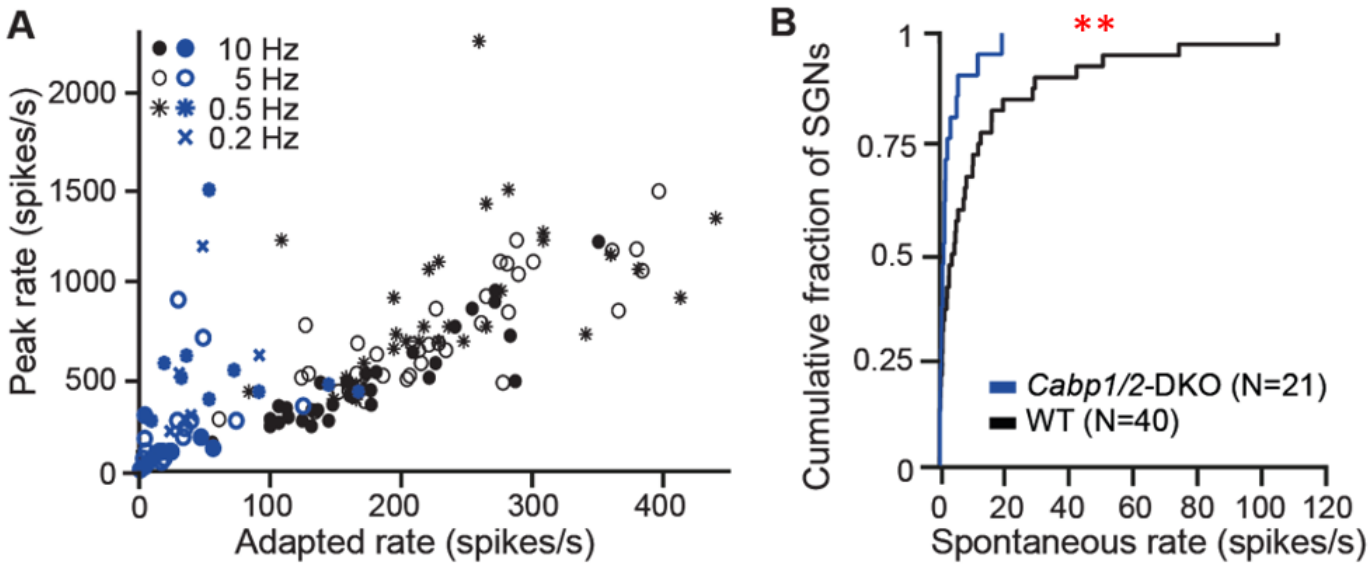

Figure 17: Spike rates in *Cabp1/2*- DKO SGNs

(A) Correlations of peak and adapted rates for different stimulus rates. (B) *Cabp1/2*- DKO neurons show lower spontaneous spike rates than WT SGNs (*, p=<0.01, Wilcoxon rank sum test)

Since the majority of neurons had a very broad frequency tuning, we often had to subjectively choose a best frequency tone burst or use white noise burst stimulation of at least 80 dB for further characterization. 16 out of 19 DKO units responded with a relatively high onset rate but strong adaptation to a minimal sustained spiking. This abnormality prevented response pattern-based unit classification. Based on their location, spike waveforms and recording stability, we assume that approximately 13 of these 16 neurons represent SGNs and 3 represent bushy cells or multipolar cells of the anteroventral cochlear nucleus. We excluded three additional units (two resembling a pauser/buildup and one displaying a clear chopper neuron-type response) from further analysis.

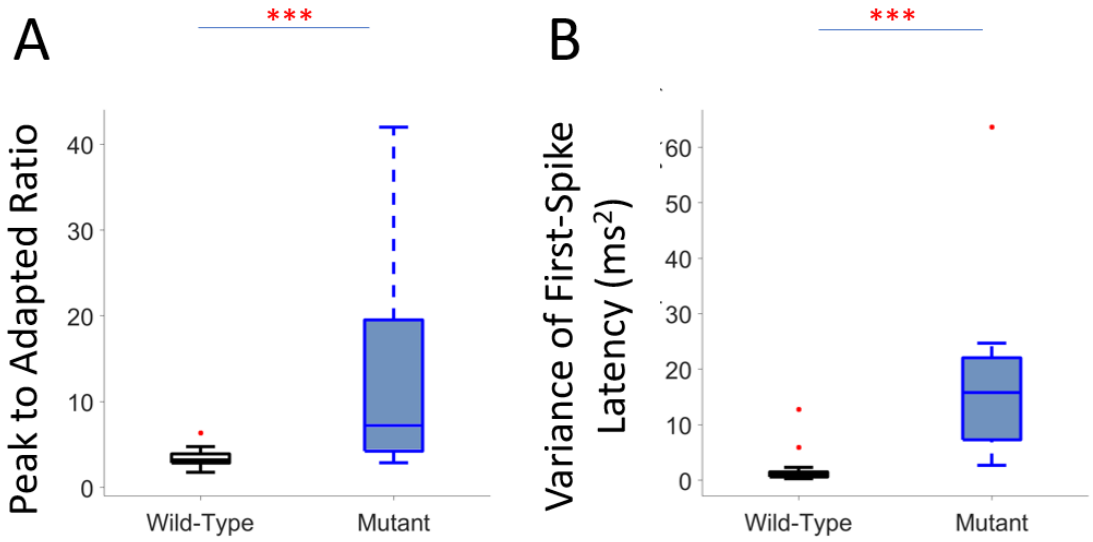

Figure 18: Functional properties of DKO

(A) The peak to adapted rate ratio is increased in the *Cabp1/2*- DKO for 5 Hz stimulus. ($p < 0.0005$, Wilcoxon rank sum test). (B) An increase in jitter was observed for the *Cabp1/2*- DKO neurons compared to WT for 5 Hz stimulus ($p < 0.0005$, Wilcoxon rank sum test)

In DKO neurons, peak and adapted rates were greatly reduced as compared to WT controls (Fig. 18 A), which came along with an increased latency (12.6 ± 2.8 ms vs WT 4.8 ± 0.2 ms; $p < 0.001$, Wilcoxon rank-sum test) (Fig. 19 A) and increased jitter (18.2 ± 5.0 vs WT 1.5 ± 0.4; $p < 0.00001$, Wilcoxon rank-sum test) (Fig. 18 B) of the first spike that follows the spike onset. On lowering the stimulus repetition rate to 0.5 Hz, the sound onset response of DKO neurons greatly improved. However, at an even lower stimulus repetition rate of 0.2 Hz, it did not increase further (Fig. 14 B, Fig. 15). We hypothesize that in DKO SGNs, recovery of $Ca_V1.3$ channels after a silent interval in the range of 1-2 seconds acts as a limiting factor for determining the maximal SGN spiking rate at the sound onset. This may be further contributed by potentially slowed re-supply of synaptic vesicles, as suggested by reduced efficiency of sustained exocytosis in the *Cabp1/2*- deficient IHCs. While in WT SGNs, the maximal spike rates are mostly recovered after a 150 ms silent interval, which may be mostly limited by vesicle replenishment at the IHC ribbon synapse (Strenzke et al. 2016, Pangršič et al. 2010). During 5-Hz sound stimulation, the strength of adaptation was greatly enhanced (peak to adapted ratio 12.5 ± 3.0 vs WT 3.4 ± 0.1; $p < 0.00001$, Wilcoxon rank-sum test) (Fig. 18 A) with an unchanged time constant of adaptation (7.9 ± 2.0 ms in DKO compared to 7.0 ± 0.4 ms in WT ($p = 0.5$, Wilcoxon rank-sum test) (Fig. 19 B).

In contrast, for the longer 500-ms tone bursts used in the 0.5 Hz stimulation, it becomes obvious that despite the strong adaptation, DKO neurons are still able to sustain spiking (albeit at a low rate) throughout the stimulation (Fig. 16). Spontaneous spiking activity in DKOs was found to be reduced (Fig. 17 B), which supports the hypothesis that already in the sound stimulation absence over tens of seconds a considerable fraction of calcium channels may be in steady-state inactivation.

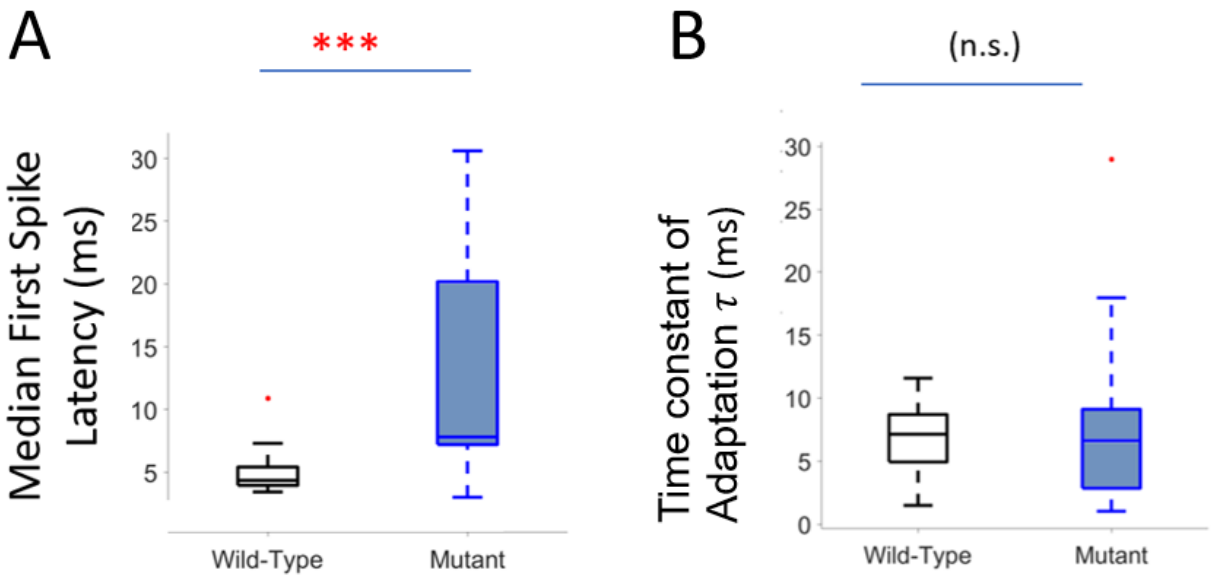

Figure 19: SGN response properties in *Cabp1/2* DKO mice

An increase in median first - spike latency was observed for the *Cabp1/2*- DKO neurons compared to WT for 5 Hz stimulus ($p < 0.0005$, Wilcoxon rank sum test) (B) The time constant of adaptation was found to be unchanged in the *Cabp1/2*- DKO for 5 Hz stimulus as compared to WT. ($p = 0.5$, Wilcoxon rank-sum test)

We have experimental bias to our data brought about by spike rate reduction and their strong dependence on the strength of stimulation. In DKO units, it was not feasible to faithfully assess sound thresholds or dynamic ranges, because threshold depended on stimulation strength in the seconds before the test pulse. Adding to it, the overall experimental yield was generally much lower in DKO animals. On average per hour of recording we hit 0.3 sound-responsive neurons in mutants, compared to 2.5 in WT. There is a high possibility that many DKO neurons failed to generate spontaneous and evoked action potentials, thus we were not able to identify them. Our DPOAE data suggest that cochlear mechanics and active amplification and thus the IHC receptor potential thresholds are mostly normal in the DKOs. It is plausible that IHC receptor potentials are decreased in amplitude, which however should rather reduce SGN adaptation. We thus assign the observed increase in adaptation and delay of recovery of SGN spiking to the effects of changed synaptic $Ca_V1.3$ channel kinetics as described above. In summary, sound responses of DKO SGNs and cochlear nucleus neurons showed a drastic reduction in spontaneous and evoked action potential rates, which was associated with sound threshold increment along with reduced temporal precision of action potential generation. Together, the poor ABR thresholds are well explained by these factors.

3.2 ATP11A

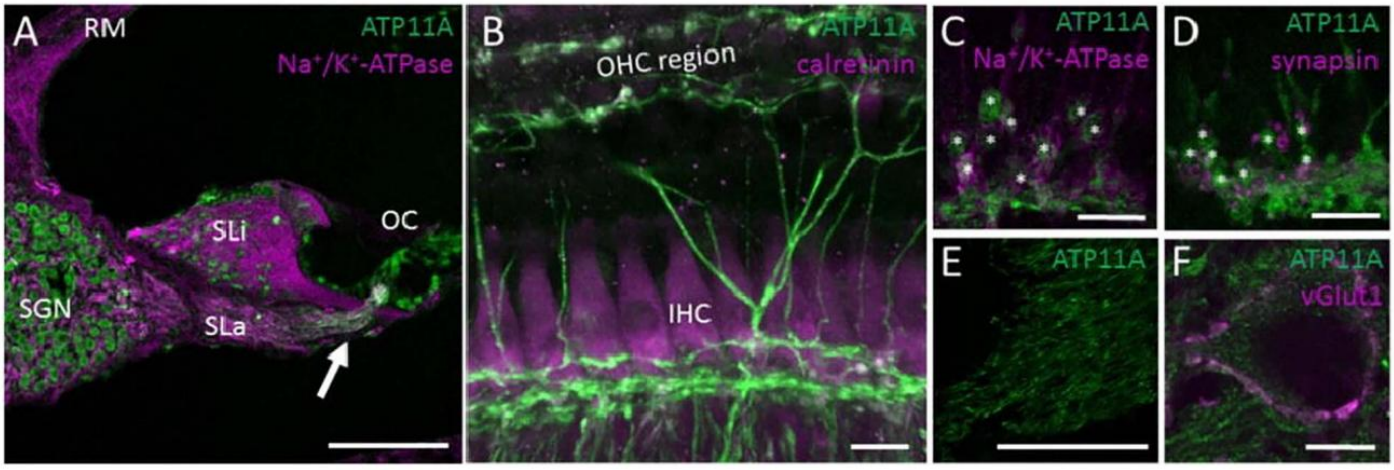

Figure 20: Atp11a expression in the organ of Corti

(A) Mouse cochlear middle turn section with immunofluorescence labeling of ATP11A (green) in SGN cell bodies and their peripheral neurites (arrow) originating from the organ of Corti (OC). Here, ATP11A colocalizes with Na+/ K^+-ATPase α3 staining (magenta). Na+/ K^+-ATPase staining in surrounding structures like the spiral limbus (SLi), spiral lamina (SLa) and Reissner's membrane (RM) is likely to be unspecific. (B) Maximum projection of a confocal image stack of the Organ of Corti with intense ATP11A staining in SGNs (green) contacting the IHCs co-labelled with calretinin (IHC, magenta) and the OHCs (not stained). (C) Single confocal section from the basal region of an IHC (not stained). The cytoplasm of the synaptic boutons (∗) of afferent type I SGNs contacting the IHCs contains ATP11A (green) and is surrounded by a Na+/ K^+-ATPase α3 (magenta) halo which labels the cell membrane. (D) Same, with colabeling for synapsin (magenta) staining the synaptic terminals of lateral olivocochlear efferents contacting the ATP11A-stained (green) afferent boutons(∗). (E/F) Single confocal sections of a brainstem cryosection, demonstrating ATP11A immunoreactivity in the auditory nerve at the entry region into the cochlear nucleus (E) and in fibers passing through and neurons of the anteroventral cochlear nucleus as well as in the cytoplasm of synaptic contacts onto those neurons (co-stained for vglut1, magenta). Scale bars in A, E: 100 μm; in B, C, D and F: 10 μm

We performed immunofluorescent labeling of whole-mount preparations and cryosections of the Organ of Corti and cochlear nucleus in mice (Fig. 20) in collaboration with Dr. Jakob Neef and Daniela Wigger. In various antibody combinations, anti ATP11A reliably and specifically labeled both type I and type II SGNs, that connect the afferent ribbon synapses of IHC and OHC with further neurons of the brainstem. While most if not all afferents appeared to be stained, there was no co-staining with synapsin which is an exclusive label for efferent synapses (Bergeron et al. 2005, Safieddine et al. 1999) (Fig. 20 D). Along with fibers, synaptic contacts in the auditory nerve and cochlear nucleus, neurons of the cochlear nucleus also showed ATP11A expression (Fig. 20 E and F).

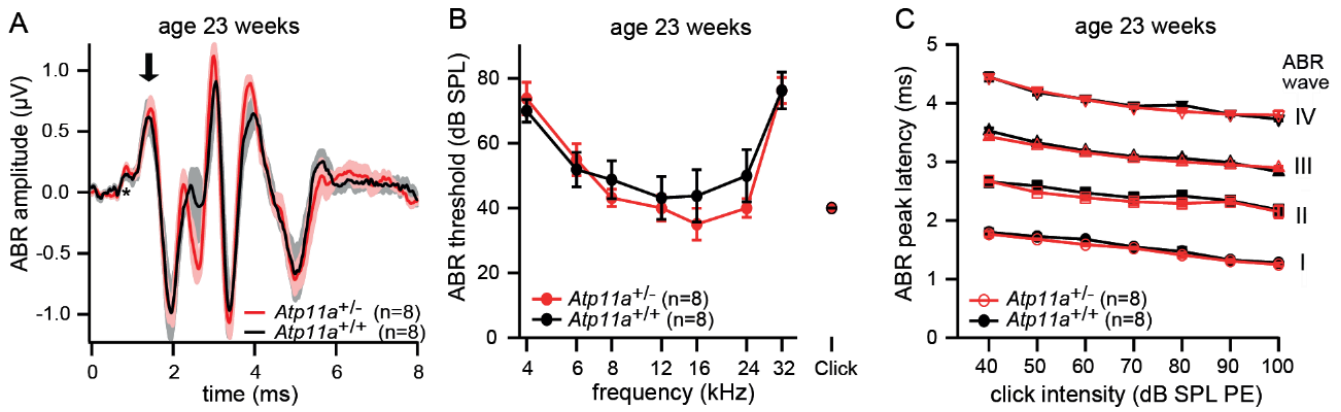

Figure 21: ABR recordings at age 23 weeks

(A, B) ABR amplitude and thresholds were not significantly different in the heterozygous *Atp1A*$^{+/-}$ mutant mice, (C) ABR peak latency was also similar to WT ATP11A mice at 23 weeks (arrow points to ABR wave I)

With a goal to independently validate the role of ATP11A in hearing function, we generated a conditional knockout (cKO) mouse which selectively lacks ATP11A in parvalbumin-expressing cells, which includes all afferent SGN subtypes (Shrestha et al. 2019). I could not find impairment in ABR in the heterozygous ATP11A (+/-) mice with conserved ABR wave amplitudes and thresholds along with unchanged ABR wave latencies (Fig. 21)

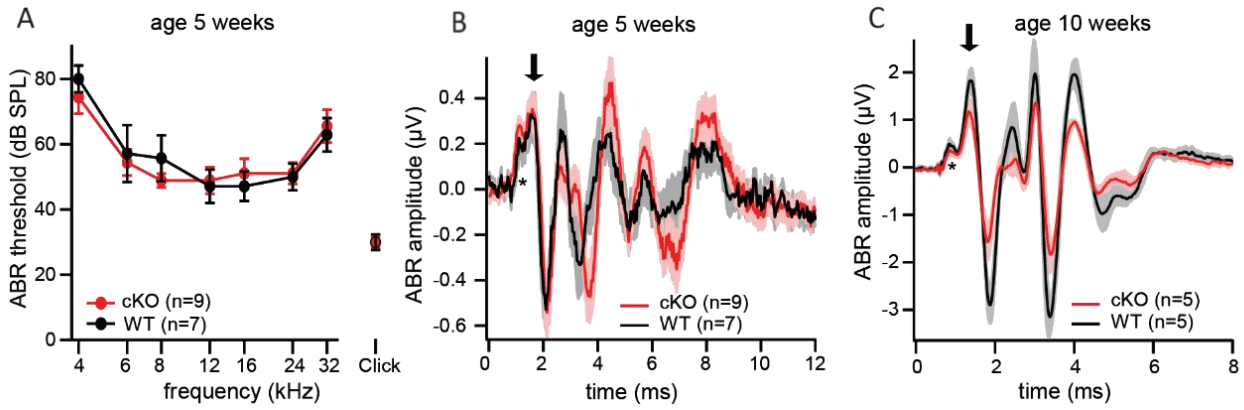

Figure 22: ABR data at lower ages

(A, B) ABR thresholds and wave amplitudes did not show a significant impairment in young 5 weeks old mice. (C) However, by 10 weeks of age a slight reduction in wave I amplitude (see arrow) as well as later waves was visible in *Atp11a*-PV-Cre conditional knockout mice.

Similarly, *Atp11a* cKO mouse at an age of 5 weeks exhibited ABR waveforms (Fig. 22 A, B) and thresholds that (not shown) were almost indistinguishable from WT littermate controls. However, by the age of 10 weeks, we observed that the amplitude of ABR wave I reduced to approximately 50% (Fig. 22 C), and by the age of 25 weeks, was reduced to about 30% of WT control values (Fig. 24 C), indicating a progressive SGN loss or

dysfunction. ABR thresholds at 10 and 25 weeks of age were moderately elevated from WT controls (Fig. 23 A, B)

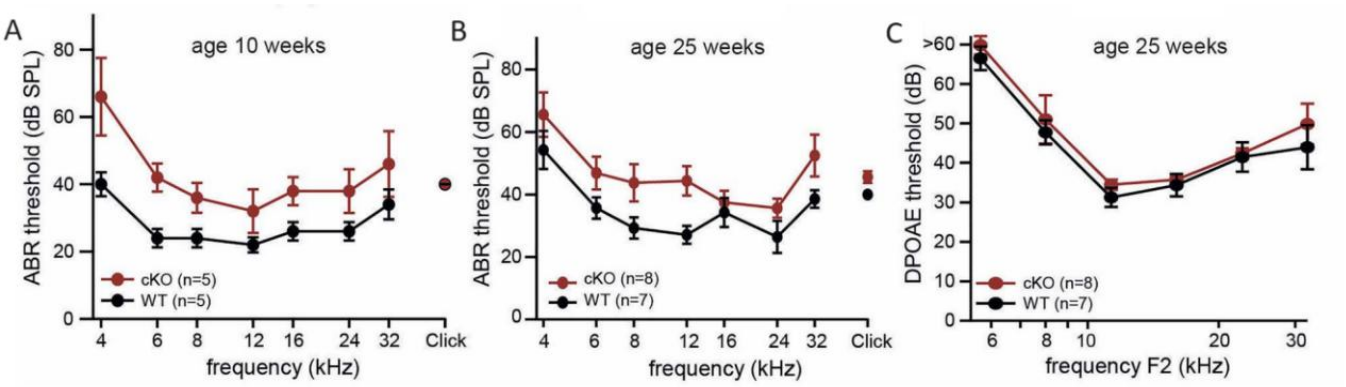

Figure 23: ABR thresholds at advanced ages

ABR thresholds at 10 (A) and 25 weeks of age (B) in *Atp11a*-PV-Cre cKO mice are moderately elevated (age 25 weeks; mean ± SEM, n as in B/C). (C) DPOAE remain normal until 25 weeks of age (mean ± SEM).

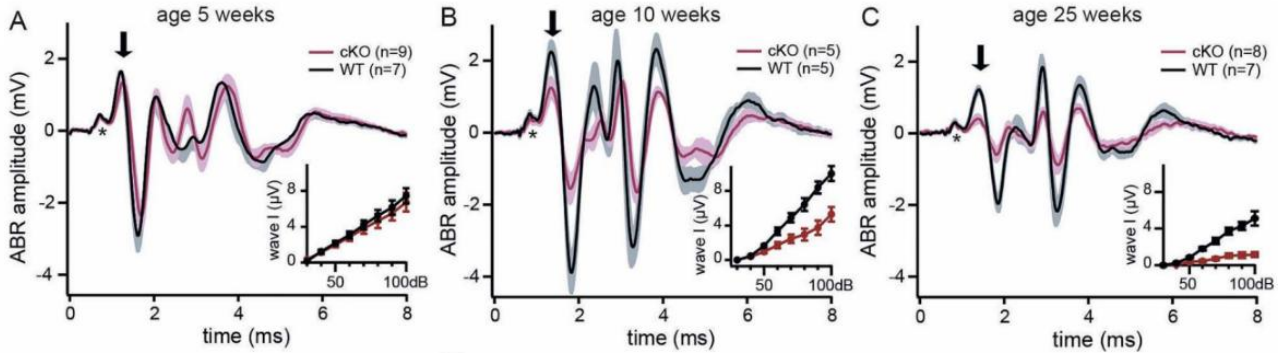

Figure 24: ABR in Atp11a cKO mice

Grand averages of ABR waveforms to 80 dB click stimulation showing normal ABR in 5 week old cKO mice (A) and a progressive reduction in ABR amplitudes at ages 10 weeks (B) and 25 weeks (C). Inset shaded areas indicate the SEM. Stars (*) mark the summating potential, reflecting hair cell depolarization. Arrows point to ABR wave I, reflecting synchronous spiking of SGNs. Insets show the peak-to-trough amplitudes of ABR wave I for different click intensities.

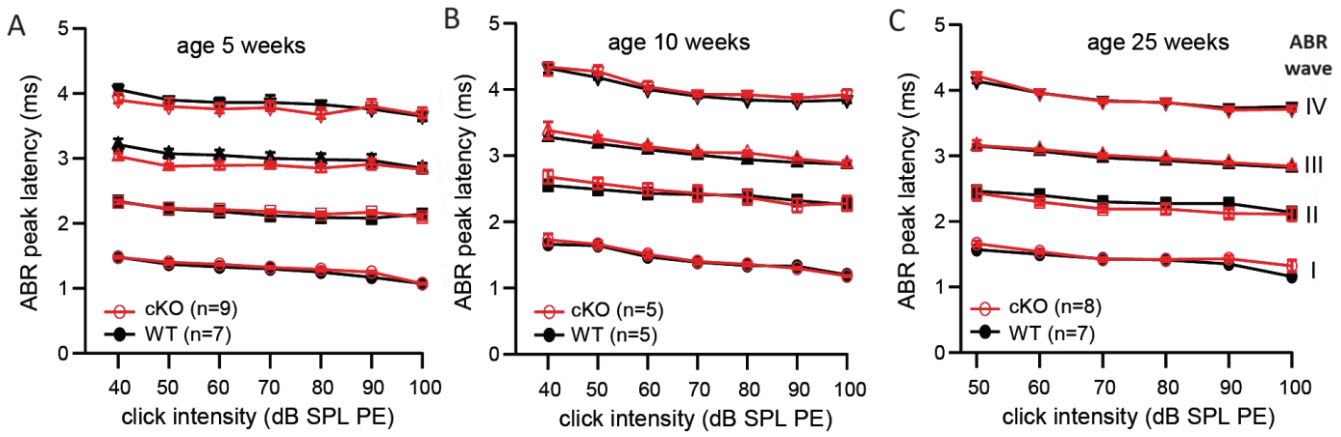

Figure 25: ABR latencies in *Atp11a* cKO mice

ABR peak latency of wave I to wave IV at 5 (A), 10 weeks of age (B) and 25 weeks of age remained unchanged between WT and mutants.

Summating potentials reflecting IHC receptor potentials were observed to be normal (Fig. 24 A–C). Although the ABR thresholds were elevated with age, the ABR wave latencies in cKO mutants did not show any changes as compared to WT (Fig. 25).

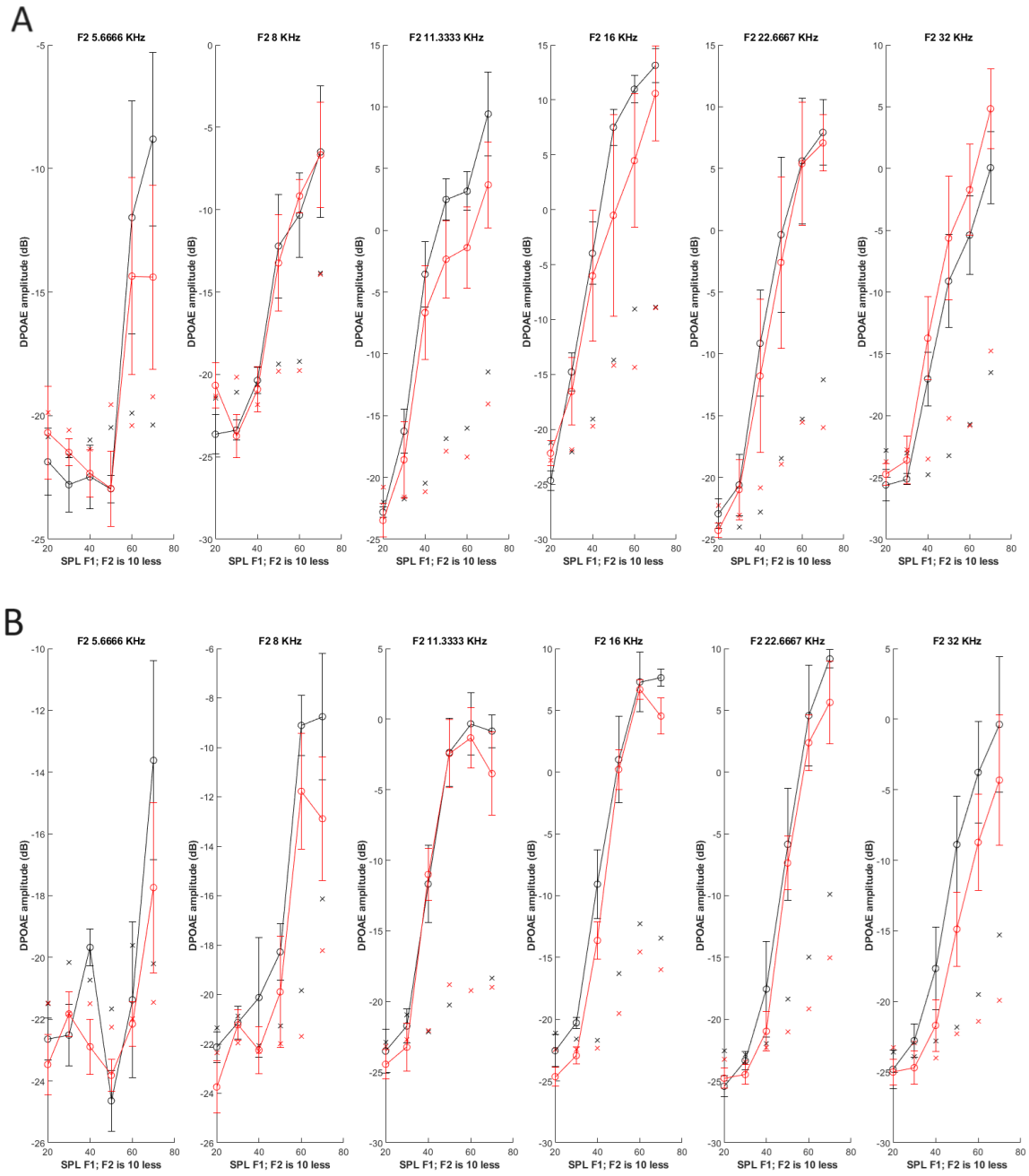

Figure 26: Normal DPOAE in *Atp11a* cKO mice

(A) DPOAE amplitudes elicited for F2 frequencies from 5.6 KHz to 32 KHz show no impairment for 8 weeks in the cKO mutant (red) compared to WT (black) (B) DPOAE amplitude for 24 weeks age mutants show normal output for the cKO mutants (red) as compared to WT (black).

Considering normal distortion product OAE (DPOAE) up to the age of 25 weeks (Fig. 23 C and Figure 26), we conclude that there was no defect of outer and middle ear mechanics, active cochlear amplification, cochlear homeostasis or mechanotransduction. In line with the expression pattern shown in Fig. 20, we conclude that the loss of ATP11A in parvalbumin-expressing cells leads to an age-progressive dysfunction, which is well comparable to the situation in human *ATP11A* associated AN.

Using the single-unit electrophysiological recordings from SGNs of the cKO mutants I observed that the peak rate showed a significant reduction (Fig. 28 A,Fig. 29 A) while the adapted rate was comparable between mutants and WT. Interestingly, I observed the distribution of spontaneous rates to be similar between the mutants and WT (Fig. 27 A).

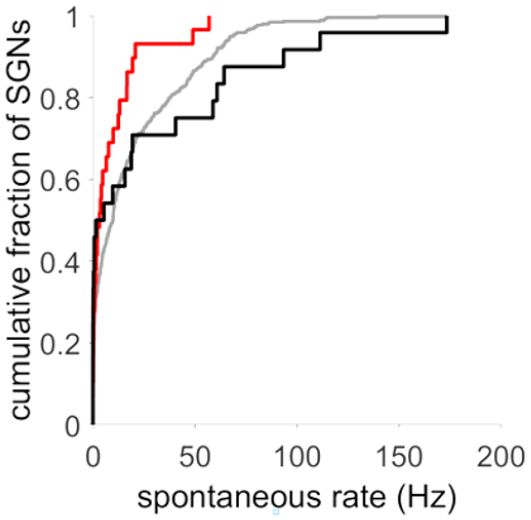

Figure 27: Spontaneous Rate in *Atp11a* cKO

It was observed that spontaneous rate is reduced among the SGNs [Red: *Atp11a* cKO (n=29), Black: WT(N=24), Grey: combined WT of all SU studies in the lab (N'=432)]

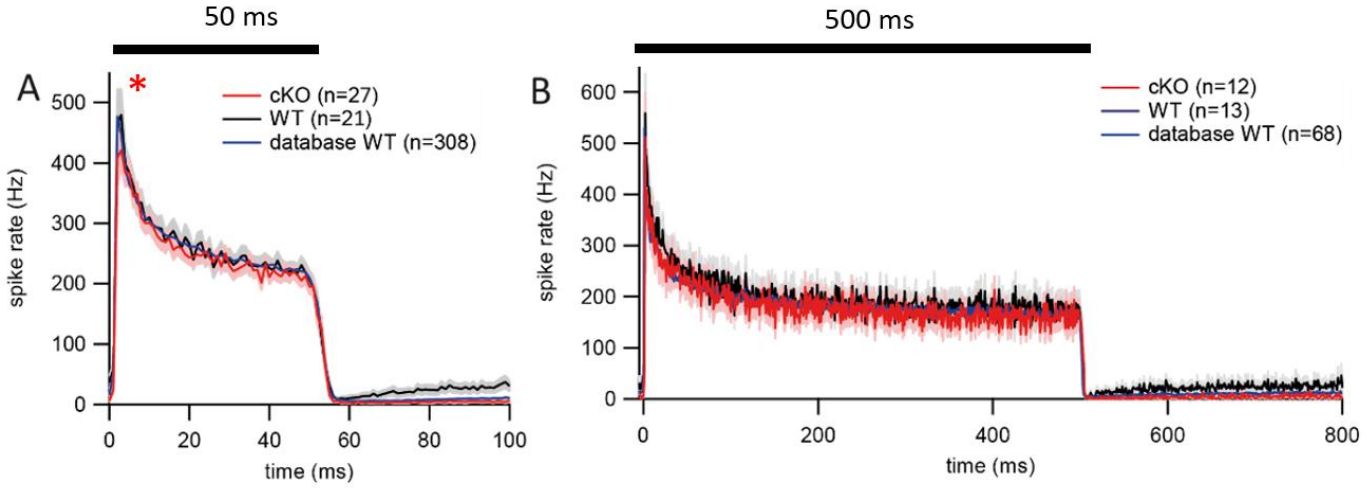

Figure 28: *Atp11a* cKO Post-stimulus time histogram (A) Peak-aligned PSTH of conditional knockout (cKO) mutant *Atp11A*-PvCre in comparison to recorded Wild-type units and with Wild-type data curated from our database containing data from several distinct experiments. A reduction in the peak rate but not the adapted rate in mutants is evident. (B) Post-stimulus time histogram to 500 ms long duration stimulus points at conserved ability to follow continuous stimuli in mutant (red) and Wild-type (black)

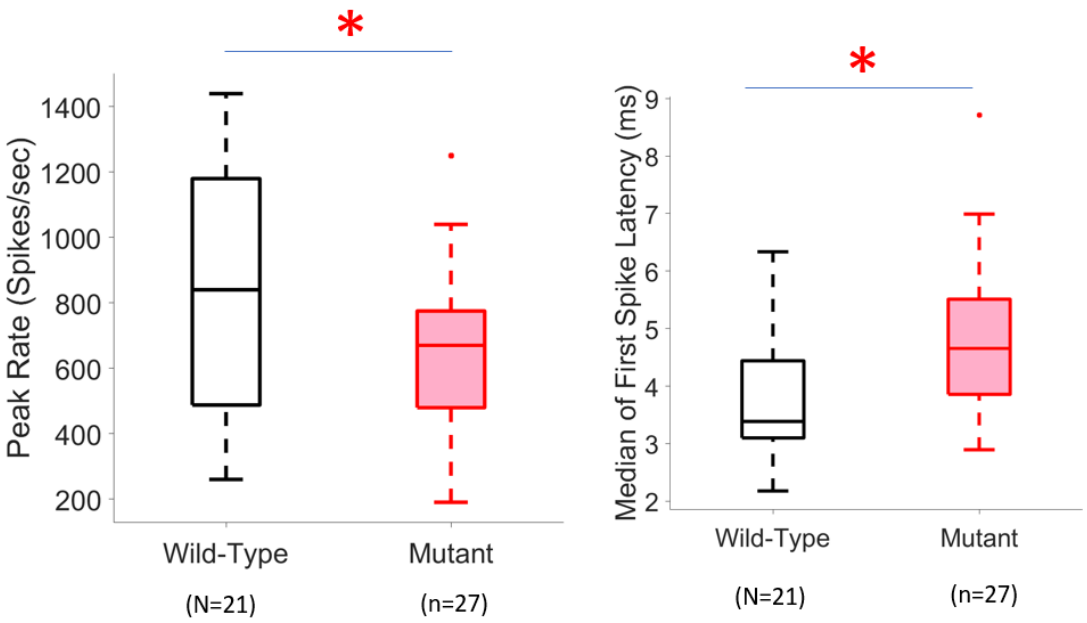

Figure 29: Functional properties of SGNs in *Atp11a* cKO mice

(A) Although mild, peak rate is significantly lowered in *Atp11a*-PV-Cre mutants ($p < 0.05$, Student's t test) (B) The median first spike latency was observed to be increased mildly but significantly ($p<0.05$, Student's t test). (Red cross denotes outliers; high-value outliers are not shown) (cKO, n=27; WT, n=21)

On probing with a long 500ms stimulus, no impairment for sustained stimulation was observed with a lack of strong response adaptation (Fig. 28 B). Responses to forward masking tones were found to be normal thus showing no impairment for post-stimulus recovery of response (Fig. 30 A). Responses to amplitude modulated tones showed no impairment (Fig. 30 B)

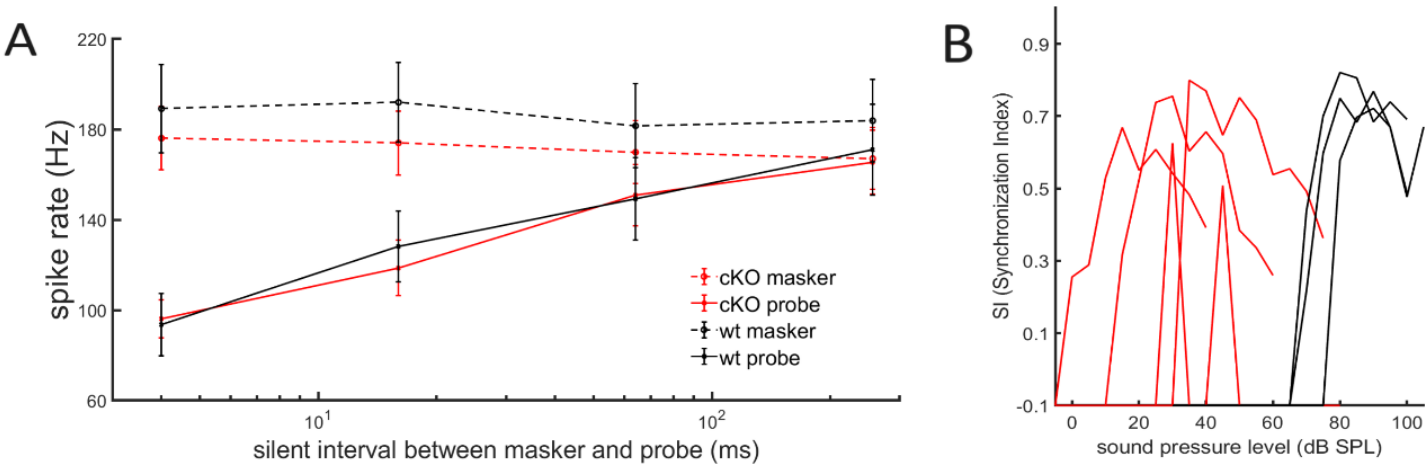

Figure 30: Properties of SGNs to complex stimuli

(A) Response for forward-masking tones in WT and *Atp11a*-PV-Cre mutants show comparable values with no significant difference. (n= 12 for cKO, 13 for WT) (B) Synchronization Index for responses to amplitude modulated tone in Wild-type (black) and mutant (red) show no impairment of sound-following response in mutants (n=4 for cKO, n=3 for WT)

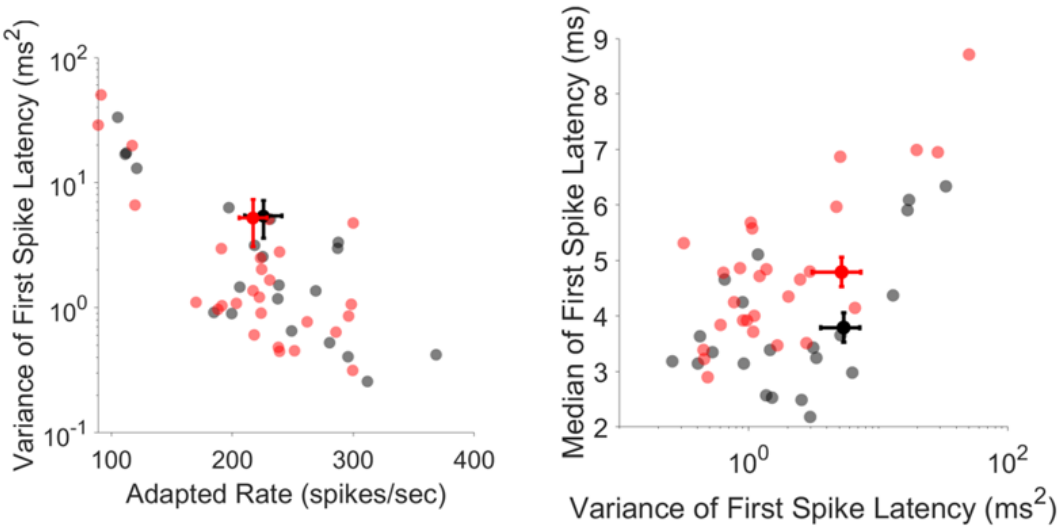

Figure 31: Correlations of functional properties

Scatter plots between (A) variance of first spike latency and adapted rate, (B) Median first spike latency and variance of first spike latency (jitter) (n=27 for mutant cKO, n=21 for WT)

Similarly, responses to Amplitude Modulated tones showed no significant difference between the mutants and WT thus hinting at a preserved ability of the cKO mutants to closely follow sound response (Fig. 30 B). Moreover, for units with varying Steady State Rates the values of jitter were similar between WT and cKO mutants (Fig. 31 A). Although median first spike latency was slightly increased in mutant cKO units, there was no change in corresponding jitter values (Fig. 31 B)

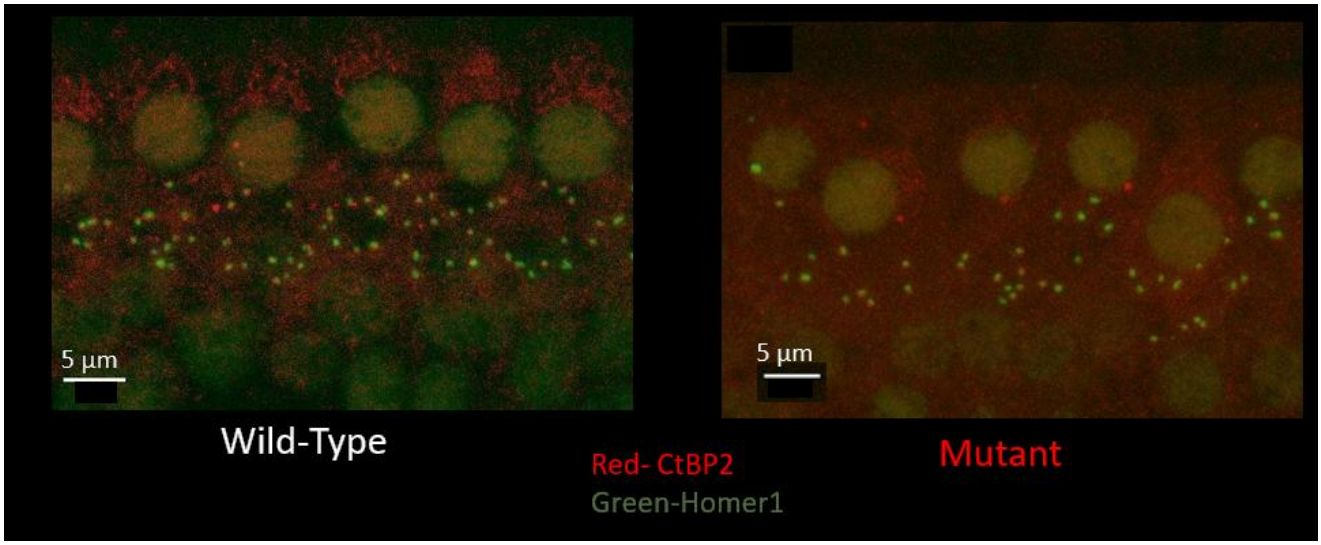

Figure 32: Images of *Atp11a* cKO inner hair cell synapses

Whole mounts preparations of the organ of Corti were immunohistochemically stained by CtBP2 (red channel) and Homer1 (green channel) antibodies to count inner hair ribbon synapses. Synapses are shown as depicted by juxtaposition of both spots. Total data collated from (N=332 WT) and (n= 251 cKO) cells with 3 mice per genotype.

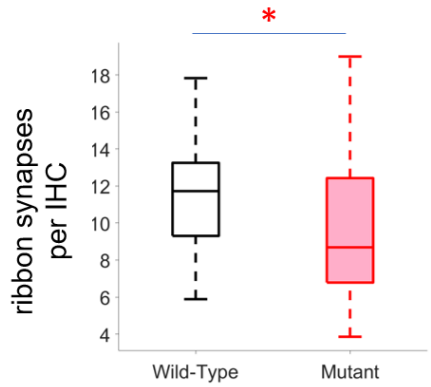

Figure 33: Reduction in synapse numbers in ATP11a cKO

Counts of IHC ribbon synapses (juxtaposed spots of CtBP2/Homer1) as a proxy of bipolar afferent SGNs revealed a reduction in SGN numbers by 30% at age 25 weeks ($p<0.05$, Student's t test).

Apart from the functional abnormalities observed in mutants, we wanted to investigate if any anatomical and morphological signatures of the pathology are present. By staining the ribbon structure as well as the adjoining post-synaptic compartment with CtBP2 and Homer1 antibodies respectively we could visualize synapses by the instances of co-localization of these two signals. In contrast to the weak ATP11A signal, these two antibodies gave robust expression making it possible to count the number of ribbon synapses. We quantified these synapses for the age group of 25 weeks observing a median reduction in synapse numbers by about 30% in mutants as compared to Wild-type ($p= 0.02$, Student's t-test) (Fig. 31 B)

3.3 OTOF TDA

Inner hair cell perforated patch clamp recordings performed by Han Chen of *Otof*$^{TDA/TDA}$ mice in the third postnatal week (P14-18) had indicated that despite normal voltage-gated Ca^{2+} influx, which is in line with the normal number of afferent synapses, *Otof*$^{TDA/TDA}$ IHCs lacked exocytosis measured as membrane capacitance increments with residual IHC exocytosis of the mutants being comparable to that of *Otof*$^{-/-}$ IHCs (Roux et al. 2006; Pangršič et al. 2010; Reisinger et al. 2011). I performed the ABRs, DPOAE and single unit recordings experiments in order to assess hearing function *in vivo* in these mice.

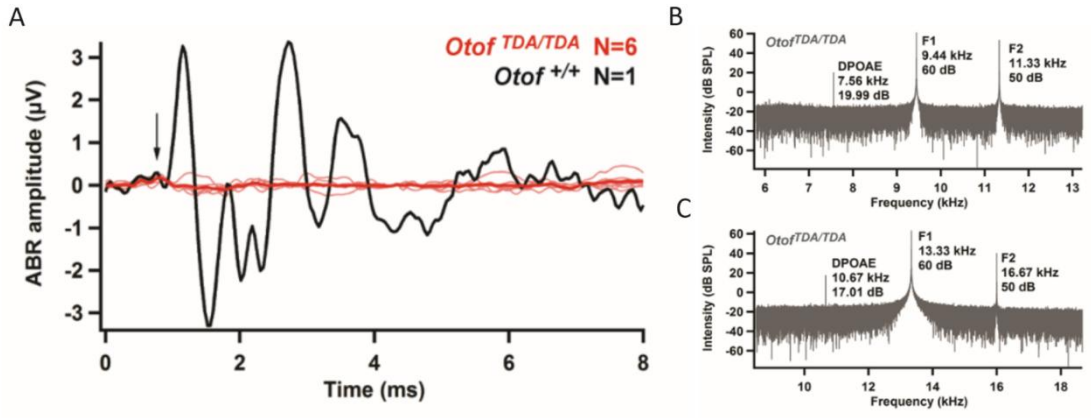

Figure 34: ABR and DPOAE in OtofTDA

(A), 100-dB click stimuli could not elicit ABR in 9–11 week-old homozygous Otof$^{TDA/TDA}$ mice (individual traces: pink, mean: red), black plot is exemplary ABR of a wt control mouse. Summating potential is denoted by the arrow, preceding ABR wave I. (B,C) exemplary frequency spectra of DPOAE recordings in an Otof $^{TDA/TDA}$ mouse aged 10 weeks, showing the expected normal-size peaks at the primary tones F1/F2 and the DPOAE frequency

ABR recordings indicated a loss of synchronized activation of spiral ganglion neurons (SGNs) (wave I reflecting the SGN compound action potential (CAP)) and further neural activity along the auditory pathway despite sizable summating potentials (reflecting the IHC receptor potential) in homozygous OtofTDA/TDA mice (Fig. 32 A). Distortion product otoacoustic emissions (DPOAEs) were observed in the mutants indicating conserved cochlear amplification by outer hair cells (OHCs, Fig. 32 B, C). Loss of ABR despite intact OHC function makes it a case of auditory synaptopathy/neuropathy (Moser & Starr, 2016).

As an increase of jitter in SGN spiking may lead to undetectable ABRs, I attempted in-vivo recordings of sound-evoked neuronal spiking activity in the region where the auditory nerve enters the cochlear nucleus. Previously, such recordings studying synaptic sound encoding at single afferent IHC synapses with great precision have been instrumental to reveal a function of otoferlin in synaptic vesicle replenishment to the readily releasable pool (Pangršič et al. 2010; Strenzke et al. 2016). However, in experiments on *Otof*$^{TDA/TDA}$ mice did not detect any obvious sound-evoked neural activity in that region. In a total recording duration of 23.5 hours in five *Otof*$^{TDA/TDA}$ mice, we never encountered any sound-evoked action potentials. For comparison, in a WT mouse dataset, I, on average, recorded from one auditory nerve fibre and one other sound-responsive neuron (e.g., bushy cells and

multipolar cells of the cochlear nucleus) per 90 minutes of the running experiment. My findings using the electrophysiological recordings support the notion of a major sound encoding failure at afferent IHC synapses of *Otof*$^{TDA/TDA}$ mice in vivo.

3.4 Current and future work

More work is required to dissect the degenerative phenotype further. Since loss of the flippase ATP11A could lead to premature exposure of PtdSer on the extracellular side of SGNs, it is probable that the cell death machinery could act on these cells leading to removal of some of the SGNs. In this regard, my lab rotation student Dominik Sobczak and I have started experiments involving cryosections of the Organ of Corti which clearly show the cluster of cell bodies of the SGNs. We have established a method for quantifying the cell numbers using Parvalbumin staining by adopting on the segmentation models developed by Anupriya Thirumalai, Jana Henseler and Dr. Antoine Huet that employs the Arivis software and Cellpose segmentation algorithm (https://www.cellpose.org/) and we plan to use Calretinin staining to study the degenerative effect on different SGN subtypes.

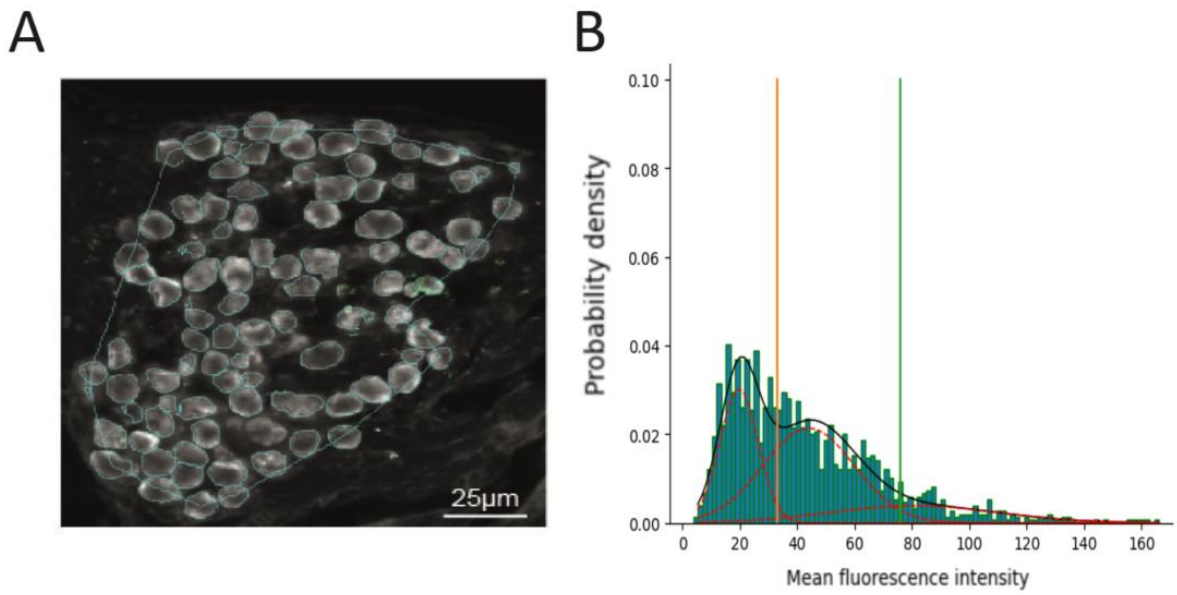

Figure 35: Image Segmentation in SGNs

(A) successful detection of SGN cellular bodies in cryosections of Organ of Corti using the cellpose method in Arivis. (B) The distribution of fluorescence intensity could be fitted with 3 clusters as depicted by the three gaussians in red (orange and green vertical lines mark the 2σ interval around the cluster maxima) with an AIC value of 13567, being higher than when using 4 clusters for fitting.

The developed python pipeline fits Gaussian curves using the Expectation-Maximization (EM) algorithm to estimate Gaussian Mixture Models. A Gaussian Mixture Model is a probability distribution modelled as a linear combination of several Gaussian distributions where each Gaussian component represents a potential cluster in the dataset. The EM algorithm estimates the parameters of the mixture distribution, including the means, covariance matrices, and weights of the individual components. The program estimates as many models as specified as the number of Gaussian curves to be fitted and calculates the AIC value (Akaike's Information Criterion) for each model. The AIC is a statistical measure used to assess the goodness of fit of a statistical model that takes into consideration both the model's goodness of fit and its complexity. Lower AIC values generally

indicate a better fit of the model to the data. We used the model to test fitting of 3, 4 and more clusters assuming the fluorescence intensity distribution would follow the three SGN subtype classification. In a dataset from aged wildtype mice, Dominik assessed the Parvalbumin and Calretinin staining intensity in the SGNs. Unfortunately, in his dataset there was no clear separation of SGNs groups with low and high Calretinin staining and the model showed that classification into three groups is not the optimum outcome. (Fig. 33 B). Thus, classifying different SGN subtypes based on their Calretinin expression level, as suggested by Shrestha et al. will likely be more difficult than initially expected.

4 Discussion

4.1 Cabp1 and Cabp2

We examined the effects of genetic disruption of the two major Cabps expressed in the cochlea on auditory function. We found strongly inactivating synaptic Ca^{2+} currents with delayed recovery from inactivation upon mild oscillatory stimulation in the IHCs of *Cabp1/2*-deficient animals, thus not supporting sufficient sustained neurotransmission. As the duration of IHC stimulation was extended, the extent of channel inactivation and impairment of IHC synaptic exocytosis aggravated. Similarly, SGN action potential rates in vivo declined at increased sound stimulation rates and exhibited very strong adaptation upon stimulation. As compared to the phenotype observed in the absence of Cabp2 alone, the impairment was significantly stronger. This suggests that under in vivo conditions, the roles of Cabp1 and 2 are partially overlapping and Cabp1 can partially compensate for the loss of Cabp2.

In the murine cochlea, a strong expression of Cabp1 and 2 is seen, while the levels of Cabp4 and 5 were observed to be negligible (Yang et al. 2016, Jean et al. 2023, Xu et al. 2022). Cabp2 has three putative splice isoforms differing in the N-terminal amino acid sequence, of which the alternative long isoform, Cabp2-alt, may be the most abundant splice variant in the IHCs (Yang et al. 2016), while in the SGNs there is no expression. In regards to Cabp1, alternative splicing generates three variants (Yang et al. 2016). Caldendrin, the long variant, is primarily expressed in the SGNs or the surrounding glial cells, while in IHCs weak expression of Cabp1-S/-L was detected (Yang et al. 2016). Our DKO model lacks Cabps in all splice isoforms. Since Cabp1 KO animals show normal hearing several weeks after birth, and Cabp2 is absent from SGNs, we interpret the hearing impairment of the *Cabp1/2* DKO animals to be mainly due to defects of hair cell function and consider the contribution by SGN dysfunction as rather unlikely, at least in the early postnatal weeks. The ABR thresholds of Cabp1 KO animals are normal at 4 weeks of age, but show deterioration with age, starting with high-frequency hearing loss at 9 weeks. Conversely, the suprathreshold ABRs in response to tone burst stimulation show increased amplitudes and reduced latencies during the first weeks after birth. The initial enhanced SGN activity, followed by slowly progressing functional decline is possibly due to overexcitability-related toxicity (Yang et al. 2018). Due to early strong impairment of hair cell synaptic function and thus no increased excitability, the latter effects are not expected to occur in the DKO animals. However, ABR thresholds for clicks were further increased with an additional reduction in the summating potential in the DKO animals at two months as compared to one month of age despite the DPOAEs being relatively well preserved.

Our results reveal that the amount of $Ca_V1.3$ inactivation increases dramatically when IHCs lack both major Cabps. This suggests a compensatory role for either of Cabp1 and 2, when one of the two Cabp members is missing. Yet it is observed that the loss of Cabp2 alone still results in progressive hearing impairment in mice and DFNB93 in humans. Here, the inability of Cabp1 to fully replace Cabp2 in the Cabp2-deficient IHCs may be due to either very low concentrations of Cabp1 (and potentially other Cabps), or from distinct properties of the two proteins. Additionally, the hearing phenotype of DKO animals could not be fully rescued by the overexpression of Cabp2. Future experiments can shed light on the potentially distinct functions performed by the two major

Cabps in the hair cells by focusing on overexpression of Cabp1 (and possibly Cabp1-2 molecular chimeras) in *Cabp2* SKO and *Cabp1/2* DKO animals further substantiated by biophysical interaction studies.

Previously, using patch-clamp recordings it was observed that normal whole-cell exocytosis existed in Cabp2-deficient IHCs despite the inactivation of calcium channels being enhanced (Picher et al. 2017). Cabp1-deficient IHCs had no obvious defects as well (Yang et al. 2018). In contrast, it was observed that IHCs deficient in both, Cabp1 and 2, displayed strongly impaired exocytosis. Transgenic overexpression of Cabp2 in IHCs resulted in a partial recovery of the Ca^{2+} influx and an even better recovery of exocytosis. These results corroborate the hypothesis of the role of Cabps in supporting sufficient synaptic exocytosis for proper sound encoding by preventing extensive steady-state inactivation of $Ca_V1.3$ channels (Picher et al. 2017). Identifying further Cabp2-interaction partners and possible functions beyond calcium channel modulation will be an important challenge for the future.

The recovery of $Ca_V1.3$ channels from inactivation upon prolonged milder stimulation (2 min sine wave) followed a single exponential course in WT IHCs, but an additional slower component was detected in the IHCs deficient in Cabp1 and 2. When a comparably shorter (500 ms) but stronger depolarization was used, the recovery of $Ca_V1.3$ from inactivation was very fast in DKO IHCs, even faster than that in WT. Our hypothesis is that this is due to faster Ca^{2+} clearance from the DKO IHC synapses. Intracellular Ca^{2+}levels are expected to rise significantly less in *Cabp1/2*- deficient IHCs because of faster channel inactivation. In contrast, higher Ca^{2+}may build up at the synapses of WT IHCs; consequently, prolonging CDI. CaPB2 may act as a slow mobile calcium buffer thus providing an alternate plausible explanation for the observed results (Picher et al. 2017). Our results of the recovery upon 500-ms depolarization may thus point towards the kinetics of the Ca^{2+} clearance from the cytosol, while the prolonged sine wave stimulation experiments may report the speed of calcium channel recovery from slow inactivation. It has to be noted that the time constant of recovery of Cav1.2 from slow VDI was comparably shorter (4 s) in our results (Ferreira et al. 2003) possibly due to variabilities in conditions such as stimulus parameters or channel subtype. Future experiments combining patch-clamp recordings with calcium imaging will be crucial to address this question. From our observations of in vitro recordings at higher holding potential or upon prolonged stimulation with small voltage oscillations we predict that in vivo a noteworthy proportion of $Ca_V1.3$ channels may be effectively inactivated and thus unavailable for mediating IHC synaptic transmission. The low experimental yield, the low "spontaneous" spiking rates of the SGNs and lower sound evoked spike rates with higher thresholds could be explained by this. Similarly, thresholds may be high for tone bursts in the ABR measurements due to a high proportion of inactivated channels upon stimuli at high repetition rate used for these recordings (20 and 40 Hz repetition rate for click and tone burst stimulation, respectively).

We believe that not only any sound stimulation but also spontaneous activity may effectively silence DKO synapses. As expected, longer interstimulus intervals may allow a larger proportion of channels to recover between stimuli, increasing the onset rates of SGN spiking and decreasing the first spike latency and jitter. Still, high-intensity stimulation had to be used in the DKO animals to evoke an increase in SGN spiking. It is possible that spontaneous activity and/or the sound stimulation used to determine the SGN characteristic frequency inactivate a majority of IHC $Ca_V1.3$ channels thus not allowing reliable assessment of the characteristic frequency. In addition to $Ca_V1.3$ channel inactivation, other factors may contribute to low hearing sensitivity, such as possible impairment of synaptic vesicle replenishment, or IHC mechanotransduction, and, in some cases, impaired cochlear

amplification. In addition, impaired DPOAE in some DKO mice and reduced summating potentials suggest that there could be like in other cases of synaptopathy, a secondary degeneration of the organ of Corti.

4.2 Atp11a

In collaboration with Dr. Christian Kubisch, we identified a 5500 bp deletion in a large German family with AN affecting the last coding exon of *ATP11A* segregating with an AN/AS phenotype in a large family by using whole-genome sequencing. The location of *ATP11A* is within the linked region on chromosome 13q34 of AUNA2. Due to the deletion a cryptic splice site is activated that gives rise to a C terminal altered protein. Subcellular localization of the mutant protein was not changed, but flippase activity for phospatidylserine was reduced. Atp11A is highly expressed in SGNs in mice. While outer and middle ear mechanics, active cochlear amplification, cochlear homeostasis and mechanotransduction were normal, a progressive SGN loss or dysfunction similar to loss of ribbon synapses could be observed. Furthermore, the conditional KO mouse mimics the age-progressive AN phenotype observed in humans.

The AUNA2 locus overlapped with DFNA33 on chromosome 13q34 (Lang-Roth et al. 2017, Bonsch et al. 2009). With the identification of a pathogenic variant in *ATP11A* as the genetic cause of AUNA2, a possible speculation could be if DFNA33 may also be related to *ATP11A*. Transitory evoked otoacoustic emissions (TEOAEs) were missing in some affected family members in the original DFNA33 family, which would argue against a typical AN/AS phenotype on first sight. However, also in the older patients in our family, TEOAEs were lost, which would be compatible with a secondary OHC degeneration in AUNA2 (Lang-Roth et al. 2017).

The exact disease mechanism leading to an AN phenotype by Atp11a dysfunction is unclear. Membrane asymmetry established by different P4-ATPases, including Atp11a is essential for a wide variety of cellular processes and future studies will have to unravel the actual cellular and organism-level consequences of *ATP11A* mutations. From a clinical point of view, it seems noteworthy that the patients in our family had an AN phenotype with pathological ABRs and OAEs being better than expected from subjective hearing thresholds, pointing to a deficit in neural sound encoding. However, speech perception in quiet and in noise was not excessively affected, unlike in other cases of AN/AS. This less severe sound encoding deficit suggests a possible primary degeneration of a subset of SGNs than with a primary defect of neuronal function in the sense of a perturbation of the extreme temporal precision of action potential generation and propagation in SGNs. From a clinical perspective, such a mild deterioration in speech perception makes it difficult to diagnose the AN phenotype. ABRs are not routinely recorded in adults with age-progressive hearing loss, and even if this test is performed, because of poor standardization a reduction of ABR amplitude may be missed.

ABR recordings in the cKO mutants confirmed an auditory deficit that is age-progressive without any signs of delays during transmission through auditory pathways as seen by intact latencies of ABR waves. The single-unit SGN recordings were useful to thoroughly characterize the auditory functions bringing to light several abnormalities. A significant reduction in peak rates in the mutant cKO animals explains the poor ABRs but intact jitter values in mutants makes it difficult to predict the mechanism of functional deficit. Non-pathological response for forward-masking and amplitude modulated tones also rules out any obvious abnormalities in recovery or

sound-following. A key finding is the inability of the mutant units to exhibit a normal peak response with a conserved ability of maintaining the adapted response. This observation points towards the mechanisms involved in reaching a high peak value probably implicating the processes regulating early events such as action-potential initiation or those that facilitate high-rate firing. Apart from functional investigations, molecular characterization proved to be crucial to uncover the preliminary mechanism of AUNA2.

The significant loss of synapses in *Atp11a*-PvCre mutants points towards a degenerative process that underlies the pathology. A loss of synapses may severely limit the amount of neurotransmitter release-coupled signal transmission events thus losing the fidelity with which the original sound signal can be conducted. The lowering of peak and adapted rates in mutants can be partially explained by the synaptic loss. Since the loss of flippase can make SGNs vulnerable to the cell-death machinery by exposing Pt-Ser there is a high possibility of cellular loss in this disease, future studies ascertaining the extent of degeneration by assessing the integrity of SGNs will be important. If the loss of synapses has been caused by an SGN-internal mechanism, a pre-synaptic process or by events outside of the synapses for example, by the cells surrounding the synapse will be an important question to study. Furthermore, if the loss is caused by inflammatory or apoptotic processes it will be crucial to determine the progression of the loss with age so that a best-choice window for drug-based intervention can be estimated. We describe the first study revealing a functionally validated IHC-SGN synaptic loss phenotype in a hearing disorder.

4.3 Perspective

To arrive at a functional understanding and molecular disease mechanism in diseases of hearing loss, studies focusing on systems physiology and specifically neural recordings from the SGNs prove to be indispensable. Through my work I have highlighted a single-unit electrophysiology centric approach to characterize important elements of pathological mechanisms in diverse hearing disorders focusing on mouse models of mutations targeting specific genes. In $Otof^{TDA/TDA}$ mutants the observations of absence of SU responses were crucial to confirm a deficit at the level of neuronal transmission thus giving a reliable picture of the severity of the phenotype. Without a direct observation of the functional status of SGNs, an accurate picture of the auditory deficit is limited. In the *Cabp* DKO experiments building upon the ex-vivo patch clamp studies, the electrophysiological recordings provided a way to directly probe our hypothesis on the limitations of neuronal transmission. Using a carefully designed stimulus paradigm involving sound stimuli with increasing silent interval between the sound pulses, we confirmed that the enhanced inactivation observed previously has a functional correlation in the SGNs. The DKO mutants cannot maintain high firing rates during a sustained auditory stimulation. Crucial parameters such as jitter, latency, strength of adaptation and time-course of adaptation gave a multi-faceted view of the observed pathology in mutants. With an observed increase in jitter in the DKO mutants, additional deficits beyond those involved in generating sustained sound response were also evident. Considering the conserved number of synapses, the auditory deficit is attributable to changes in the events in IHCs. Inability to maintain a steady response towards sustained stimuli can limit the coding of continuous auditory events in the animal. In humans, such mutation can lead to impaired perception of speech and appreciation of music. Further studies relating such functional observations at the level of neurons with perceptual changes can help build a cohesive neuronal property-perception mapping for the auditory system. The synergistic role of Cabp1 and Cabp2 in maintaining a steady

response towards sustained stimuli focusing on their shared role through interaction studies will be important by bringing focus to multi-protein events in the auditory system.

Combining immunohistochemical studies and systems physiology approaches of ABR and DPOAE and single unit recordings I could gain a preliminary understanding of the Atp11a deficiency mediated autosomal dominant auditory phenotype. As the pathology was characterized as auditory neuropathy, discovering a common mechanism of Auditory Neuropathies was one of our goals apart from understanding the molecular mechanism of the disease. Neuronal recording from the SGNs showed a significant decrease in peak rate in the mutants and an important observation is the significant loss of synapses which hints at a degenerative phenotype, the extent of which needs to be studied in greater detail. Future studies should focus on the distribution of degenerative load on specific SGN subtypes. It is surprising that the increase in jitter in the mutants is not statistically significant suggesting that the degenerative phenotype could underlie the disease without a transmission deficit. I observed that more low-spontaneous rate SGNs were intercepted while recording in mutants leading to a hypothesis that high-spontaneous rate SGNs are specifically targeted in the mutants thus changing the coding dynamics. Although a loss of synapses would translate to less signal conducting units lowering the overall strength of transmitted signal, the differential effects on different subtypes will determine the specific nature of coding deficit. The temporal nature of disease progression needs to be further illuminated answering the questions of whether the synapse loss progresses with time. This will help better design the delivery of therapeutic interventions at the right-time.

While degenerative and specifically neuro-degenerative diseases have been amply studied in the central nervous system a considerable effort is still warranted in understanding the mechanism of degenerative diseases of the sensory periphery. A degenerative loss of cells or functional components such as synapses in the auditory system may have a more severe implication as functional compensation by neighbouring partners may be further limited in the peripheral nervous system. If there are native adaptive mechanisms that safeguard against a degenerative process in the auditory system would be a further interesting direction to explore. How the auditory system is robust towards loss of a small number of functional units and how the sound encoding is affected as a result will be an important question as many other genetic diseases of deafness are expected to have a hitherto undetected degenerative aspect.

Elucidation of disease mechanisms is a crucial aspect of medical science and involves multi-disciplinary approaches with molecular, cellular and systems level investigations. Frequently studied diseases such as diabetes, Alzheimer's disease, cancer, etc have a steady influx of new insights being generated by the scientific community. However, a miniscule effort is dedicated to study rare diseases creating a dearth of knowledge surrounding their etiology and mechanism. In the auditory system, a large number of genetic diseases are categorized as rare diseases hence to design interventions it is important to de-orphanize these diseases in the context of their mechanism. Studying rare diseases is scientifically rewarding because many of them function via interesting unknown pathways which may have larger implications in other diseases. While a significant effort has been focused on the cochlear system to find drivers of pathology, there is a gap in understanding the auditory nerve and further auditory pathway. My study through investigations on multiple mutants establishes the importance of single-unit SGN recordings as a go to choice for functional assessment and mechanism elucidation. An elevation of median of first-spike latency in SGNs is a common pathological hallmark in my study and this could serve as a driver of deficit in higher auditory functions. The role of first-spike latency in encoding sound stimuli with fidelity could

involve effects ranging from reduced synchronicity in the auditory nerve to impaired computations involving spike co-incidences higher up in the auditory system and the brain. I hope that the findings in this work on Cabp proteins and ATP11a will inform new studies on their role in the auditory system and further facilitate clinical interventions in diagnosis and treatment of patients with allied mutations. I also hope that many more studies focusing on the auditory nerve specifically its functional capabilities and vulnerabilities along with a cohesive picture of IHC-auditory nerve interplay will emerge thus advancing a crucial understanding in the field.

5 References

Korver, A. M. H., Smith, R. J. H., Van Camp, G., Schleiss, M. R., Bitner-Glindzicz, M. A. K., Lustig, L. R., Usami, S., & Boudewyns, A. N. (2017). Congenital hearing loss. Nature Reviews Disease Primers, 3(1), 16094. https://doi.org/10.1038/nrdp.2016.94

Finitzo, T., Albright, K., & Neal, J. O. (1998). The Newborn With Hearing Loss: Detection in the Nursery. Pediatrics, 102(6), 1452–1460. https://doi.org/10.1542/peds.102.6.1452

Oghalai, J. S. (2004). The cochlear amplifier: augmentation of the traveling wave within the inner ear. Current Opinion in Otolaryngology & Head and Neck Surgery, 12(5), 431.

Sukharev, S., & Corey, D. P. (2004). Mechanosensitive Channels: Multiplicity of Families and Gating Paradigms. Science's STKE, 2004(219), re4–re4. https://doi.org/10.1126/stke.2192004re4

Siemens, J., Lillo, C., Dumont, R. A., Reynolds, A., Williams, D. S., Gillespie, P. G., & Müller, U. (2004). Cadherin 23 is a component of the tip link in hair-cell stereocilia. Nature, 428(6986), 950–955.

Bartsch, T. F., & Hudspeth, A. J. (2018). A new twist on tip links. Neuron, 99(3), 423–425.

Fettiplace, R., & Nam, J.-H. (2019). Tonotopy in calcium homeostasis and vulnerability of cochlear hair cells. Hearing Research, 376, 11–21.

Kros, C. J. (2007). How to build an inner hair cell: Challenges for regeneration. In Hearing Research (Vol. 227, Issues 1–2, pp. 3–10). Elsevier. https://doi.org/10.1016/j.heares.2006.12.005

Fuchs, P. A., Glowatzki, E., & Moser, T. (2003). The afferent synapse of cochlear hair cells. In Current Opinion in Neurobiology (Vol. 13, Issue 4, pp. 452–458). Elsevier Ltd. https://doi.org/10.1016/S0959-4388(03)00098-9

Lenzi, D., Runyeon, J.W., Crum, J., Ellisman, M.H., Roberts, W.M. 1999. Synaptic vesicle populations in saccular hair cells reconstructed by electron tomography. J. Neurosci. 19:119–132

Zenisek, D., Horst, N. K., Merrifield, C., Sterling, P., & Matthews, G. (2004). Visualizing synaptic ribbons in the living cell. Journal of Neuroscience, 24(44), 9752–9759.

Khimich, D., Nouvian, R., Pujol, R., Tom Dieck, S., Egner, A., Gundelfinger, E.D., Moser, T. 2005. Hair cell synaptic ribbons are essential for synchronous auditory signalling. Nature 434:889–894

Lenzi, D., Crum, J., Ellisman, M. H., & Roberts, W. M. (2002). Depolarization redistributes synaptic membrane and creates a gradient of vesicles on the synaptic body at a ribbon synapse. Neuron, 36(4), 649–659.

Sterling, P., & Matthews, G. (2005). Structure and function of ribbon synapses. In Trends in Neurosciences (Vol. 28, Issue 1, pp. 20–29). Elsevier Current Trends. https://doi.org/10.1016/j.tins.2004.11.009

Keen EC, Hudspeth AJ. Transfer characteristics of the hair cell's afferent synapse. Proc Natl Acad Sci U S A 103: 5537-5542, 2006.

Schnee ME, Lawton DM, Furness DN, Benke TA, Ricci AJ. Auditory hair cell-afferent fiber synapses are specialized to operate at their best frequencies. Neuron 47: 243-254, 2005

Schmitz F, Konigstorfer A, Sudhof TC. RIBEYE, a component of synaptic ribbons:Aprotein's journey through evolution provides insight into synaptic ribbon function. Neuron 28: 857-872, 2000.

Dick O, Hack I, Altrock WD, Garner CC, Gundelfinger ED, Brand- statter JH. Localization of the presynaptic cytomatrix protein Piccolo at ribbon and conventional synapses in the rat retina: Comparison with Bassoon. JCompNeurol 439: 224-234, 2001.

Khimich D, Nouvian R, Pujol R, Tom Dieck S, Egner A, Gundelfinger ED, Moser T. Hair cell synaptic ribbons are essential for synchronous auditory signalling. Nature 434: 889-894, 2005.

Vogl C, Cooper BH, Neef J, Wojcik SM, Reim K, Reisinger E, Brose N, Rhee JS, Moser T, Wichmann C. Unconventional molecular regulation of synaptic vesicle replenishment in cochlear inner hair cells. JCell Sci 128: 638-644, 2015.

Roux I, Safieddine S, Nouvian R, Grati M, Simmler MC, Bahloul A, Perfettini I, Le Gall M, Rostaing P, Hamard G, Triller A, Avan P, Moser T, Petit C. Otoferlin, defective in a human deafness form, is essential for exocytosis at the auditory ribbon synapse. Cell 127: 277-289, 2006.

Safieddine S, El-Amraoui A, Petit C. The auditory hair cell ribbon synapse: From assembly to function. Annu Rev Neurosci 35: 509-528, 2012.

Yasunaga S, Grati M, Cohen-Salmon M, El-Amraoui A, Mustapha M, Salem N, El-Zir E, Loiselet J, Petit C. A mutation in OTOF, encoding otoferlin, a FER-1-like protein, causes DFNB9, a nonsyndromic form of deafness. Nat Genet 21: 363-369, 1999

Pangršič T, Lasarow L, Reuter K, Takago H, Schwander M, Riedel D, Frank T, Tarantino LM, Bailey JS, Strenzke N, Brose N, Muller U, Reisinger E, Moser T. Hearing requires otoferlin-dependent efficient replenishment of synaptic vesicles in hair cells. Nat Neurosci 13: 869- 876, 2010.

Vogl, C., Cooper, B. H., Neef, J., Wojcik, S. M., Reim, K., Reisinger, E., Brose, N., Rhee, J.-S., Moser, T., & Wichmann, C. (2015). Unconventional molecular regulation of synaptic vesicle replenishment in cochlear inner hair cells. Journal of Cell Science, 128(4), 638–644.

Ruel J, Emery S, Nouvian R, Bersot T, Amilhon B, Van Rybroek JM, Rebillard G, Lenoir M, Eybalin M, Delprat B, Sivakumaran TA, Giros B, El Mestikawy S, Moser T, Smith RJ, Lesperance MM, Puel JL. Impairment of SLC17A8

encoding vesicular glutamate transporter-3, VGLUT3, underlies nonsyndromic deafness DFNA25 and inner hair cell dysfunction in null mice. Am J Hum Genet 83: 278-292, 2008.

Seal RP, Akil O, Yi E, Weber CM, Grant L, Yoo J, Clause A, Kandler K, Noebels JL, Glowatzki E, Lustig LR, Edwards RH. Sensorineural deafness and seizures in mice lacking vesicular glutamate transporter 3. Neuron 57: 263-275, 2008.

Marcotti W, Johnson SL, Rusch A, Kros CJ. Sodium and calcium currents shape action potentials in immature mouse inner hair cells. J Physiol 552: 743-761, 2003

Kiang NYS. Peripheral neural processing of auditory information. In: Handbook of Physiology, The Nervous System, Sensory Processes: American Physiological Society, pp. 639-674, 1984

Rose JE, Brugge JF, Anderson DJ, Hind JE. Phase-locked response to low-frequency tones in single auditory nerve fibers of the squirrel monkey. J Neurophysiol 30: 769-793, 1967.

Liberman MC.Auditory-nerve response from cats raised in a low-noise chamber. J Acoust Soc Am 63: 442-455, 1978.

Liberman MC. Morphological differences among radial afferent fibers in the cat cochlea: An electron-microscopic study of serial sections. Hear Res 3: 45-63, 1980.

Ohn TL, Rutherford MA, Jing Z, Jung S, Duque-Afonso CJ, Hoch G, Picher MM, Scharinger A, Strenzke N, Moser T. Hair cells use active zones with different voltage dependence of Ca^{2+} influx to decompose sounds into complementary neural codes. Proc Natl Acad Sci U S A 113: E4716-4725, 2016.

Matsubara, A., Laake, J.H., Davanger, S., Usami, S., Ottersen, O.P. 1996. Organization of AMPA receptor subunits at a glu- tamate synapse: a quantitative immunogold analysis of hair cell synapses in the rat organ of Corti. J. Neurosci. 16:4457–4467

Furness, D.N., Lehre, K.P. 1997. Immunocytochemical localiza- tion of a high-affinity glutamate-aspartate transporter, GLAST, in the rat and guinea-pig cochlea. Eur. J. Neurosci. 9:1961–1969

Furness, D.N., Lawton, D.M. 2003. Comparative distribution of glutamate transporters and receptors in relation to afferent innervation density in the mammalian cochlea. J. Neurosci. 23:11296–11304

Rebillard, G., Ruel, J., Nouvian, R., Saleh, H., Pujol, R., Dehnes, Y., Raymond, J., Puel, J.L., Devau,G. 2003. Glutamate transporters in the guinea-pig cochlea: partial mRNA sequences, cellular expression and functional implications. Eur. J. Neurosci. 17:83– 92

Liberman, M.C. 1982. Single-neuron labeling in the cat auditory nerve. Science 216:1239–1241

Moser, T., Beutner, D. 2000. Kinetics of exocytosis and endocy- tosis at the cochlear inner hair cell afferent synapse of the mouse. Proc. Natl. Acad. Sci. USA 97:883–888

Rutherford, M.A., Roberts, W.M. 2006. Frequency selectivity of synaptic exocytosis in frog saccular hair cells. Proc. Natl. Acad. Sci. USA 103:2898–2903

Edmonds, B.W., Gregory, F.D., Schweizer, F.E. 2004. Evidence that fast exocytosis can be predominantly mediated by vesicles not docked at active zones in frog saccular hair cells. J. Physiol. 560:439–450

Spassova, M.A., Avissar, M., Furman, A.C., Crumling, M.A., Saunders, J.C., Parsons, T.D. 2004. Evidence that rapid vesicle replenishment of the synaptic ribbon mediates recovery from short-term adaptation at the hair cell afferent synapse. J. Assoc. Res. Otolaryngol. 5:376–390

Melcher, J. R., Knudson, I. M., Fullerton, B. C., Guinan, J. J., Norris, B. E., Kiang, N. Y. E. 1996. Generators of brainstem auditory evoked potential in cat. I. An experimental approach to their identification. Hear. Res., 93, 1-27.

Lorente de No R. Action potentials of the motoneurons of the hypoglossus nucleus. J Cell Comp Physiol 29: 207–287, 1947

Rüttiger, L., Zimmermann, U., & Knipper, M. (2017). Biomarkers for Hearing Dysfunction: Facts and Outlook. ORL, 79(1–2), 93–111. https://doi.org/10.1159/000455705

Kim, D. O., Molnar, C. E., Matthews, J. W. 1980. Cochlear mechanics: nonlinear behavior in two-tone responses as reflected in cochlear-nerve-fiber responses and in ear-canal sound pressure. J. Acoust. Soc. Am., 67, 1704-1721

Shera, C. A., Guinan, Jr., J. J. 1999. Evoked otoacoustic emissions arise by two fundamentally different mechanisms: a taxonomy of mammalian OAEs. J. Acoust. Soc. Am., 105, 782-798.

Knight, R. D., Kemp, D. T. 2000. Indications of different distortion product otoacoustic emission mechanisms from a detailed f1,f2 area study. J. Acoust. Soc. Am., 107, 457-473.

Abdala, C. (1996). Distortion product otoacoustic emission ($2f1 - f2$) amplitude as a function of $f2 / f1$ frequency ratio and primary tone level separation in human adults and neonates . The Journal of the Acoustical Society of America, 100(6), 3726–3740. https://doi.org/10.1121/1.417234

Lacas-Gervais, S., Guo, J., Strenzke, N., Scarfone, E., Kolpe, M., Jahkel, M., De Camilli, P., Moser, T., Rasband, M. N., & Solimena, M. (2004). βIVΣ1 spectrin stabilizes the nodes of Ranvier and axon initial segments. Journal of Cell Biology, 166(7), 983–990. https://doi.org/10.1083/jcb.200408007

Werner, H. B., Krämer-Albers, E. M., Strenzke, N., Saher, G., Tenzer, S., Ohno-Iwashita, Y., De Monasterio-Schrader, P., Möbius, W., Moser, T., Griffiths, I. R., & Nave, K. A. (2013). A critical role for the cholesterol-associated proteolipids PLP and M6B in myelination of the central nervous system. Glia, 61(4), 567–586. https://doi.org/10.1002/glia.22456

Giuliani, N., Holte, L., Shy, M., & Grider, T. (2019). The audiologic profile of patients with Charcot-Marie Tooth neuropathy can be characterised by both cochlear and neural deficits. International Journal of Audiology, 58(12), 902–912. https://doi.org/10.1080/14992027.2019.1633022

Moore, S., Meschkat, M., Ruhwedel, T., Tzvetanova, I. D., Trevisiol, A., Battefeld, A., Kusch, K., Kole, M., Strenzke, N., Möbius, W., Hoz, L. de, & Nave, K.-A. (2019). A role of oligodendrocytes in information processing independent of conduction velocity. BioRxiv, 736975. https://doi.org/10.1101/736975

Giraudet, F., Charles, P., Mom, T., Boespflug-Tanguy, O., Dürr, A., Deltenre, P., & Avan, P. (2018). Rapid exhaustion of auditory neural conduction in a prototypical mitochondrial disease, Friedreich ataxia. Clinical Neurophysiology, 129(6), 1121–1129. https://doi.org/10.1016/j.clinph.2018.03.005

Yorgason, J.G., Fayad, J.N., and Kalinec, F. (2006). Understanding drug ototoxicity: molecular insights for prevention and clinical management. Expert Opin. Drug Saf. 5, 383–399.

Morton CC, Nance WE. Newborn hearing screening: a silent revolution. N Engl J Med 2006;354:2151-2164.

Dror, A. A., & Avraham, K. B. (2010). Hearing impairment: A panoply of genes and functions. In Neuron (Vol. 68, Issue 2, pp. 293–308). Cell Press. https://doi.org/10.1016/j.neuron.2010.10.011

Starr, A., Picton, T.W., Sininger, Y., Hood, L.J., and Berlin, C.I. (1996). Auditory neuropathy. Brain 119, 741–753.

Starr, A., Picton, T. W., Sininger, Y., Hood, L. J., & Berlin, C. I. (1996). Auditory neuropathy. Brain, 119(3), 741–753.

Starr, A., Sininger, Y.S., and Pratt, H. (2000). The varieties of auditory neurop- athy. J. Basic Clin. Physiol. Pharmacol. 11, 215–230.

Seal, R.P., Akil, O., Yi, E., Weber, C.M., Grant, L., Yoo, J., Clause, A., Kandler, K., Noebels, J.L., Glowatzki, E., et al. (2008). Sensorineural deafness and seizures in mice lacking vesicular glutamate transporter 3. Neuron 57, 263–275.

Ruel, J., Emery, S., Nouvian, R., Bersot, T., Amilhon, B., Van Rybroek, J.M., Rebillard, G., Lenoir, M., Eybalin, M., Delprat, B., et al. (2008). Impairment of SLC17A8 encoding vesicular glutamate transporter-3, VGLUT3, underlies nonsyndromic deafness DFNA25 and inner hair cell dysfunction in null mice. Am. J. Hum. Genet. 83, 278–292.

Chaïb H, Place C, Salem N, Chardenoux S, Vincent C, Weissenbach J, El-Zir E, Loiselet J, Petit C. A gene responsible for a sensorineural nonsyndromic recessive deafness maps to chromosome 2p22–23. Human molecular genetics. 1996 Jan 1;5(1):155-8.

Yasunaga, S., Grati, M., Cohen-Salmon, M., El-Amraoui, A., Mustapha, M., Salem, N., El-Zir, E., Loiselet, J., and Petit, C. (1999). A mutation in OTOF, encoding otoferlin, a FER-1-like protein, causes DFNB9, a nonsyndromic form of deafness. Nat. Genet. 21, 363–369.

Roux, I., Safieddine, S., Nouvian, R., Grati, M., Simmler, M.C., Bahloul, A., Perfettini, I., Le Gall, M., Rostaing, P., Hamard, G., et al. (2006). Otoferlin, defective in a human deafness form, is essential for exocytosis at the auditory ribbon synapse. Cell 127, 277–289.

Yasunaga, S., Grati, M., Chardenoux, S., Smith, T.N., Friedman, T.B., Lalwani, A.K., Wilcox, E.R., and Petit, C. (2000). OTOFencodes multiple long and short isoforms: Genetic evidence that the long ones underlie recessive deafness DFNB9. Am. J. Hum. Genet. 67, 591–600.

Beurg, M., Safieddine, S., Roux, I., Bouleau, Y., Petit, C., and Dulon, D. (2008). Calcium- and otoferlin-dependent exocytosis by immature outer hair cells. J. Neurosci. 28, 1798–1803.

Dulon, D., Safieddine, S., Jones, S.M., and Petit, C. (2009). Otoferlin is critical for a highly sensitive and linear calcium-dependent exocytosis at vestibular hair cell ribbon synapses. J. Neurosci. 29, 10474–10487.

Delmaghani, S.; Del Castillo, F.J.; Michel, V.; Leibovici, M.; Aghaie, A.; Ron, U.; Van Laer, L.; Ben-Tal, N.; Van Camp, G.; Weil, D.; et al. Mutations in the Gene Encoding Pejvakin, a Newly Identified Protein of the Afferent Auditory Pathway, Cause DFNB59 Auditory Neuropathy. Nat. Genet. 2006, 38, 770–778.

Defourny, J.; Aghaie, A.; Perfettini, I.; Avan, P.; Delmaghani, S.; Petit, C. Pejvakin-Mediated Pexophagy Protects Auditory Hair Cells against Noise-Induced Damage. Proc. Natl. Acad. Sci. USA 2019, 116, 8010–8017.

Schwander, M.; Sczaniecka, A.; Grillet, N.; Bailey, J.S.; Avenarius, M.; Najmabadi, H.; Steffy, B.M.; Federe, G.C.; Lagler, E.A.; Banan, R.; et al. A Forward Genetics Screen in Mice Identifies Recessive Deafness Traits and Reveals That Pejvakin Is Essential for Outer Hair Cell Function. J. Neurosci. 2007, 27, 2163–2175.

Brandt, A.; Striessnig, J.; Moser, T. $Ca_V1.3$ Channels Are Essential for Development and Presynaptic Activity of Cochlear Inner Hair Cells. J. Neurosci. 2003, 23, 10832–10840.

Baig, S.M.; Koschak, A.; Lieb, A.; Gebhart, M.; Dafinger, C.; Nürnberg, G.; Ali, A.; Ahmad, I.; Sinnegger-Brauns, M.J.; Brandt, N.; et al. Loss of Ca v 1.3 (CACNA1D) Function in a Human Channelopathy with Bradycardia and Congenital Deafness. Nat. Neurosci. 2011, 14, 77–86.

Platzer, J.; Engel, J.; Schrott-Fischer, A.; Stephan, K.; Bova, S.; Chen, H.; Zheng, H.; Striessnig, J. Congenital Deafness and Sinoatrial Node Dysfunction in Mice Lacking Class D L-Type Ca^{2+} Channels. Cell 2000, 102, 89–97.

Haeseleer, F.; Imanishi, Y.; Sokal, I.; Filipek, S.; Palczewski, K. Calcium-Binding Proteins: Intracellular Sensors from the Calmodulin Superfamily. In Biochemical and Biophysical Research Communications; Academic Press Inc.: Cambridge, MA, USA, 2002; pp. 615–623.

Christel, C.; Lee, A. Ca 2 +-Dependent Modulation of Voltage-Gated Ca 2 + Channels. Biochim. Biophys. Acta Gen. Subj. 2012, 1820, 1243–1252.

Schrauwen, I.; Helfmann, S.; Inagaki, A.; Predoehl, F.; Tabatabaiefar, M.A.; Picher, M.M.; Sommen, M.; Seco, C.Z.; Oostrik, J.; Kremer, H.; et al. A Mutation in CABP2, Expressed in Cochlear Hair Cells, Causes Autosomal-Recessive Hearing Impairment. Am. J. Hum. Genet. 2012, 91, 636–645.

Alexander, C.; Votruba, M.; Pesch, U.E.A.; Thiselton, D.L.; Mayer, S.; Moore, A.; Rodriguez, M.; Kellner, U.; Leo-Kottler, B.; Auburger, G.; et al. OPA1, Encoding a Dynamin-Related GTPase, Is Mutated in Autosomal Dominant Optic Atrophy Linked to Chromosome 3q28. Nat. Genet. 2000, 26, 211–215.

Delettre, C.; Lenaers, G.; Griffoin, J.M.; Gigarel, N.; Lorenzo, C.; Belenguer, P.; Pelloquin, L.; Grosgeorge, J.; Turc-Carel, C.; Perret, E.; et al. Nuclear Gene OPA1, Encoding a Mitochondrial Dynamin-Related Protein, Is Mutated in Dominant Optic Atrophy. Nat. Genet. 2000, 26, 207–210.

Diaz-Horta, O.; Abad, C.; Sennaroglu, L.; Ii, J.F.; DeSmidt, A.; Bademci, G.; Tokgoz-Yilmaz, S.; Duman, D.; Cengiz, F.B.; Grati, M.; et al. ROR1 Is Essential for Proper Innervation of Auditory Hair Cells and Hearing in Humans and Mice. Proc. Natl. Acad. Sci. USA 2016, 113, 5993–5998.

Nicolaides, P.; Appleton, R.E.; Fryer, A. Cerebellar Ataxia, Areflexia, Pes Cavus, Optic Atrophy, and Sensorineural Hearing Loss (CAPOS): A New Syndrome. J. Med. Genet. 1996, 33, 419–421.

Kim, T. B., Isaacson, B., Sivakumaran, T. A., Starr, A., Keats, B. J. B., & Lesperance, M. M. (2004). A gene responsible for autosomal dominant auditory neuropathy (AUNA1) maps to 13q14-21. Journal of Medical Genetics, 41(11), 872–876.

Schoen, C. J., Burmeister, M., & Lesperance, M. M. (2013). Diaphanous homolog 3 (Diap3) Overexpression Causes Progressive Hearing Loss and Inner Hair Cell Defects in a Transgenic Mouse Model of Human Deafness. PLoS ONE, 8(2), e56520. https://doi.org/10.1371/journal.pone.0056520

Goswamy, J.; Bruce, I.A.; Green, K.M.J.; O'Driscoll, M.P. Cochlear Implantation in a Patient with Sensori-Neural Deafness Secondary to Charcot-Marie-Tooth Disease. Cochlear Implants Int. 2012, 13, 184–187.

Verhagen, W.I.M.; Huygen, P.L.M.; Gabreëls-Festen, A.A.W.M.; Engelhart, M.; Van Mierlo, P.J.W.B.; Van Engelen, B.G.M. Sensorineural Hearing Impairment in Patients with Pmp22 Duplication, Deletion, and Frameshift Mutations. Otol. Neurotol. 2005, 26, 405–414.

Varga, R.; Kelley, P.M.; Keats, B.J.; Starr, A.; Leal, S.M.; Cohn, E.; Kimberling, W.J. Non-Syndromic Recessive Auditory Neuropathy Is the Result of Mutations in the Otoferlin (OTOF) Gene [2]. J. Med. Genet. 2003, 40, 45–50.

Kabzi´nska, D.; Korwin-Piotrowska, T.; Drechsler, H.; Drac, H.; Hausmanowa-Petrusewicz, I.; Kocha´nski, A. Late-Onset Charcot-Marie-Tooth Type 2 Disease with Hearing Impairment Associated with a Novel Pro105Thr Mutation in the MPZ Gene. Am. J. Med. Genet. Part A 2007, 143, 2196–2199.

Rance, G.; Fava, R.; Baldock, H.; Chong, A.; Barker, E.; Corben, L.; Delatycki, M.B. Speech Perception Ability in Individuals with Friedreich Ataxia. Brain 2008, 131, 2002–2012.

Tranebjærg, L. Deafness-Dystonia-Optic Neuronopathy Syndrome.; Adam, M.P., Ardinger, H.H., Pagon, R.A., Wallace, S.E., Bean, L.J.H., Stephens, K., Amemiya, A., Eds.; University of Washington: Seattle, WA, USA, 2003.

Bahmad, F.; Merchant, S.N.; Nadol, J.B.; Tranebjærg, L. Otopathology in Mohr-Tranebjærg Syndrome. Laryngoscope 2007, 117, 1202–1208.

Brookes, J.T.; Kanis, A.B.; Tan, L.Y.; Tranebjærg, L.; Vore, A.; Smith, R.J.H. Cochlear Implantation in Deafness-Dystonia-Optic Neuronopathy (DDON) Syndrome. Int. J. Pediatr. Otorhinolaryngol. 2008, 72, 121–126.

Simon, M.; Richard, E.M.; Wang, X.; Shahzad, M.; Huang, V.H.; Qaiser, T.A.; Potluri, P.; Mahl, S.E.; Davila, A.; Nazli, S.; et al. Mutations of Human NARS2, Encoding the Mitochondrial Asparaginyl-TRNA Synthetase, Cause Nonsyndromic Deafness and Leigh Syndrome. PLoS Genet. 2015, 11, e1005097.

Lang-Roth, R., Fischer-Krall, E., Kornblum, C., Nurnberg, G., Meschede, D., Goebel, I., Nurnberg, P., Beutner, D., Kubisch, C., Walger, M. et al. (2017) AUNA2: a novel type of non-syndromic slowly progressive auditory synaptopathy/auditory neuropathy with autosomal-dominant inheritance. Audiol. Neurootol., 22, 30–40.

Shashank Chepurwar, Sarah M von Loh, Daniela C Wigger, Jakob Neef, Peter Frommolt, Dirk Beutner, Ruth Lang-Roth, Christian Kubisch, Nicola Strenzke, Alexander E Volk, A mutation in ATP11A causes autosomal-dominant auditory neuropathy type 2, Human Molecular Genetics, Volume 32, Issue 7, 1 April 2023, Pages 1083–1089, https://doi.org/10.1093/hmg/ddac267

Andersen, J. P., Vestergaard, A. L., Mikkelsen, S. A., Mogensen, L. S., Chalat, M., & Molday, R. S. (2016). P4-ATPases as Phospholipid Flippases—Structure, Function, and Enigmas. In Frontiers in Physiology (Vol. 7). https://www.frontiersin.org/articles/10.3389/fphys.2016.00275

Lopez-Marques, R. L., Theorin, L., Palmgren, M. G., & Pomorski, T. G. (2014). P4-ATPases: lipid flippases in cell membranes. Pflügers Archiv - European Journal of Physiology, 466(7), 1227–1240. https://doi.org/10.1007/s00424-013-1363-4

Zachowski, A. (1993). Phospholipids in animal eukaryotic membranes: transverse asymmetry and movement. Biochemical Journal, 294(1), 1–14. https://doi.org/10.1042/bj2940001

Lenoir, G., Williamson, P., & Holthuis, J. C. (2007). On the origin of lipid asymmetry: the flip side of ion transport. Current Opinion in Chemical Biology, 11(6), 654–661. https://doi.org/10.1016/j.cbpa.2007.09.008

Katoh, Y., & Katoh, M. (2004). Identification and characterization of CDC50A, CDC50B and CDC50C genes in silico. Oncology Reports, 12(4), 939–943.

Saito, K., Fujimura-Kamada, K., Furuta, N., Kato, U., Umeda, M., & Tanaka, K. (2004). Cdc50p, a protein required for polarized growth, associates with the Drs2p P-type ATPase implicated in phospholipid translocation in Saccharomyces cerevisiae. Molecular Biology of the Cell, 15(7), 3418–3432.

Folmer, D. E., Elferink, R. P. J. O., & Paulusma, C. C. (2009). P4 ATPases - Lipid flippases and their role in disease. Biochimica et Biophysica Acta (BBA) - Molecular and Cell Biology of Lipids, 1791(7), 628–635. https://doi.org/10.1016/j.bbalip.2009.02.008

Liou, A. Y., Molday, L. L., Wang, J., Andersen, J. P., & Molday, R. S. (2019). Identification and functional analyses of disease-associated P4-ATPase phospholipid flippase variants in red blood cells. Journal of Biological Chemistry, 294(17), 6809–6821. https://doi.org/10.1074/jbc.RA118.007270

Fadok VA, Voelker DR, Campbell PA, Cohen JJ, Bratton DL, Henson PM. Exposure of phosphatidylserine on the surface of apoptotic lymphocytes triggers specific recognition and removal by macrophages. Journal of immunology (Baltimore, Md.: 1950). 1992 Apr 1;148(7):2207-16.

Gardai SJ, Bratton DL, Ogden CA, Henson PM. Recognition ligands on apoptotic cells: a perspective. Journal of leukocyte biology. 2006 May;79(5):896-903.

Leventis PA, Grinstein S. The distribution and function of phosphatidylserine in cellular membranes. Annual review of biophysics. 2010 Jun 9;39:407-27.

Tanaka, Y. and Schroit, A.J. (1983) Insertion of fluorescent phosphatidylserine into the plasma membrane of red blood cells. Recognition by autologous macrophages. J. Biol. Chem. 258, 11335–11343 5.

Van den Eijnde SM, Boshart L, Baehrecke EH, De Zeeuw CI, Reutelingsperger C, Vermeij-Keers C. Cell surface exposure of phosphatidylserine during apoptosis is phylogenetically conserved. Apoptosis. 1998 Jan;3:9-16.

Venegas, V. and Zhou, Z. (2007) Two alternative mechanisms that regulate the presentation of apoptotic cell engulfment signal in Caenorhabditis elegans. Mol. Biol. Cell 18, 3180–3192

Segawa, K., & Nagata, S. (2015). An Apoptotic 'Eat Me' Signal: Phosphatidylserine Exposure. Trends in Cell Biology, 25(11), 639–650. https://doi.org/10.1016/j.tcb.2015.08.003

Balasubramanian K, Schroit AJ. Aminophospholipid asymmetry: A matter of life and death. Annual review of physiology. 2003 Mar;65(1):701-34.

Nagata, S., Suzuki, J., Segawa, K., & Fujii, T. (2016). Exposure of phosphatidylserine on the cell surface. Cell Death and Differentiation, 23(6), 952–961. https://doi.org/10.1038/cdd.2016.7

Martin SJ, Finucane DM, Amarante-Mendes GP, O'Brien GA, Green DR. Phosphatidylserine externalization during CD95-induced apoptosis of cells and cytoplasts requires ICE/CED-3 protease activity. Journal of Biological Chemistry. 1996 Nov 15;271(46):28753-6.

Verhoven B, Schlegel R, Williamson P. Mechanisms of phosphatidylserine exposure, a phagocyte recognition signal, on apoptotic T lymphocytes. The Journal of experimental medicine. 1995 Nov 1;182(5):1597-601.

Bratton DL, Fadok VA, Richter DA, Kailey JM, Guthrie LA, Henson PM. Appearance of phosphatidylserine on apoptotic cells requires calcium-mediated nonspecific flip-flop and is enhanced by loss of the aminophospholipid translocase. Journal of Biological Chemistry. 1997 Oct 17;272(42):26159-65.

Segawa K, Kurata S, Yanagihashi Y, Brummelkamp TR, Matsuda F, Nagata S. Caspase-mediated cleavage of phospholipid flippase for apoptotic phosphatidylserine exposure. Science. 2014 Jun 6;344(6188):1164-8.

Suzuki J, Fujii T, Imao T, Ishihara K, Kuba H, Nagata S. Calcium-dependent phospholipid scramblase activity of TMEM16 protein family members. Journal of Biological Chemistry. 2013 May 10;288(19):13305-16.

deCathelineau AM, Henson PM. The final step in programmed cell death: phagocytes carry apoptotic cells to the grave. Essays in biochemistry. 2003 Oct 1;39:105-17.

Gordon S, Plüddemann A, Martinez Estrada F. Macrophage heterogeneity in tissues: phenotypic diversity and functions. Immunological reviews. 2014 Nov;262(1):36-55.

Bevers EM, Williamson PL. Phospholipid scramblase: an update. FEBS letters. 2010 Jul 2;584(13):2724-30.

Sahu SK, Gummadi SN, Manoj N, Aradhyam GK. Phospholipid scramblases: an overview. Archives of biochemistry and biophysics. 2007 Jun 1;462(1):103-14.

Wolf A, Schmitz C, Böttger A. Changing story of the receptor for phosphatidylserine-dependent clearance of apoptotic cells. EMBO reports. 2007 May;8(5):465-9.

Seidenbecher CI, Langnaese K, Sanmartí-Vila L, Boeckers TM, Smalla KH, Sabel BA, Garner CC, Gundelfinger ED, Kreutz MR (1998) Caldendrin, a novel neuronal calcium-binding protein con fined to the somato-dendritic compartment. J Biol Chem 273: 21324–21331.

Menger N, Seidenbecher CI, Gundelfinger ED, Kreutz MR (1999) The cytoskeleton-associated neuronal calcium-binding protein caldendrin is expressed in a subset of amacrine, bipolar and ganglion cells of the rat retina. Cell Tissue Res 298:21–32.

Haeseleer F, Sokal I, Verlinde C, Erdjument-Bromage H, Tempst P, Pronin A, Benovic J, Fariss R, Palczewski K (2000) Five members of a novel Ca2 -binding protein (CABP) subfamily with similarity to calmodulin. J Biol Chem 275:1247–1260.

Haeseleer F, Imanishi Y, Maeda T, Possin DE, Maeda A, Lee A, Rieke F, Palczewski K (2004) Essential role of Ca2 -binding protein 4, a Ca(v)1.4 channel regulator, in photoreceptor synaptic function. Nat Neurosci 7:1079–1087.

Yang PS, Alseikhan BA, Hiel H, Grant L, Mori MX, Yang WJ, Fuchs PA, Yue DT (2006) Switching of Ca2 -dependent inactivation of Ca(V)1.3 channels by calcium binding proteins of auditory hair cells. J Neurosci 26:10677–10689.

Cui G, Meyer A, Calin-Jageman I, Neef J, Haeseleer F, Moser T, Lee A (2007) Ca2 -binding proteins tune Ca2 -feedback to $Ca_V1.3$ Ca^{2+} channels in auditory hair cells. J Physiol 585:791–803.

Kim KY, Scholl ES, Liu X, Shepherd A, Haeseleer F, Lee A (2014) Localization and expression of Cabp1/caldendrin in the mouse brain. Neuroscience 268:33–47.

Yang, T., Scholl, E. S., Pan, N., Fritzsch, B., Haeseleer, F., & Lee, A. (2016). Expression and localization of Cabp Ca^{2+} binding proteins in the mouse cochlea. PLoS ONE, 11(1), 1–15. https://doi.org/10.1371/journal.pone.0147495

Yang, T., Hu, N., Pangršič, T., Green, S., Hansen, M., & Lee, A. (2018). Functions of Cabp1 and Cabp2 in the peripheral auditory system. Hearing Research, 364, 48–58. https://doi.org/https://doi.org/10.1016/j.heares.2018.04.001

Zhou H, Kim SA, Kirk EA, Tippens AL, Sun H, Haeseleer F, Lee A (2004) Ca2 -binding protein-1 facilitates and forms a postsynaptic complex with Ca(v)1.2 (L-Type) Ca2 channels. J Neurosci 24:4698–4708

Hardie J, Lee A (2016) Decalmodulation of Cav1 channels by Cabps. Channels (Austin) 10:33–37

Findeisen F, Minor DL (2010) Structural basis for the differential effects of Cabp1 and calmodulin on Ca(v)1.2 calcium-dependent inactivation. Structure 18:1617–1631.

Oz, S., Benmocha, A., Sasson, Y., Sachyani, D., Almagor, L., Lee, A., Hirsch, J. A., & Dascal, N. (2013). Competitive and non-competitive regulation of calcium-dependent inactivation in Cav1.2 L-type Ca^{2+} channels by calmodulin and Ca^{2+}-binding protein 1. Journal of Biological Chemistry, 288(18), 12680–12691. https://doi.org/10.1074/jbc.M113.460949

Yang, P. S., Johny, M. Ben, & Yue, D. T. (2014). Allostery in Ca^{2+} channel modulation by calcium-binding proteins. Nature Chemical Biology, 10(3), 231–238. https://doi.org/10.1038/nchembio.1436

Picher, M. M., Gehrt, A., Meese, S., Ivanovic, A., Predoehl, F., Jung, S., Schrauwen, I., Dragonetti, A. G., Colombo, R., Van Camp, G., Strenzke, N., & Moser, T. (2017). Ca^{2+}-binding protein 2 inhibits Ca^{2+}-channel inactivation in mouse inner hair cells. Proceedings of the National Academy of Sciences of the United States of America, 114(9), E1717–E1726. https://doi.org/10.1073/pnas.1617533114

Schrauwen, I., Helfmann, S., Inagaki, A., Predoehl, F., Tabatabaiefar, M. A., Picher, M. M., Sommen, M., Seco, C. Z., Oostrik, J., Kremer, H., Dheedene, A., Claes, C., Fransen, E., Chaleshtori, M. H., Coucke, P., Lee, A., Moser, T., & Van Camp, G. (2012). A mutation in CABP2, expressed in cochlear hair cells, causes autosomal-recessive hearing impairment. American Journal of Human Genetics, 91(4), 636–645. https://doi.org/10.1016/j.ajhg.2012.08.018

Moser T & Starr A (2016) Auditory neuropathy — neural and synaptic mechanisms. Nat Rev Neurol 12: 135–149

Santarelli R, Del Castillo I, Cama E, Scimemi P & Starr A (2015) Audibility, speech perception and processing of temporal cues in ribbon synaptic disorders due to OTOF mutations. Hear Res 330: 200–212

Moser T & Starr A (2016) Auditory neuropathy — neural and synaptic mechanisms. Nat Rev Neurol 12: 135–149

Vogl C, Panou I, Yamanbaeva G, Wichmann C, Mangosing SJ, Vilardi F, Indzhykulian AA, Pangršič T, Santarelli R, Rodriguez-Ballesteros M, et al (2016) Tryptophan-rich basic protein (WRB) mediates insertion of the tail-anchored protein otoferlin and is required for hair cell exocytosis and hearing. EMBO J 35: 2536–2552

Roux I, Safieddine S, Nouvian R, Grati M, Simmler M-C, Bahloul A, Perfettini I, Le Gall M, Rostaing P, Hamard G, et al (2006) Otoferlin, Defective in a Human Deafness Form, Is Essential for Exocytosis at the Auditory Ribbon Synapse. Cell 127: 277–289

Lek A, Evesson FJ, Sutton RB, North KN & Cooper ST (2012) Ferlins: Regulators of Vesicle Fusion for Auditory Neurotransmission, Receptor Trafficking and Membrane Repair. Traffic 13: 185–194

McNeil PL & Kirchhausen T (2005) An emergency response team for membrane repair. Nat Rev Mol Cell Biol 6: 499–505

Pangršič T, Reisinger E & Moser T (2012) Otoferlin: a multi-C2 domain protein essential for hearing. Trends Neurosci 35: 671–680

Pangršič T, Lasarow L, Reuter K, Takago H, Schwander M, Riedel D, Frank T, Tarantino LM, Bailey JS, Strenzke N, et al (2010) Hearing requires otoferlin-dependent efficient replenishment of synaptic vesicles in hair cells. Nat Neurosci 13: 869–876

Revelo NH, Kamin D, Truckenbrodt S, Wong AB, Reuter-Jessen K, Reisinger E, Moser T & Rizzoli SO (2014) A new probe for super-resolution imaging of membranes elucidates trafficking pathways. J Cell Biol 205: 591–606

Vogl C, Panou I, Yamanbaeva G, Wichmann C, Mangosing SJ, Vilardi F, Indzhykulian AA, Pangršič T, Santarelli R, Rodriguez-Ballesteros M, et al (2016) Tryptophan-rich basic protein (WRB) mediates insertion of the tail-anchored protein otoferlin and is required for hair cell exocytosis and hearing. EMBO J 35: 2536–2552

Tertrais M, Bouleau Y, Emptoz A, Belleudy S, Sutton RB, Petit C, Safieddine S & Dulon D (2019) Viral Transfer of Mini-Otoferlins Partially Restores the Fast Component of Exocytosis and Uncovers Ultrafast Endocytosis in Auditory Hair Cells of Otoferlin Knock-Out Mice. J Neurosci Off J Soc Neurosci 39: 3394–3411

Johnson, C. P., & Chapman, E. R. (2010). Otoferlin is a calcium sensor that directly regulates SNARE-mediated membrane fusion. Journal of Cell Biology, 191(1), 187–197.

Michalski NA, Goutman JD, Auclair SM, Monvel JB de, Tertrais M, Emptoz A, Parrin A, Nouaille S, Guillon M, Sachse M, et al (2017) Otoferlin acts as a Ca^{2+} sensor for vesicle fusion and vesicle pool replenishment at auditory hair cell ribbon synapses. eLife 6: e31013

Vogl C, Cooper BH, Neef J, Wojcik SM, Reim K, Reisinger E, Brose N, Rhee J-S, Moser T & Wichmann C (2015) Unconventional molecular regulation of synaptic vesicle replenishment in cochlear inner hair cells. J Cell Sci 128: 638–644

Jung SY, Maritzen T, Wichmann C, Jing ZZ, Neef A, Revelo NH, Al-Moyed H, Meese S, Wojcik SM, Panou I, et al (2015) Disruption of adaptor protein 2 mu (AP-2 mu) in cochlear hair cells impairs vesicle reloading of synaptic release sites and hearing. Embo J 34: 2686–2702

Strenzke N, Chakrabarti R, Al-Moyed H, Muller A, Hoch G, Pangršič T, Yamanbaeva G, Lenz C, Pan K-T, Auge E, et al (2016) Hair cell synaptic dysfunction, auditory fatigue and thermal sensitivity in otoferlin Ile515Thr mutants. EMBO J 35: 2519–2535

Kroll J, Jaime Tobón LM, Vogl C, Neef J, Kondratiuk I, König M, Strenzke N, Wichmann C, Milosevic I & Moser T (2019) Endophilin-A regulates presynaptic Ca^{2+} influx and synaptic vesicle recycling in auditory hair cells. EMBO J 38

Kroll J, Özçete ÖD, Jung S, Maritzen T, Milosevic I, Wichmann C & Moser T (2020) AP180 promotes release site clearance and clathrin-dependent vesicle reformation in mouse cochlear inner hair cells. J Cell Sci 133

Shrestha, B. R., Chia, C., Wu, L., Kujawa, S. G., Liberman, M. C., & Goodrich, L. V. (2018). Sensory Neuron Diversity in the Inner Ear Is Shaped by Activity. Cell, 174(5), 1229-1246.e17. https://doi.org/10.1016/j.cell.2018.07.007

Liberman MC (1978) Auditory-nerve response from cats raised in a low-noise chamber. J Acoust Soc Am 63:442–455.

Ohlemiller KK, Echteler SM, Siegel JH (1991) Factors that influence rate-versus intensity relations in single cochlear nerve fibers of the gerbil. J Acoust Soc Am 90: 274–287.

Winter IM, Robertson D, Yates GK (1990) Diversity of characteristic frequency rate intensity functions in guinea pig auditory nerve fibres. Hear Res 45:191–202.

Liberman MC (1982) Single-neuron labeling in the cat auditory nerve. Science 216: 1239–1241.

Merchan-Perez A, Liberman MC (1996) Ultrastructural differences among afferent synapses on cochlear hair cells: Correlations with spontaneous discharge rate. J Comp Neurol 371:208–221.

Ochiai, Y., Suzuki, C., Segawa, K., Uchiyama, Y., & Nagata, S. (2022). Inefficient development of syncytiotrophoblasts in the ATP11A -deficient mouse placenta. 1–11.

Harris DM, Dallos PE. Forward masking of auditory nerve fiber responses. Journal of neurophysiology. 1979 Jul 1;42(4):1083-107.

Frank, T., Rutherford, M. A., Strenzke, N., Neef, A., Pangršič, T., Khimich, D., Fejtova, A., Gundelfinger, E. D., Liberman, M. C., & Harke, B. (2010). Bassoon and the synaptic ribbon organize Ca^{2+} channels and vesicles to add release sites and promote refilling. Neuron, 68(4), 724–738.

Bernstein LR, Trahiotis C. Enhancing sensitivity to interaural delays at high frequencies by using "transposed stimuli". The Journal of the Acoustical Society of America. 2002 Sep 1;112(3):1026-36.

Buran BN, Strenzke N, Neef A, Gundelfinger ED, Moser T, Liberman MC. Onset coding is degraded in auditory nerve fibers from mutant mice lacking synaptic ribbons. Journal of Neuroscience. 2010 Jun 2;30(22):7587-97.

Yang, T. et al. Functions of Cabp1 and Cabp2 in the peripheral auditory system. Hear. Res. 364, 48–58 (2018).

Picher, M. M. et al. Ca^{2+}-binding protein 2 inhibits Ca^{2+}-channel inactivation in mouse inner hair cells. Proc. Natl. Acad. Sci. 114, E1717–E1726 (2017).

Oestreicher, D., Picher, M. M., Rankovic, V., Moser, T. & Pangršič, T. Cabp2-Gene Therapy Restores Inner Hair Cell Calcium Currents and Improves Hearing in a DFNB93 Mouse Model. Front. Mol. Neurosci. 14, 689415 (2021).

Bezanilla, F., Taylor, R. E. & Fernández, J. M. Distribution and kinetics of membrane dielectric polarization. 1. Long-term inactivation of gating currents. J. Gen. Physiol. 79, 21–40 (1982).

Payandeh, J., Gamal El-Din, T. M., Scheuer, T., Zheng, N. & Catterall, W. A. Crystal structure of a voltage-gated sodium channel in two potentially inactivated states. Nature 486, 135–139 (2012).

Olcese, R., Latorre, R., Toro, L., Bezanilla, F. & Stefani, E. Correlation between Charge Movement and Ionic Current during Slow Inactivation in Shaker K^+ Channels. J. Gen. Physiol. 110, 579–589 (1997).

Ferreira, G., Ríos, E. & Reyes, N. Two components of voltage-dependent inactivation in Ca(v)1.2 channels revealed by its gating currents. Biophys. J. 84, 3662–3678 (2003).

Tadross, M. R., Ben Johny, M. & Yue, D. T. Molecular endpoints of Ca^{2+}/calmodulin- and voltage-dependent inactivation of Ca(v)1.3 channels. J. Gen. Physiol. 135, 197–215 (2010).

Khimich, D. et al. Hair cell synaptic ribbons are essential for synchronous auditory signalling. Nature 434, 889–894 (2005).

Strenzke, N. et al. Hair cell synaptic dysfunction, auditory fatigue and thermal sensitivity in otoferlin Ile515Thr mutants. EMBO J. 35, e201694564 (2016).

Bharadwaj, H. M., Verhulst, S., Shaheen, L., Liberman, M. C. & Shinn-Cunningham, B. G. Cochlear neuropathy and the coding of supra-threshold sound. Front. Syst. Neurosci. 8, 26 (2014).

Jean, P. et al. The synaptic ribbon is critical for sound encoding at high rates and with temporal precision. eLife 7, e29275 (2018).

Jing, Z. et al. Disruption of the presynaptic cytomatrix protein bassoon degrades ribbon anchorage, multiquantal release, and sound encoding at the hair cell afferent synapse. J. Neurosci. 33, 4456–4467 (2013).

Taberner, A. M. & Liberman, M. C. Response Properties of Single Auditory Nerve Fibers in the Mouse. J. Neurophysiol. 93, 557–569 (2005).

Vogl C, Butola T, Haag N, Hausrat TJ, Leitner MG, Moutschen M, Lefèbvre PP, Speckmann C, Garrett L, Becker L, Fuchs H. The BEACH protein LRBA is required for hair bundle maintenance in cochlear hair cells and for hearing. EMBO reports. 2017 Nov;18(11):2015-29.

Pangršič T, Lasarow L, Reuter K, Takago H, Schwander M, Riedel D, Frank T, Tarantino LM, Bailey JS, Strenzke N, Brose N. Hearing requires otoferlin-dependent efficient replenishment of synaptic vesicles in hair cells. Nature neuroscience. 2010 Jul;13(7):869-76.

Roux I, Safieddine S, Nouvian R, Grati M, Simmler MC, Bahloul A, Perfettini I, Le Gall M, Rostaing P, Hamard G, Triller A, Avan P, Moser T, Petit C. Otoferlin, defective in a human deafness form, is essential for exocytosis at the auditory ribbon synapse. Cell 127: 277-289, 2006.

Bergeron, A.L., Schrader, A., Yang, D., Osman, A.A. and Simmons, D.D. (2005) The final stage of cholinergic differentiation occurs below inner hair cells during development of the rodent cochlea. J. Assoc. Res. Otolaryngol., 6, 401–415.

Safieddine, S. and Wenthold, R.J. (1999) SNARE complex at the ribbon synapses of cochlear hair cells: analysis of synaptic vesicle- and synaptic membrane-associated proteins. Eur. J. Neurosci., 11, 803–812.

Reisinger E, Bresee C, Neef J, Nair R, Reuter K, Bulankina A, Nouvian R, Koch M, Bückers J, Kastrup L, Roux I. Probing the functional equivalence of otoferlin and synaptotagmin 1 in exocytosis. Journal of Neuroscience. 2011 Mar 30;31(13):4886-95.

Yang, T. et al. Expression and Localization of Cabp Ca^{2+} Binding Proteins in the Mouse Cochlea. PLoS ONE 11, (2016)

Jean, P. et al. Single-cell transcriptomic profiling of the mouse cochlea: An atlas for targeted therapies. Proc. Natl. Acad. Sci. 120, e2221744120 (2023).

Xu, Z. et al. Profiling mouse cochlear cell maturation using 10× Genomics single-cell transcriptomics. Front. Cell. Neurosci. 16, 962106 (2022).

Yang, T. et al. Functions of Cabp1 and Cabp2 in the peripheral auditory system. Hear. Res. 364, 48–58 (2018).

Bonsch, D., Schmidt, C.M., Scheer, P., Bohlender, J., Neumann, C., Am Zehnhoff-Dinnesen, A. and Deufel, T. (2009) A new gene locus for an autosomal-dominant non-syndromic hearing impairment (DFNA 33) is situated on chromosome 13q34-qter. HNO, 57, 371–376.